OCS Study
BOEM 2012-004

Ultra-Deepwater Circulation Processes in the Gulf of Mexico

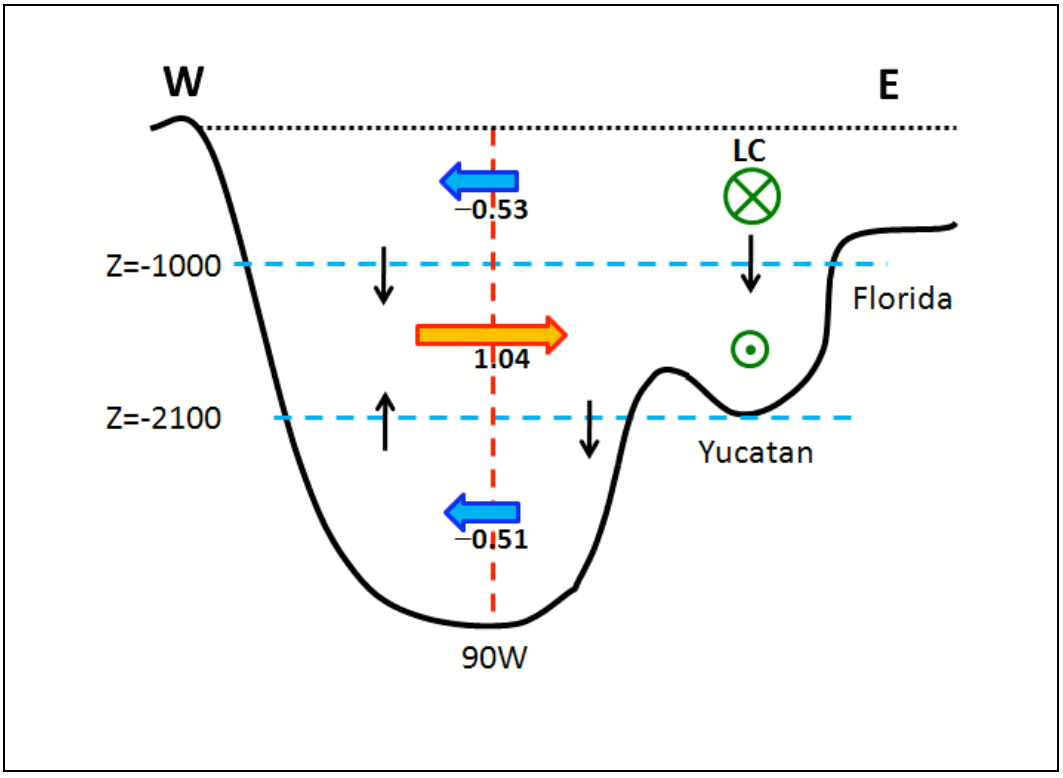

U.S. Department of the Interior
Bureau of Ocean Energy Management
Gulf of Mexico OCS Region

OCS Study
BOEM 2012-004

Ultra-Deepwater Circulation Processes in the Gulf of Mexico

Authors

Lie-Yauw Oey
Peter Hamilton

Prepared under BOEM Contract
M08PC20007
by
Princeton University
Program in Atmospheric and Oceanic Sciences
Sayre Hall
Princeton, NJ 08544

Published by

U.S. Department of the Interior
Bureau of Ocean Energy Management
Gulf of Mexico OCS Region

New Orleans
May 2012

DISCLAIMER

This report was prepared under contract between the Bureau of Ocean Energy Management (BOEM) and Princeton University. This report has been technically reviewed by BOEM, and it has been approved for publication. Approval does not signify that the contents necessarily reflect the views and policies of BOEM, nor does mention of trade names or commercial products constitute endorsement or recommendation for use. It is, however, exempt from review and compliance with BOEM editorial standards.

REPORT AVAILABILITY

This report is available only in compact disc format from the Bureau of Ocean Energy Management, Gulf of Mexico OCS Region, at a charge of $15.00, by referencing OCS Study BOEM 2012-004. The report may be downloaded from the BOEM website through the Environmental Studies Program Information System (ESPIS). You will be able to obtain this report also from the National Technical Information Service in the near future. Here are the addresses. You may also inspect copies at selected Federal Depository Libraries.

U.S. Department of the Interior
Bureau of Ocean Energy Management
Gulf of Mexico OCS Region
Public Information Office (MS 5034)
1201 Elmwood Park Boulevard
New Orleans, Louisiana 70123-2394
Phone: (504) 736-2519, 1-800-200-GULF
Fax: (504) 736-2620

U.S. Department of Commerce
National Technical Information Service
5301 Shawnee Road
Springfield, Virginia 22312
Phone: (703) 605-6000, 1-800-553-6847
Fax: (703) 605-6900
Email: orders@ntis.gov

CITATION

Oey, L.-Y. and P. Hamilton, 2012. Ultra-deepwater circulation processes in the Gulf of Mexico. U.S. Dept. of the Interior, Bureau of Ocean Energy Management, Gulf of Mexico OCS Region, New Orleans, LA. OCS Study BOEM 2012-004. 72 pp.

ABOUT THE COVER

Modeled 3-layer mean circulation in a west(W)-east(E) section of the Gulf of Mexico with Loop Current (LC). Horizontal arrows indicate transports (in Sv) at 90^{o}W. Vertical arrows show the corresponding vertical mass fluxes across z = -1000 m and z = -2100 m.

ACKNOWLEDGMENTS

Sponsor Acknowledgments: The study was sponsored by the Bureau of Ocean Energy Management/DOI, under Contract No. M08PC20007. The Contract Officer's Representative was Dr. Alexis Lugo-Fernandez and period of study was from June 2008 through June 2010.

Other Acknowledgments: We benefited from discussions with Drs. Kathy Donohue and Dong-Ping Wang. Contributions by co-authors (listed in each chapter) are also acknowledged; in particular those from Yu-Lin Chang for the modeling and analysis work, and from Peter Hamilton for the detailed model-data comparison work. Drs. Alexis Lugo-Fernandez, Walter Johnson and Ronald Lai are thanked for their encouragements throughout the course of this project.

TABLE OF CONTENTS

FIGURES

Page

TABLES

SUMMARY

Deep circulation (approximately 1000 m below the free surface) in the Gulf of Mexico is poorly known and its dynamics are not well-understood. Despite increased observations in recent decades, they still give incomplete and sometimes confusing and misleading pictures of the circulation—hence often misinterpretations of the related dynamics. Models are simpler but also often give misleading conclusions if not carefully analyzed. Moreover, models are imperfect and have errors due to their numerics (e.g., truncation errors), forcing, and incomplete physics. This work therefore first attempts to identify these imperfections in the models, and then conducts a series of carefully controlled model experiments that do not crucially depend on the detailed (hence imperfect) model physics. These experiments are analyzed to identify essential physics that govern the deep circulation in the Gulf of Mexico and how they are forced by, and are coupled to, the Loop Current and eddies in the upper layer.

The primary goal of this study is then to describe and explain the dynamical process(es) that govern the deep circulation in the Gulf of Mexico—how it is produced, how it is coupled to the upper layer (surface to approximately z = -1000 m below the surface), and how the coupling affects the Loop Current separation process. A second goal is to skill-assess the model against observations. For this purpose, data assimilation is used.

To meet the first goal, we conducted a series of carefully designed experiments and theoretical analyses to understand both the deep eddy-kinetic-energy (EKE) as well as the mean circulation. We then related these processes to upper-layer forcing by the Loop Current and rings, and also to the ring-separation process itself. To meet the second goal, we compared a data-assimilated version of our circulation model outputs against deep observations in central Gulf of Mexico.

We showed that topographic Rossby waves (TRW's), which previously have been identified to contribute to the largest portion of EKE in the deep Gulf, can focus in regions of closed contours of $N|\nabla H|$ (N is buoyancy frequency and H is bottom topographic depth below the mean surface), which we dubbed as "topocaustics" where deep EKE can accumulate, leading to intense bottom currents. Such intense currents are shown to occur in the Sigsbee escarpment, for example. The TRW (energy) rays are shown to follow the same rule as internal-wave rays in (simpler) two-dimensional xz-plane, but topocaustics are uniquely TRW's because these low-frequency rotational waves have preferential propagation direction with shallow depths on the right in the northern hemisphere, leading to energy accumulation in the western side of closed contours of $N|\nabla H|$ for H that shallows northward.

We then analyzed mass balances in a special 'box' defined over the deep eastern Gulf of Mexico (EG) bounded by 90°W to the west, the Gulf's bottom at the lower boundary, the z = -1000 m planar surface at the upper boundary, the sill wall of the Straits of Florida at the east, the northern Gulf's continental slope topography at the north and the Yucatan channel in the south. There are only 3 openings: 90°W, z = -1000 m plane and the deep Yucatan channel. By calculating transport balances in this box (across the 3 openings) over repeating Loop Current shedding cycles, we were able to explain the coupling between stages of Loop Current Cycle: intrusion and formation, incipient shedding, eddy-propagation, and the deep flows in *both* the eastern and western Gulf of Mexico.

We showed that previously widely-believed correlations between Loop expansion and Yucatan deep flows is weak at best and, more importantly, is based on a physically incorrect misconception of the upper-lower coupling that neglects the deep interaction between the eastern

and western Gulf of Mexico. We showed that this deep interaction results in what we call the Gulf of Mexico Oscillator, in which the western Gulf thermocline at z = -1000 m rises while that at the eastern Gulf falls and vice versa over the Loop Current shedding cycle. We showed that the net vertical transport in the eastern Gulf is downward across the z = -1000 m and deeper through z = -2000 m because the Loop spends more time "reforming" (i.e., accumulating its mass) than shedding eddies. As a result, since the deep Gulf is closed below the sill depth of the Yucatan Channel at z ≈-2000 m, the net circulation is zero and the eastern Gulf's downwelling results in anticyclonic mean circulation in the east and cyclonic circulation in the west. To the best of our knowledge, this is the first time that the cause for the deep cyclonic circulation in the western Gulf of Mexico has been robustly explained without resorting to complicated arguments involving, for example, TRW's. Moreover, since the deep western cyclonic gyre necessitates an influx of deep water from eastern to western Gulf, it results in upwelling across the z = -2000 m plane in the western Gulf, which together with downwelling across the z = -1000 m plane results in convergence and eastward transport in the middle layer across 90°W from west to east. Since the upper layer (0 to -1000 m) transport is westward due to eddies carrying mass westward, the circulation across 90°W is of a 3-layer structure: westward from surface to z = -1000 m and from z = -2000 m to bottom, and eastward in between from z = -1000 m to z = -2000 m.

We showed that the Yucatan deep flow is towards the south throughout the Loop Current Cycle. However, at incipient shedding, the Yucatan deep flow is very weak, so that deep perturbation in the channel at this stage can significantly affect the timing of eddy separation from the Loop Current.

Finally, as we pointed out previously in a related study (Chang and Oey, 2010a), changes in flow condition in the Straits of Florida may affect shedding of eddies. Our results (and previous modeling works) show that this downstream condition is not necessary. We pointed out then that a recently published claim of observed downstream-triggered mechanism to eddy-shedding is misleading.

1. TOPOCAUSTICS—THE GENERATION OF INTENSE CURRENTS NEAR THE SIGSBEE ESCARPMENT[1]

Synopsis

Why are strong, deep currents often observed near the Sigsbee escarpment in the northern Gulf of Mexico? We showed a mechanism for the generation of these strong currents by way of focusing and trapping of topographic Rossby wave energy.

Summary of the Main Results

Deep (~2000 m) observations near the Sigsbee escarpment in the Gulf of Mexico showed short-period (5~12 days) energetic currents due to topographic Rossby waves (TRW's). We suggested that the phenomenon is due to the focusing and accumulation of TRW energy by the slopes coupled with a bend in isobaths, in a topographic caustic (topocaustic). The idea draws on a simple mathematical equivalence between the propagation of internal waves and of TRW's. Topocaustics occur near regions of maximum $N_T = N|\nabla h|$ (N = Brunt-Vaisala frequency; h = water depth). Because of the one-sided propagation property of TRW's, energy also tends to accumulate at the "western" end of closed contours of N_T. The process is demonstrated here using a non-linear primitive-equation numerical model with idealized bathymetry and forcing. A Gulf of Mexico simulation initialized with a data-assimilated analysis covering the period of the Sigsbee observation is then conducted. The mooring is near a localized maximum N_T, and Intrinsic Mode Functions confirm the existence of energetic bursts of short-period deep current events. The strong currents are locally forced from above, either by an extended Loop Current or a warm ring.

1.1. INTRODUCTION

Near the Sigsbee Escarpment in the Gulf of Mexico (Figure 1.1; water depths ≈ 2000 m), Hamilton and Lugo-Fernandez (2001), Lai and Huang (2005), and Hamilton (2007) observed short-period (5~12 days) bottom-trapped topographic Rossby waves (TRW's) consisting of bursts of current fluctuations with amplitudes which are typically 0.2~0.3 m s^{-1} near the bottom (Figure 1.1). These intense TRW's appear to emanate from the south and southeast, from frontal eddies of the Loop Current and propagating rings, and also from deep eddies (Oey and Lee, 2002; Hamilton, 2007; Oey, 2008). Across the escarpment, a few kilometers to the northwest (of the mooring shown in Figure 1.1), current fluctuations rapidly decay, which may indicate that the TRW's are reflected off the escarpment (Hamilton, 2007). In this work, we used the mathematical equivalence between the propagation of TRW's and internal waves (IW's) to explain the build-up and rapid decay of TRW's near the escarpment.

Topographic Rossby wave energy propagates along rays the direction and (group) speed of which depend on the horizontal wavelength ($2\pi/K$) and period ($2\pi/\sigma$), as well as on environmental parameters such as the water depth (h), depth gradients (∇h), Brunt-Vaisala frequency (N) and also the background mean current ($\mathbf{V}$) and its shears if these exist (Rhines, 1970; Oey and Lee, 2002).

[1] This chapter is based on Oey et al. (2009): Topocaustics. Ocean Modeling, 29, 277-286. This work was also partially supported by BOEM Contract M07PC1133.

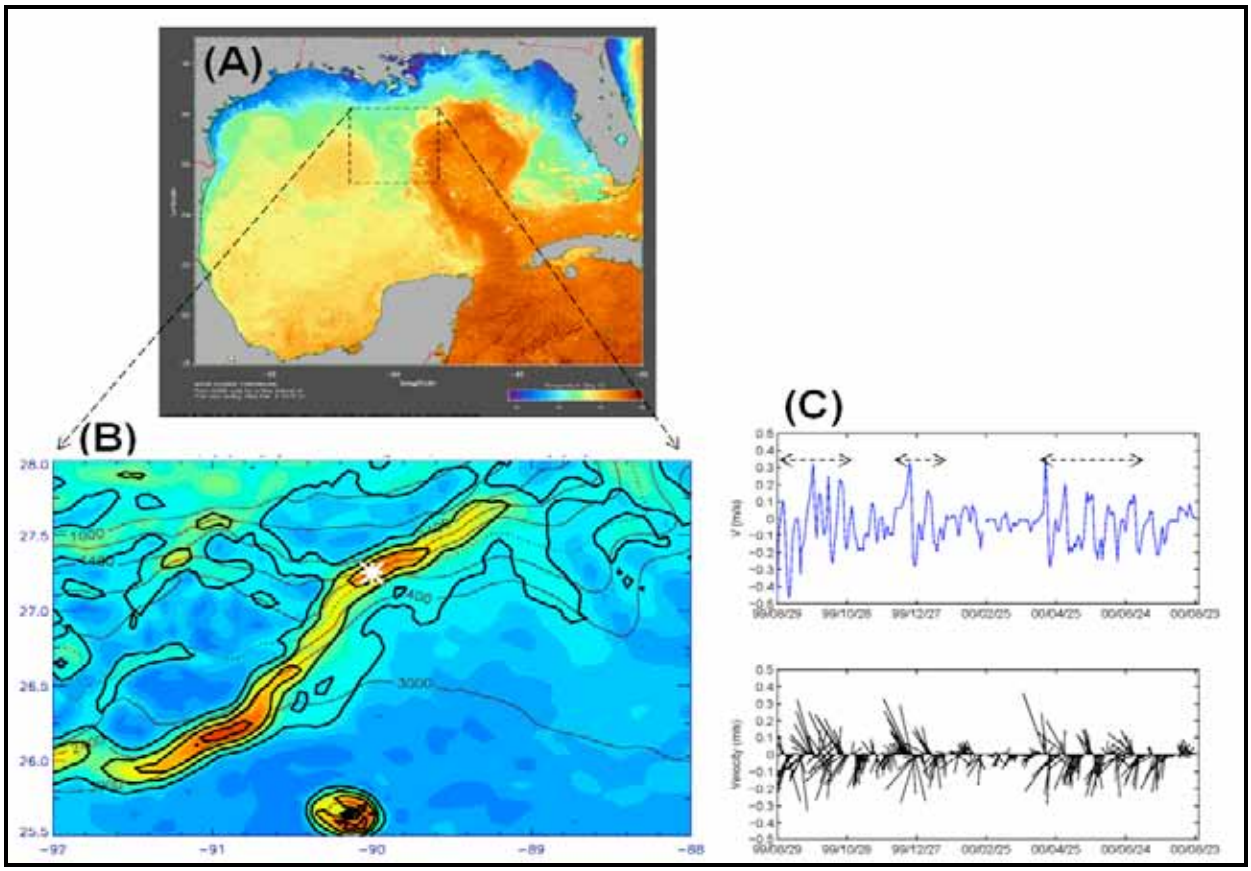

Figure 1.1. (A) AVHRR (Advanced Very High Resolution Radiometry; http://fermi.jhuapl.edu/avhrr/gm/averages/) seven-day composite sea-surface temperature in the Gulf of Mexico in Feb/1993 showing the Loop Current and a warm-core ring further west; (B) contours (dark lines and color shading) of maximum allowable TRW frequency NT = N|(h| (cycles/day or cpd) in the vicinity of the Sigsbee escarpment (box in panel A). Here the N = 6(10-4 s-1. Thin brown contours are isobaths, and the dotted line = 2000 m. The escarpment is identified with the band of high NT oriented northeast to southwest, approximately along the 2000 m isobaths in the north and along the 3000 m isobaths in the south. The "*" is one mooring from Hamilton (2007) and the along-isobath velocity component (daily-averaged, 200 m above the bottom) is plotted in (C) which also shows the corresponding vector sticks. The dashed arrowed lines in the time-series plot in (C) indicate periods when bursts of TRW's were identified by Hamilton (2007). (Data courtesy of Dr. Peter Hamilton).

A tacit assumption is that these parameters are slowly varying over the TRW wavelengths and periods. Formulae (2) and (3) (Oey and Lee, 2002) below are approximately valid provided that

$$NhK/|f| = h/h_{trap} \approx O(1) \text{ or larger,} \qquad (1)$$

where $h_{trap} = |f|/(NK)$ is the trapping depth of TRW's ($h_{trap} \approx 1000$ m for $2\pi/K \approx 100$ km, $f \approx 6.7\times10^{-5}$ s^{-1} and $N \approx 10^{-3}$ s^{-1}). Thus,

$$\sigma \approx N_T \sin(\theta) \qquad (2)$$

where $N_T = N|\nabla h|$, θ is the clockwise angle the wavenumber vector $\mathbf{K}$ makes with ∇h (Oey and Lee, 2002); also,

$$\mathbf{C_g} \times \mathbf{K} \approx N_T \cos(\theta) \mathbf{n}_u, \qquad (3)$$

where $\mathbf{C_g} = \nabla_{\mathbf{K}} \sigma$ is the group velocity, and $\mathbf{n}_u$ is an 'upward' unit vector perpendicular to both x and y. Equation (2) says that σ depends only on the wavenumber direction θ, but not its magnitude $|\mathbf{K}|$. Therefore $\mathbf{K}.\nabla_{\mathbf{K}} \sigma = 0$ since it is (proportional to) the component in the fixed $\mathbf{K}$-direction of the rate of change of σ in the $\mathbf{K}$-space, and is non-zero only if σ changes with $|\mathbf{K}|$ (Lighthill, 1978). Thus $\mathbf{C_g}$ and $\mathbf{K}$ are perpendicular to each other, and equation (3) says moreover that if $\mathbf{C_g}$ has an upslope component then $\mathbf{K}$ has a downslope component and vice versa. These properties make TRW's different from planetary Rossby waves, continental shelf waves or coastally trapped waves (Gill, 1982) but more similar to IW's for which the frequency is also a function of the wavenumber direction only. Indeed, TRW-propagation ($f > 0$) is identical to two-dimensional IW-propagation in the left half of the xz-plane, in which the z-direction may be identified as the y-direction pointing in the $\mathbf{n_{hy}}$ ($= -\nabla h/|\nabla h|$) direction (towards deceasing water depth). For IW's the maximum possible frequency of (local) oscillations is N; for TRW's it is N_T. Figure 1.2 illustrates the similarities and differences between IW's and TRW's.

Figure 1.1b plots N_T in the vicinity of the Sigsbee escarpment in the Gulf of Mexico. The escarpment appears as the high-N_T region inside the 0.2 cpd contour, i.e., where TRW's with periods shorter than 5 days are trapped. Mathematically, this is equivalent to IW-trapping in a thermocline. It is helpful to think of the trapping region as an n-day 'TRW-valley' within which TRW's with periods shorter than the (contour of the) bounding period of n days are trapped (Figure 1.2). Figure 1.1b indicates that TRW's with periods shorter than 10 days propagating upslope onto the Sigsbee escarpment may be trapped, since beyond (i.e., north of) the escarpment there exist elevated N_T^{-1} ("TRW-ridges") where the allowable periods are longer than 10 days; though in this case the waves may escape upslope through one of the narrow valleys. The existence of short-period TRW-valleys near the Sigsbee escarpment explains why predominantly shorter-period TRW's are found there (Lai and Huang, 2005; Hamilton, 2007; Oey, 2008).

The equivalence between TRW and IW rays means that one may utilize tools well-developed for the latter (Lighthill, 1978) to analyze TRW's. There are some differences, but once they are understood, most of the analytical treatments for IW-rays carry over to TRW's. Firstly, as mentioned above, TRW's are confined only to the left half (for $f > 0$) of the equivalent xz-plane of IW's. Secondly, as seen in Figure 1.1b, the n-day 'TRW-valleys' may be closed. With some exceptions,[2] the thermocline is unbounded for trapped IW's to propagate. Finally, whereas a trapped IW can reflect off side boundaries and therefore propagate back and forth ad infinitum within the thermocline (if inviscid), a trapped TRW cannot; the TRW phase, hence also its energy (irrespective of the wavelength, by equation 3), is constrained to propagate with the shallower water on the right (in northern hemisphere). When there is more than one group of waves, the possibility exists that TRW's may focus at the "western" end of a TRW-valley.

[2] Side boundaries or bounding well-mixed regions with low N's.

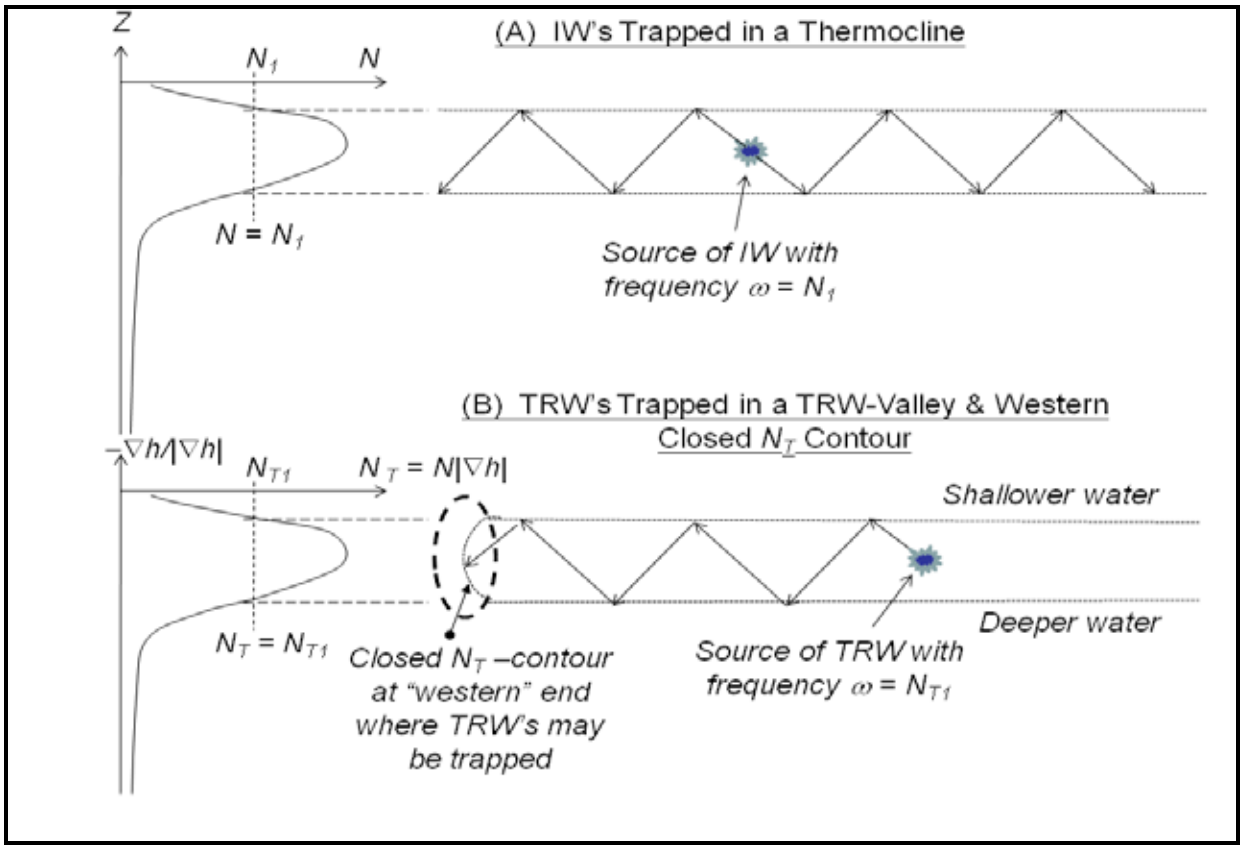

Figure 1.2. Similarities and differences between (A) internal waves trapped in a thermocline (upper panel; for clarity only one set of rays are sketched) and (B) topographic Rossby waves in a TRW-valley (lower panel). See text for details.

In analogy with IW caustics (Lighthill, 1978), the phenomenon when two or more TRW groups coalesce at a trapping boundary will be called topographic caustics or topocaustics. Near a trapping boundary, $\theta \sim \pi/2$, and the $\mathbf{n}_{hy}$-component of the wavenumber and the corresponding group velocity approach zero (rays form $\mathbf{n}_{hy}$-cusps in the absence of a mean flow). Since the $\mathbf{n}_{hy}$-component of the wave energy flux (= energy density × group velocity) is constant, the energy (hence wave amplitude) itself is predicted to become infinite. The theory of caustics utilizes the fact when rays coalesce the group velocity is stationary; the theory then predicts a finite amplitude by way of the Airy integral. The trapping boundary can be a critical "level" (latitude) either reflective or absorbing (when a mean flow is present) analogous to IW's, or it can be uniquely TRW's at a western TRW-valley (explained above), in which case it will be referred to as a "western topocaustic."

The above ideas are based on linear equations, slowly-varying parameters for rays and quasi-geostrophy for TRW's. Experience with these types of approximations suggests however that they often give useful insights on the properties of the solutions in more complete formulations. Essential aspects of linear theories also often show up in fully nonlinear models, and the ray theory is often successful when applied to environments which are not necessarily slowly varying (Lighthill, 1978). In this chapter, the ideas of trapped waves within closed N_T-contours and topocaustics are tested using a nonlinear primitive-equation numerical model under both simple (i.e., idealized topography and forcing; Sections 2 and 3) and Gulf of Mexico (i.e.

simulation with realistic forcing; Section 4) conditions. Results are discussed in Section 5 and Section 6 provides a summary.

The Loop Current is the dominant feature of the circulation in the eastern Gulf of Mexico and the formation region of the Florida Current-Gulf Stream system (Figures 1.1 and 1.2). It originates at the Yucatan Channel through which approximately 23~27 Sv (1 Sv = 10^6 m^3 s^{-1}) transport passes with a large minimum-maximum range of 14~36 Sv (Johns et al. 2002; Sheinbaum et al. 2002). Peak speeds of 1.5 to 1.8 m s^{-1} have been observed near the surface in the Loop Current (e.g., Nowlin, 1972; Forristal et al. 1992; see Oey et al. 2005a for other references). The Loop Current feeds the Florida Current which transports significant amounts of heat poleward. The Loop episodically sheds warm-core rings (e.g., Cochrane, 1972; Vukovich, 1995) at intervals of approximately 3 to 18 months (Sturges and Leben, 2000; Leben, 2005). These rings have diameters ≈ 200~300 km, vertical extent ≈ 1000 m, and swirl speeds ≈ 1.8~2 m s^{-1}; they generally translate westward at 2~5 km day^{-1} and have lifetimes of months to approximately a year (Nowlin, 1972; Elliott, 1982; Vukovich and Crissman, 1986; Cooper et al. 1990; Forristal et al. 1992). The Loop Current and its rings are powerful oceanic features that affect, either directly or indirectly through their smaller-scale subsidiaries, just about every aspect of oceanography of the Gulf (Oey et al. 2005a).

1.2. A PROCESS MODEL WITH IDEALIZED TOPOGRAPHY AND FORCING

The Princeton Ocean Model (POM; Mellor, 2004) was used. The model solves the primitive equations with hydrostatic and Boussinesq approximations on the Arakawa C-grid, and sigma (terrain-following) grid in the vertical. Leap-frog time-stepping was used with Asselin filter to reduce the computational mode. A channel domain, periodic in x (500 km long) and with walls at north and south in y (250 km wide) was used. Grid sizes $\Delta x = \Delta y = 2.5$ km in the horizontal and there are 50 equal-spaced terrain-following (sigma) levels in the vertical. These resolutions are sufficient to resolve TRW wavelengths of 50~150 km and vertical trapping depths of 500~1500 m (Oey and Lee, 2002; Lai and Huang, 2005; Hamilton, 2007). The Mellor-Yamada turbulence closure scheme (default in POM, Mellor, 2004) was used for the vertical eddy viscosity (K_M) and diffusivity (K_H). The horizontal viscosity was modeled using the Smagorinsky's shear-dependent formula with constant = 0.1, and the corresponding diffusivity is set 10 times smaller.

The topography (Figure 1.3) is deep (~3500 m) and nearly flat near the southern wall and is shallower (~1260 m) and also nearly flat near the northern wall. A canyon is placed in the center and large topographic gradients exist at the canyon head. This canyon topography mimics the local topography in the vicinity of the Sigsbee Escarpment in the Gulf of Mexico (Figure 1.1). Contours of N_T are also shown in Figure 1.2 assuming $N = 6\times10^{-4}$ s^{-1}, a middle value of those used by Hamilton (2007; $N = 10^{-3}$ s^{-1}) and Reid and Wang (2004; $N = 2\times10^{-4}$ s^{-1}). In the model, the salinity is set constant, S = 35 psu, and in place of the full (nonlinear) equation of state used by POM, the density is linear in the temperature T (see Gill, 1982, Appendix 3):

$$\rho = 1027.514485 \square 0.0952189\ T \qquad (4)$$

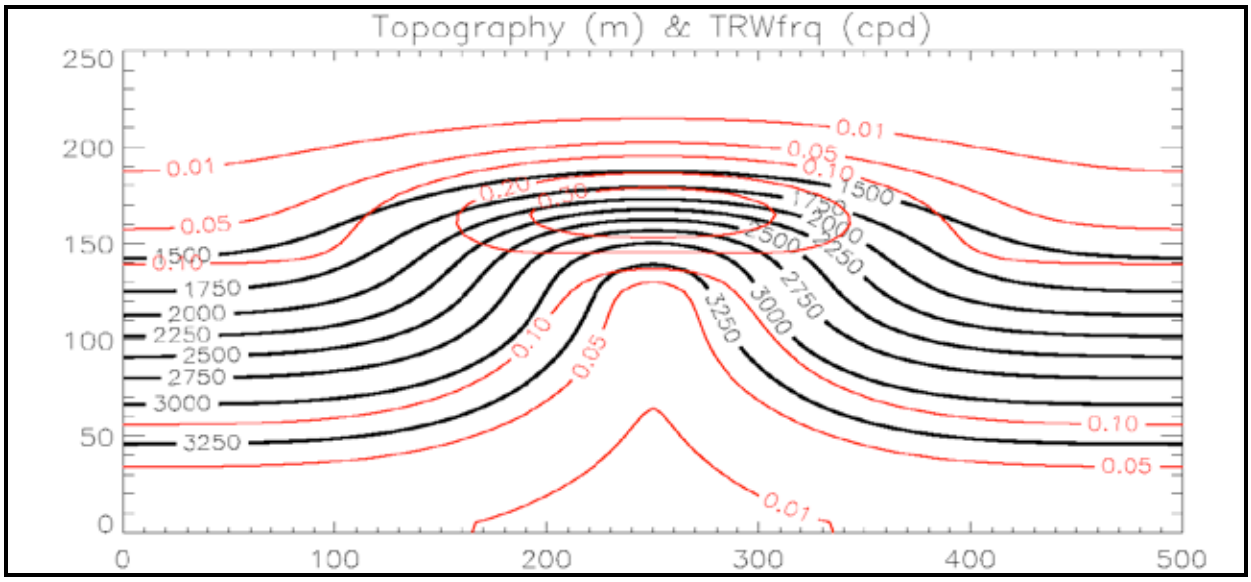

Figure 1.3. Model's 500 km (250 km domain with contours of (canyon) topography) (black; meters) and of maximum permissible TRW frequency NT (red; cycles/day). The x and y axes are in km.

The initial $T = T_o(z)$ is linear in z at all (x, y) except near the forcing described below, such that it yields a density profile (also linear in z)[3] with $N = 6\times10^{-4}$ s^{-1}. To generate waves with a wide spectrum, we put the forcing as a pressure source centered at (x_s, y_s) southeast of the canyon's head, and trapped at the bottom with a trapping height = z_s. A temperature anomaly T_s (with the corresponding density anomaly ρ_s) is specified

$$T_s = -0.5\, T_o(z)\, \exp[-(r/R_s)^2]\, \exp[-(z+h)/z_s], \qquad (5)$$

where r = radial distance from (x_s, y_s), R_s = 10 km and z_s = 500 m. These parameters yield an initial $T \approx 5^oC$ at the source center, some 5^oC cooler than the far-field T at the same depth. The pressure source is then obtained from (5), (4) and the hydrostatic equation $\partial p/\partial z = -\rho g$, and appears as the pressure gradient terms ∇p on the right hand side of the (x and y) momentum equations. For the experiment to be discussed below, the forcing is centered at (x_s, y_s) = (400, 70) km. Extensive sensitivity experiments have also been conducted as summarized in the Section 6. The pressure forcing is held steady throughout the integration period of 300 days; note that it is applied only in the small, localized region defined by equation (5).

While the forcing is steady, the solution is not. Through geostrophic balance, a cold dome (as in (5)) over the sloping topography is produced. Such a configuration is baroclinically unstable; the fastest growth is on the down-slope side of the dome (Swaters, 1991). The energy is derived from the release of available potential energy as the density slumps down-slope. This is the case in our simulation (not shown) though with only six grid points across the dome, the process was clearly under-resolved. However, details of the unstable dome are not of concern

[3] That ρ is linear in z yields zero truncation error for the so-called pressure gradient errors (Mellor et al. 1998). Subsequent evolution will yield profiles that depart from strict linearity, though the departures are slight in the TRW regions of interest. The errors are in any case small because of the fine grid, and also because the background density has been removed before computing ∇p (Mellor et al. 1998).

here, provided that disturbances with a wide spectrum are produced. The pressure specification above accomplishes this well.

1.3. RESULTS FROM THE IDEALIZED MODEL

The pressure source produces strong localized eddies and excites TRW's that propagate north-northwestward into the Canyon. An example is given in Figure 1.4 which shows snapshot (day 138) velocity vectors superimposed on a color map of relative vorticity non-dimensionalized by the Coriolis parameter, ζ/f, at z = –1300 m. Away from the source, disturbances are seen approximately along-isobaths. Note the appearance of strong ζ/f pattern of relatively short spatial scales near y = 160 km and 100 km < x < 190 km, a region where short-period TRW energy tends to build up as will be shown next (see Figure 1.5).

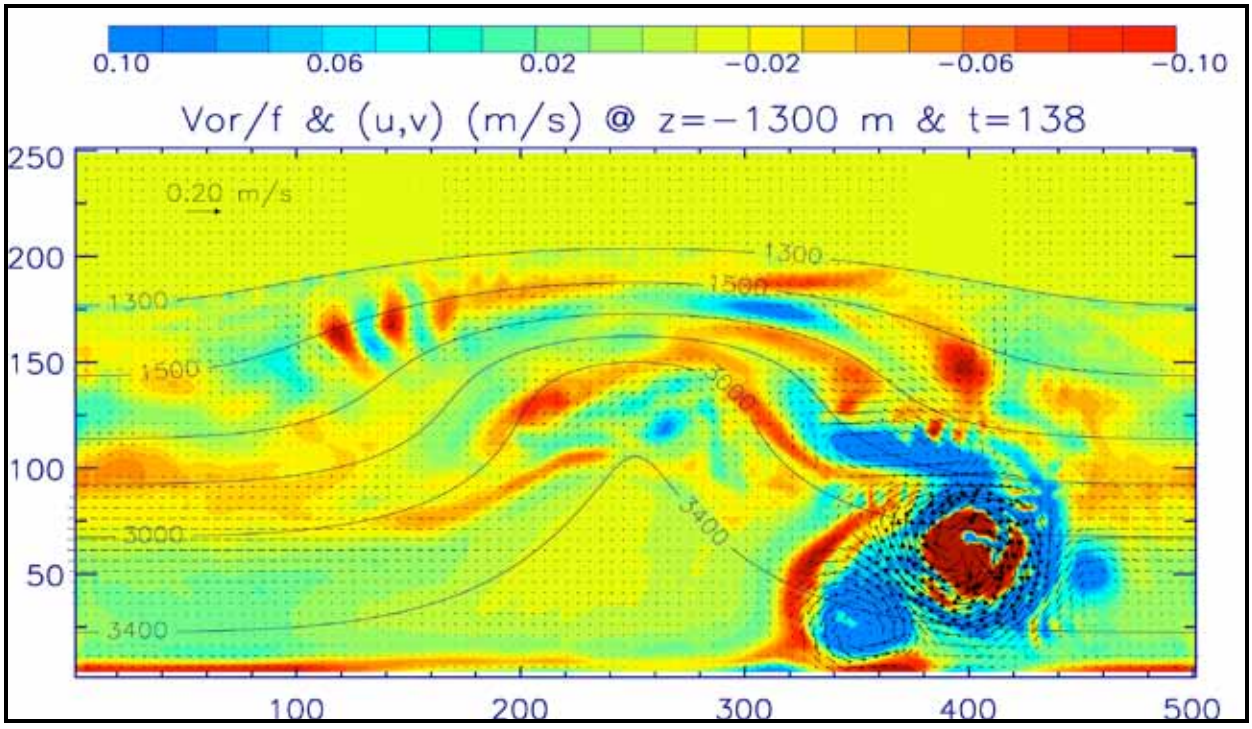

Figure 1.4. Velocity vectors superimposed on a color map of relative vorticity non-dimensionalized by the Coriolis parameter (ζ/f (blue is cyclonic and red is anti-cyclonic)) at the indicated depth and time; showing the strong forcing (pressure source) in the southeast and disturbances to the north and west. Contours are isobaths = 3400, 3000, 1500 and 1300 m. The x and y axes are in km.

We focused on short-period motions of about 5 and 10 days. As mentioned before, these were energetic motions observed near the Sigsbee Escarpment by Lai and Huang (2005) and Hamilton (2007), and are ones that are likely trapped in TRW-valleys. In Figures 1.1 and 1.3, the TRW-valleys are closed (partially closed) contours of N_T = 0.2 (0.1) cpd. Although topocaustics are based on rays, our goal was to demonstrate their existence in a nonlinear model that does not assume quasi-geostrophy.

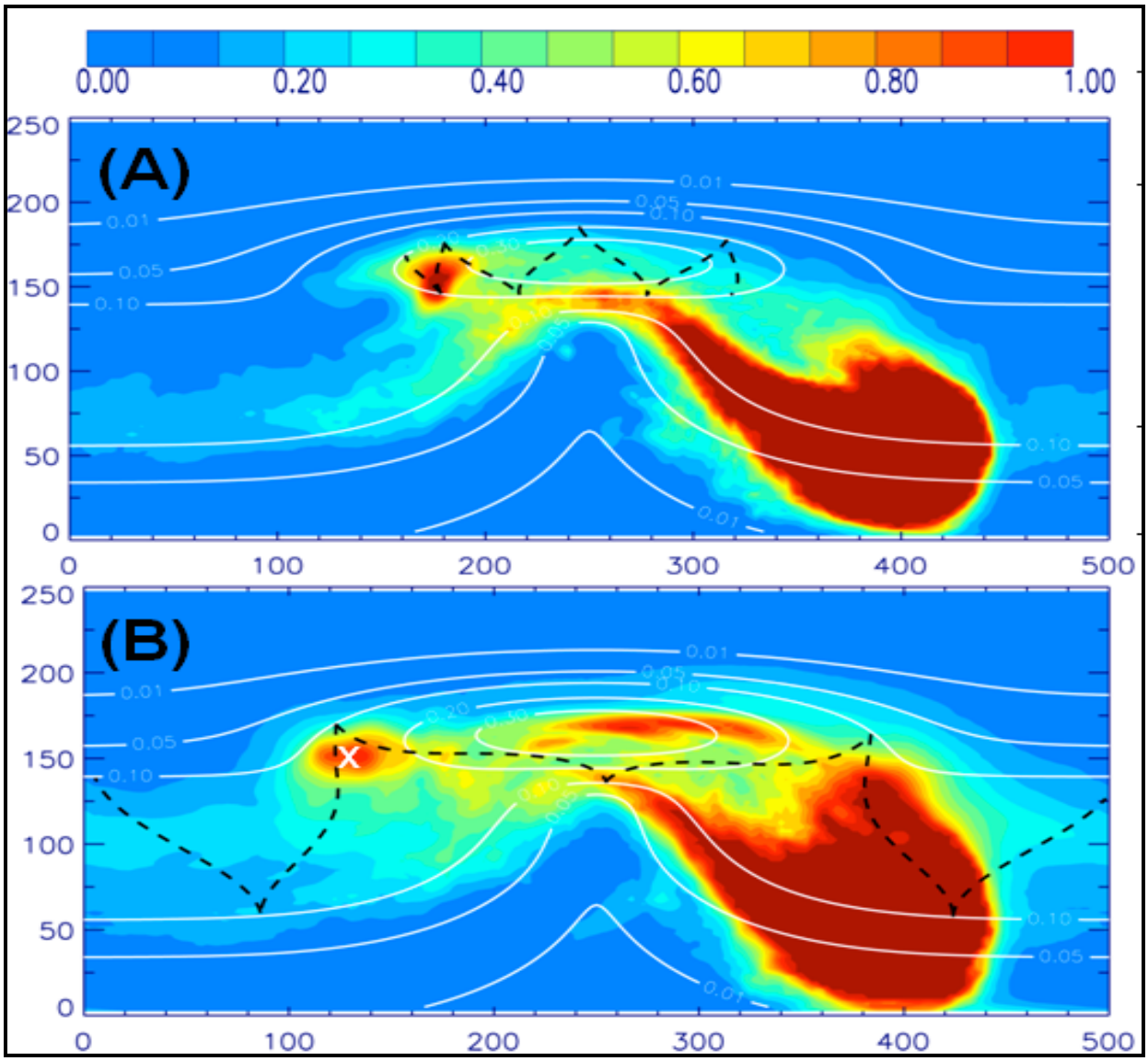

Figure 1.5a,b. Panels A & B: color is near-bottom energy (200 m off the bottom; non-dimensionalized by source energy) with periods (A) less than 5 days and (B) between 5 to 10 days. The (initial) NT contours (= 0.01 (outermost), 0.05, 0.1, 0.2 and 0.3 cycles/day) are shown in white and TRW rays in black dashed line. In each case, the ray corresponds to wavelengths that vary between 70 km and 130 km. The x and y axes are in km.

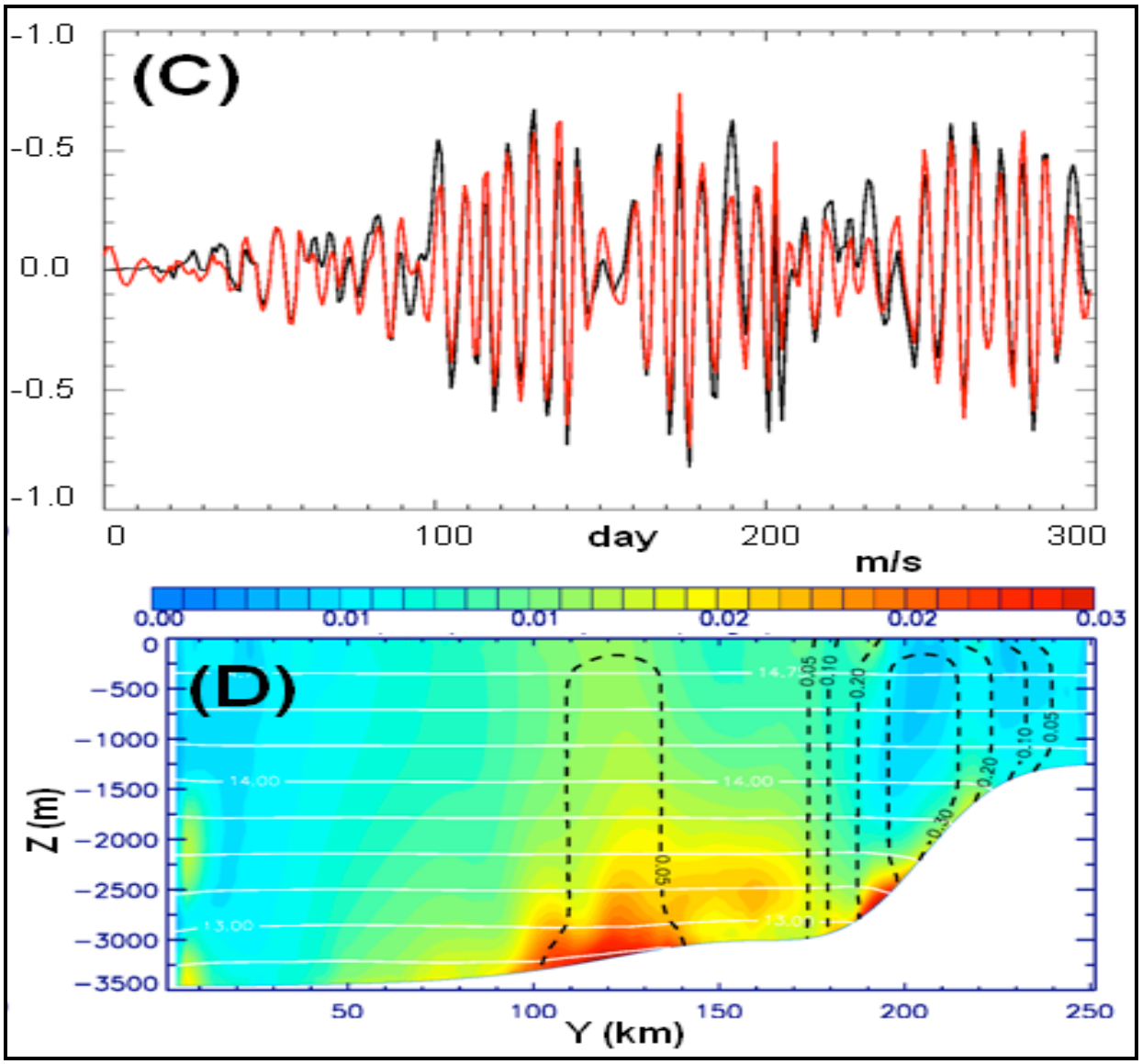

Figure 1.5c,d. (C) Time series of v at (x,y) = (130,150) km near the left edge of the northwestern topocaustic seen in Figure 1.5B (indicated by a white cross); black is total (i.e., original) v and red is v with periods < 10 days. The velocity is normalized by the standard deviation of the 10-day current (0.1 m s-1) at the center of the pressure forcing. (D) Vertical section (zy) contours (color) of mean square-root of the eddy kinetic energy $<(u'^2+v'^2)1/2>$, <.> = 300d-mean of the total (u,v), along the south-north section at mid-channel x = 250 km. White contours are temperature from 12.75 °C (near bottom) to 14.75 °C (near surface) at an interval = 0.25 °C, and black dashed contours are NT-contours = 0.05 (outermost), 0.1, 0.2 and 0.3 cycles/day. (The round-top of the NT-contours near the surface is a plot artifice).

Figure 1.5 shows the near-bottom energy with periods shorter than 5 days (Figure 1.5a) and for periods between 5 and 10 days (Figure 1.5b); the energies are non-dimensionalised (somewhat arbitrarily) by the respective (< 5 days, and 5-10 days) energies at the source (x_s, y_s). The N_T contours (white) and TRW rays (black dashed lines) are also plotted. For the 5-day periods, there are high energies around the source; these are not necessarily TRW's (indeed, the

gentle slope near the source does not support 5-day TRW's), but are caused by vigorous eddy motions noted above (Figure 1.4). Away from the source and within the N_T = 0.2 cpd contour, TRW's prevail. Figure 1.5a shows that the energy is concentrated near the western edge of the N_T = 0.2 cpd contour at (x,y) ≈ (180,150) km, i.e. a western topocaustic. The 5-day ray (black dashed line) indicates that its energy source is located on top of the canyon near the channel center, and also further east.

The 5-10 day energy (Figure 1.5b) shows two peaks: one near the western edge of the N_T = 0.1 cpd contour at (x,y) ≈ (130,150) km and the other one north of the canyon's top at (x,y) ≈ (260,170) km. Both are topocaustics as a result of TRW's being unable to cross over the N_T = 0.1 cpd contour. The first peak (at (130,150) km) is similar to the 5-day western topocaustic (described above) because of the bend in the N_T = 0.1 cpd contour. Figure 1.5c shows the corresponding v time-series. It shows that short-period (< 10 days) fluctuations make up almost the entire portion of the total current. Over the 300-day simulation, the trapped TRW's appear as three bursts of amplified currents, each lasting 30~50 days before they rapidly decay.

Finally, the existence of the model TRW's, described above, has been carefully checked using various diagnostic analyses including calculations of the trapping depths, wavelengths and frequencies based on the dispersion relation, as well as tracing the corresponding ray paths (c.f. Oey and Lee, 2002; Oey, 2008); details are not presented here. Bottom trapping is seen, for example, in the plot of vertical section contours of eddy kinetic energy, shown for the south-to-north section at x = 250 km in Figure 1.5d. Below the canyon in the lower slope, 100 km < y < 150 km, bottom trapping is seen with h_{trap} ≈ 1000 m corresponding to a TRW wavelength of about 150 km and a period of about 20 days. Near the canyon head the h_{trap} is smaller ≈ 400 m corresponding to a TRW wavelength of about 60 km and a period of less than 10 days.

In addition to the local topocaustics, described above, Figure 1.5b also shows a band of high energy along the contour of N_T ≈ 0.05~0.1 cpd approximately following the canyon topography. This is the same bottom-trapped energy seen in the yz-section plot for 100 km < y < 150 km in Figure 1.5d. The energy directly extends from the pressure source to the canyon; it then decays westward. Figure 1.6 plots the mean (u,v) superimposed on color ζ/f, and shows an approximately "westward" isobathic flow at the foot of the canyon near y ≈ 125 ~ 150 km, where u ≈ –0.05 m s^{-1}. Analogously to IW's critical-layer absorption in the presence of a mean flow (Lighthill, 1978), the westward decay of TRW-energy (seen in Figure 1.5b) may be linked also to the existence of the mean isobathic flow that extracts energy from the waves.

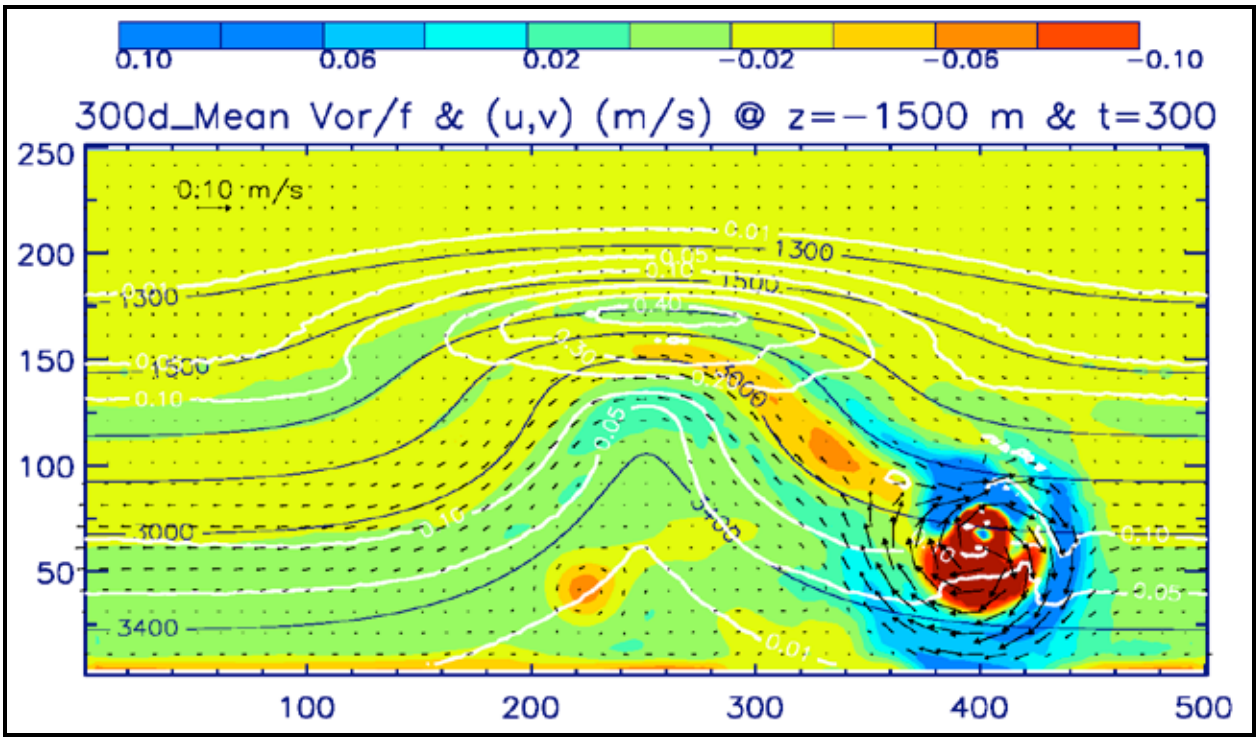

Figure 1.6. Color: 300-day mean vorticity/f at z = (1500 m, and the corresponding (u,v) vectors (plotted every 4 grid points) for the experiment described in the text. Contours: mean NT in cpd (white) and isobaths in meters (black). This figure illustrates the existence of a mean flow approximately off-slope of the 3000 m isobaths. The mean flow allows a critical-layer absorption near the foot of the canyon, y (125 ~ 150 km). The x and y axes are in km.

1.4. GULF OF MEXICO SIMULATION

At the start of the Sigsbee measurements in late August 1999, the Loop Current was about to shed an eddy, and a large warm-core ring (Eddy Juggernaut) eventually separated from the Loop approximately 1.5 months later in October 1999. We have previously studied this event in great detail (Oey et al. 2005a; Lin et al. 2006) and have compared the modeled results with observations. The focus was on the upper-layer currents and sea-surface height (SSH), and both data-assimilated (i.e., hindcast) and "free-running" model results were used. By "free-running" we mean that the model is initialized from a hindcast and then is continued without any data assimilation.

Observations (Hamilton and Lugo-Fernandez, 2001; Lai and Huang, 2005; Hamilton, 2007) show that short-period, intense deep currents at Sigsbee occurred in Sep-Oct of 1999 (Figure 1.1c), and that they were likely related to the Loop Current northward expansion and shedding of Eddy Juggernaut. Measurements at later dates (Figure 1.1c) and during other more recent field work (Donohue et al., 2006) suggest also that the Sigsbee escarpment is a site where short-period, intense deep currents tend to occur. Our goal is to show that a high-resolution simulation with realistic forcing and topography of the Gulf of Mexico also can generate such bursts of intense currents (at the Sigsbee mooring), and that these currents result in energy build-up that is consistent with the existence of topocaustics as suggested by the idealized model of the previous section. To accomplish this objective, we analyzed deep currents obtained from a free-running model initialized from a hindcast experiment approximately one month prior (July 24, 1999) to

the start of the observation on August 29, 1999. Then we captured the first intense deep-current event shown in Figure 1.1c, and also analyzed later events. The set-up was the same as detailed in Oey et al. (2005a) and Lin et al. (2007), except that the horizontal grid resolution in the Gulf of Mexico (west of 77°W) was doubled following the procedure described in Oey and Zhang (2004), and the topography was also improved incorporating the latest 1-minute resolution ETOPO1 data (http://www.ngdc.noaa.gov/mgg/global/global.html). The resulting grid size near the Sigsbee escarpment is approximately 3 km, and there are 25 vertical sigma levels. A fourth-order scheme was used to evaluate the pressure-gradient terms (Berntsen and Oey, 2010), and guarantees (in combination with high resolution and subtracting of the mean ρ-profile) very small truncation errors of O(mm/s) (c.f. Oey et al. 2003).

1.4.1. Data Assimilation and Hindcast

To produce the initial Loop Current and eddy fields on July 24, 1999 for the free-running model, a hindcast experiment that assimilates satellite SSH anomaly up to that date was conducted, using the Mellor and Ezer's (1991) and Ezer and Mellor's (1994) scheme. The SSH anomaly is projected into the subsurface density field using correlation functions pre-computed from the model's eddy statistics. This method is simple, yet it yields fairly accurate upper-layer structures ($z = 0$ to approximately -800 m) of the Loop Current and eddy fields (Oey et al. 2005a; Lin et al. 2007; Yin and Oey, 2007). No assimilation is done in the deep layers (below $z \approx -800$ m) where the simulated currents rely entirely on the model's dynamics. In the Gulf of Mexico, deep current fluctuations are caused by TRW's and perhaps also by small-scale (chaotic) eddies (Hamilton, 1990, 2007; Lai and Huang, 2005; Oey et al., 2005b; Oey, 2008); they are not likely to be simulated accurately. However, while our focus was more on verifying the existence of topocaustics near the Sigsbee escarpment (i.e., whether localized region of intense deep currents is also found in a realistic environment), rather than in accurately simulating the deep currents in details, it was necessary to verify that the model, when forced by the eddy field from above (through the Mellor-Ezer scheme), does reproduce the observed deep current variability. Figure 1.7 compares the observed and modeled current variance ellipses from surface to deep layers using the comprehensive year-long dataset collected by BOEM (Donohue et al. 2006) in the east-central Gulf of Mexico (the "L-moorings"). Generally good agreements are seen both in the amplitudes and orientations of the ellipses. A comparison at the Sigsbee location (I1-mooring; Figure 1.7) also shows reasonably good agreement. The orientations of current ellipses near the bottom give estimates of the directions of TRW propagation (Hamilton, 2007), and agreements between modeled and observed ellipses suggest that both the deep energy and its direction of propagation are represented reasonably well by the model.

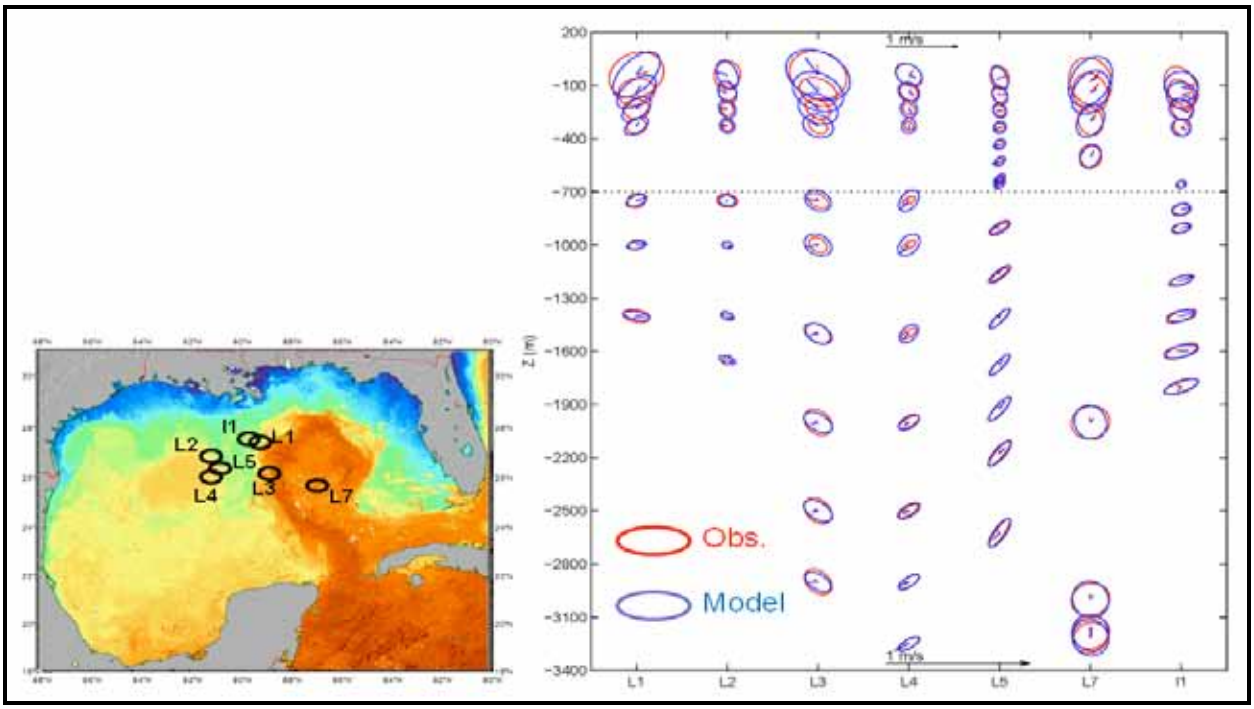

Figure 1.7. A comparison of observed and modeled current variance ellipses at six tall (L) moorings in the east-central Gulf of Mexico (left inset) for the period April 2003 through April 2004, and also at the Sigsbee (I1) mooring for the period August 1999 through August 2000, i.e. the "*" mooring shown in Figure 1. Vectors at ellipse centers are 1-year mean velocities but these are not representatives of the long-term means because they were dominated by a few strong current events. Note that scales are different above and below z = (700 m (as indicated by the dotted line). The observational data are courtesy of Dr. Peter Hamilton of SAIC.

1.4.2. The Free-Running Model

The Mellor-Ezer scheme was used to initialize a 2-year, free-running model experiment starting from July 24, 1999. The model Loop Current sheds a warm ring on September 28, 1999, approximately 2~3 weeks earlier than the actual shedding date of Eddy Juggernaut on October 13~18, 1999; this mismatch was to be expected, as the model generally has a predictability of about 6~8 weeks (c.f. Yin and Oey, 2007). Apart from this mismatch, the position of the model eddy relative to the Sigsbee mooring, shown in Figure 1.8a as SSH and surface velocity on t = 50 day (or October 22, 1999), was similar to the observed (see Oey et al. 2005a); both show the deep mooring being directly located under the northwestern edge of the eddy. The close proximity of the forcing (the eddy) to the mooring in a steep-topographic region with closed contours of high N_T values (> 0.1 cpd) suggests that short-period TRW's would be locally trapped and enhanced (see also Oey, 2008), as has been observed (Lai and Huang, 2005; Hamilton, 2007). If the theory is correct, the realistic simulation should also produce a similar response.

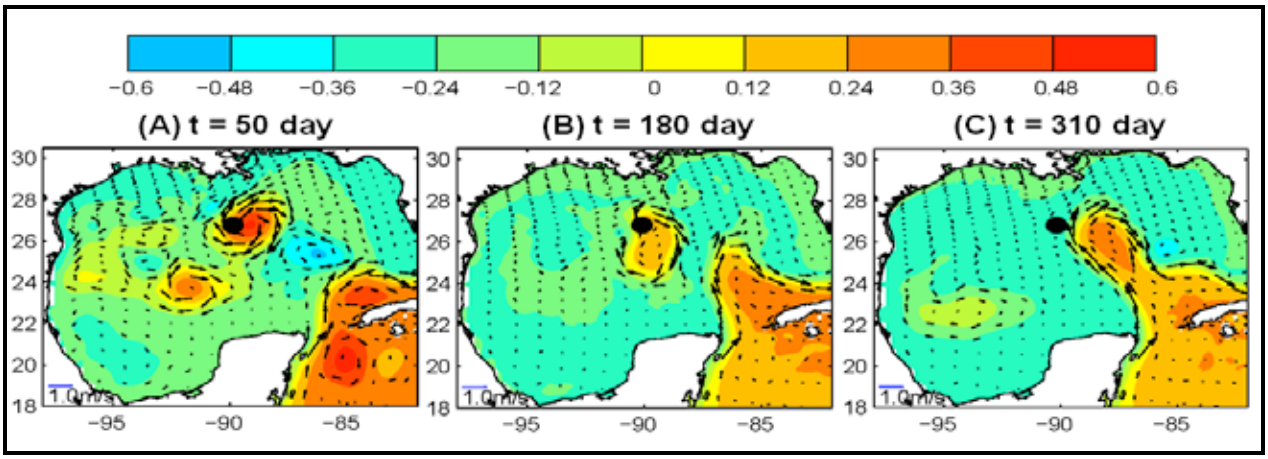

Figure 1.8. Modeled sea-surface height (color; red = +0.6m, blue = -0.6 m) and velocity (vectors) on (A) t = 50 day showing the warm-core ring Eddy Juggernaut over the mooring location at the Sigsbee escarpment (solid dot). Panels (B) and (C) show the corresponding plots 130 and 260 days later, respectively. The time "t" is Julian day from September 2, 1999, the same as that used in Figure 1.10.

1.4.3. Energy Spectra

Figure 1.9 shows the spectral energy for deep fluctuations with periods between 2 and 20 days. The currents are depth-averaged from z = –1000 m to the bottom; previous works (Oey and Lee, 2002; Hamilton, 2007; Oey, 2008) indicate that deep currents are nearly depth-independent. Energetic fluctuations exist over the lower slope and continental rise where the influence of the Loop Current and warm rings prevail. Energy generally deceases northward and westward but intensifies as one approaches the Sigsbee Escarpment, at two local maxima of N_T: southwest of the Escarpment near (91°W, 26°N) and northeast of the Escarpment near (90°W, 27.2°N; i.e., the "Sigsbee mooring"). The energy drops sharply north of the escarpment especially for the Sigsbee mooring. The energy is also weak between the two (southwest and northeast) maxima along the escarpment, even though the bottom slope remains steep and energetic warm eddies also pass over that region. These results support the idealized model prediction that energy tends to accumulate near the local maxima of N_T, or near a bend in the N_T contour (c.f. Figure 1.5b).

1.4.4. Intrinsic Mode Functions

The Intrinsic Mode Functions (IMF's; Huang et al. 1998; the method is generally called the Hilbert-Huang Transform or HHT) are used to characterize the frequency and energy of the current fluctuations at the Sigsbee mooring as a function of time. Unlike Fourier-based methods, HHT adaptively sieves through a non-stationary time-series and orders it into IMF's each with its own characteristic frequencies and amplitudes that vary with time. In oceanography, the method has been applied successfully by Lai and Huang (2005) and Oey et al. (2008) to highly non-stationary data. Figure 1.10 compares the observed (a) and modeled (b) first six IMF's at the Sigsbee mooring over a one-year period beginning on September 2, 1999. Both observed and modeled IMF#1's have very short periods 5~10 days, and show bursts of intense fluctuations during the first 50 days when the Loop Current extended northward and Eddy Juggernaut was shed (Figure 1.8a). The modeled IMF became weak after Eddy Juggernaut (t > 50 days) and only became intense again at t ≈ 180 days when another (slightly weaker) eddy was shed over

the Sigsbee mooring (Figure 1.8b). The modeled IMF became strong again at t ≈ 310 days when the modeled Loop Current extended far northward over the Sigsbee mooring (Figure 1.8c). These variations in the (modeled) IMF#1 can be seen also in IMF's#2 (periods ~ 10 days), 3 (~20 days) and 4 (30~40 days), but the signals are most distinct for the shorter-period IMF's#1

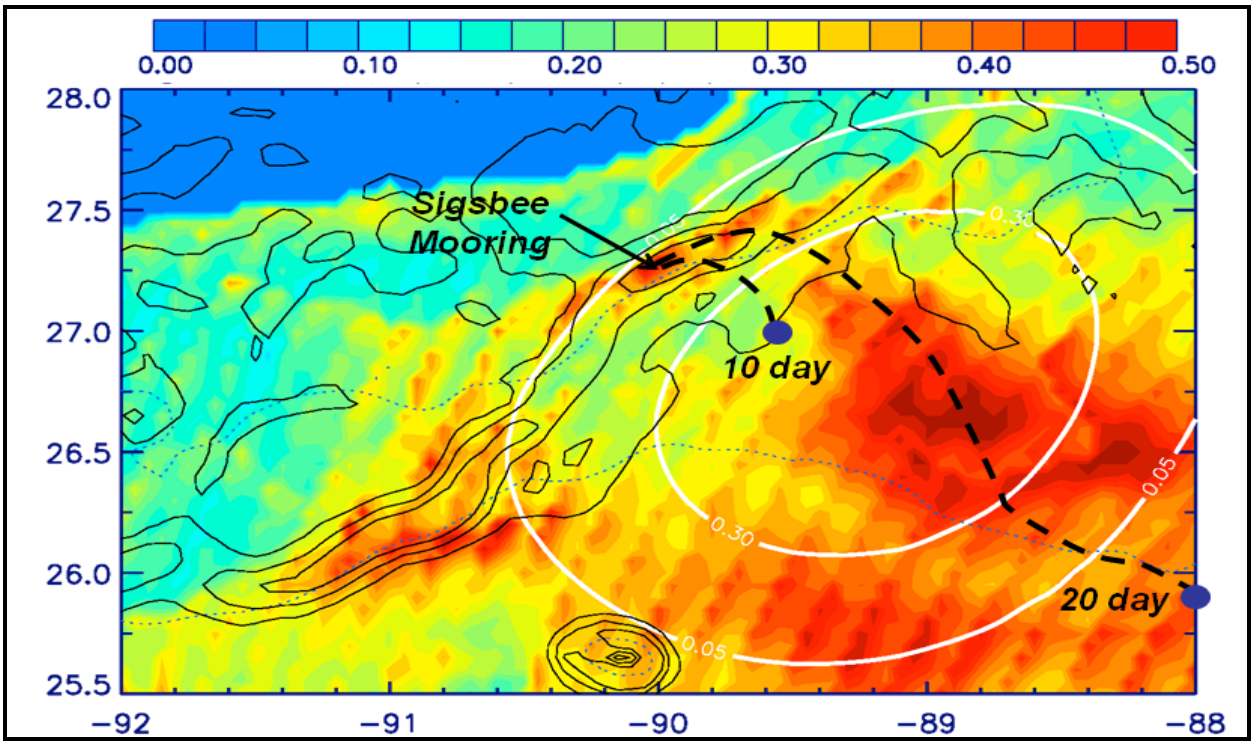

Figure 1.9. Power spectral energy (color, plotted as $10\times((u^2+v^2)$ m/s; thus red (0.05 m/s) of currents depth-averaged below z = (1000 m for the 2 20-day periods) calculated from the 2-year free-running model experiment initialized at July 24, 1999 from a satellite SSH data-assimilated hindcast. Black contours are NT = 0.1, 0.2 and 0.3 in cycles per day. White lines are SSH = 0.05 and 0.3 m contours indicating the outlines of (the simulated) Eddy Juggernaut on October 2, 1999. Thick dashed lines are 10 and 20-day TRW rays traced backward from the Sigsbee mooring (as indicated). Thin dotted contours are the 3000 m (southern contour) and 2000 m isobaths.

and 2. These results suggest that (a) the Sigsbee mooring location tends to harbor short-period, intense current fluctuations, and (b) these fluctuations are forced locally either when a warm ring arrives, or when the Loop Current extends far northward over the mooring.

The observed IMF's display a more complicated behavior, but some useful inferences may be made. Eddy Juggernaut excites intense short-period (5~10 days; IMF's#1 and 2) motions before day 60 in Figure 1.10a. These are similar to those seen for the modeled IMF's (Figure 1.10b), though the observed IMF's are stronger, and persist for a longer time. Beyond day 60 (after Eddy Juggernaut), the next major warm ring was not shed until 18 months later. However, data-assimilated model hindcast[4] indicates active eddy activities (cyclones and anticyclones) on the northwestern portion of the Loop Current; these eddies could excite northwestward propagating, low-frequency (periods > 20 days) TRW's (Oey, 2008). Such eddy activities are

[4] For 5-daily animation of the satellite SSH data-assimilated analyses, visit ftp://aden.princeton.edu/pub/lyo/mms/walt/xtnhcast_work/anim_DAILY_GOM27_xhcast_0_gulf_sshuvk0on2000_5d.gif

weaker in the free-running experiment. This inference that after Eddy Juggernaut the TRW's observed at the Sigsbee mooring are of lower-frequencies and remotely-forced is consistent with the observed period-lengthening in the IMF-oscillations after day 60, e.g., days 120, 230 and 300 in Figure 1.10a (IMF's#1 and 2 in particular; c.f. Hamilton, 2007).

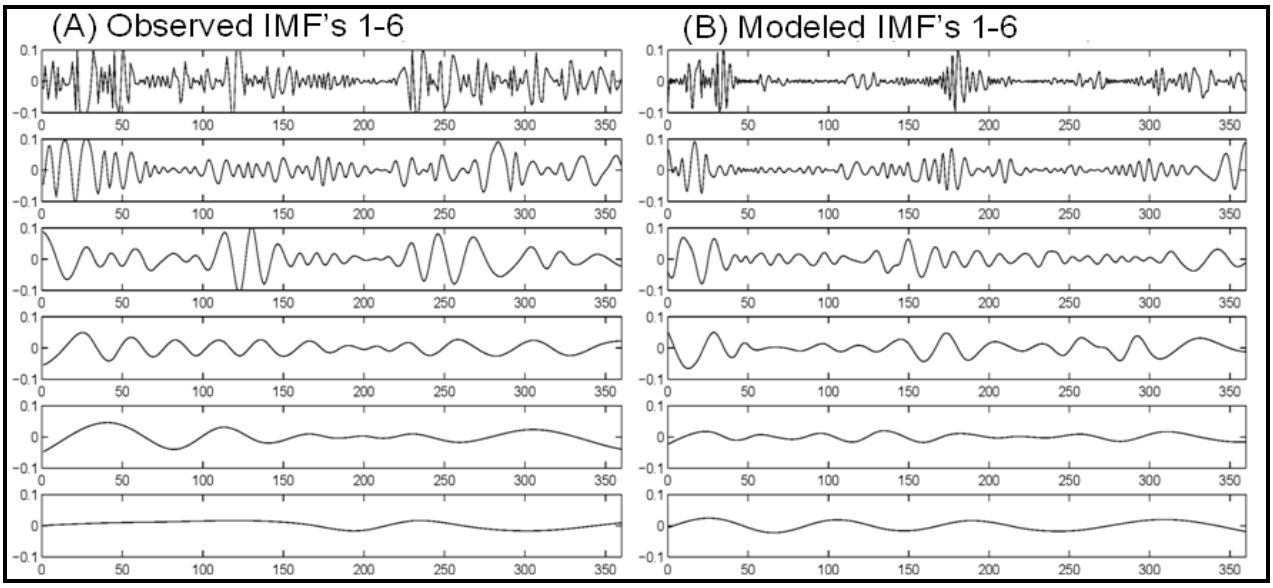

Figure 1.10. Observed (A) and modeled (B) first six Intrinsic Mode Functions (IMF's,1-6 shown from top to bottom) of the south-to-north (v) component velocity at the Sigsbee mooring. Units are m/s (ordinate) and days since September 2, 1999 (abscissa). The velocity is 200 m above the bottom (water depth (2000 m).

1.5. DISCUSSION

The Sigsbee measurements were made within the TRW-valleys where contours of N_T = 0.1~0.2 cpd also bend southward (Figure 1.1). The Gulf of Mexico simulation above suggests that high energies occur at localized topocautics. This idea of a trapped-wave solution is also consistent with observed and simulated rapid energy decays north of the escarpment, and with the fact that short-period fluctuations are neither observed nor simulated farther west (c.f. Hamilton, 2007).

Near a topocaustic, in addition to energy accumulation, short scales also tend to develop (e.g. near y = 160 km and 100 km < x < 190 km, mentioned previously in conjunction with Figure 1.4). In the model, motions with very short scales (~ grid sizes) are damped by the model's viscous terms. In reality wave-breaking may develop and topocaustics may therefore contribute to deep mixing in the oceans. Real topography is complicated, and regions where topocaustics can potentially develop are quite common; we have demonstrated this in the Gulf of Mexico. Figure 1.11 shows potential topocaustics in the Atlantic Ocean. In addition to the steep-slope regions of the western boundary where strong currents and eddies can provide the necessary sources of TRW's, the topography under the Antarctic Circumpolar Current may also be a rich region of topocaustics.

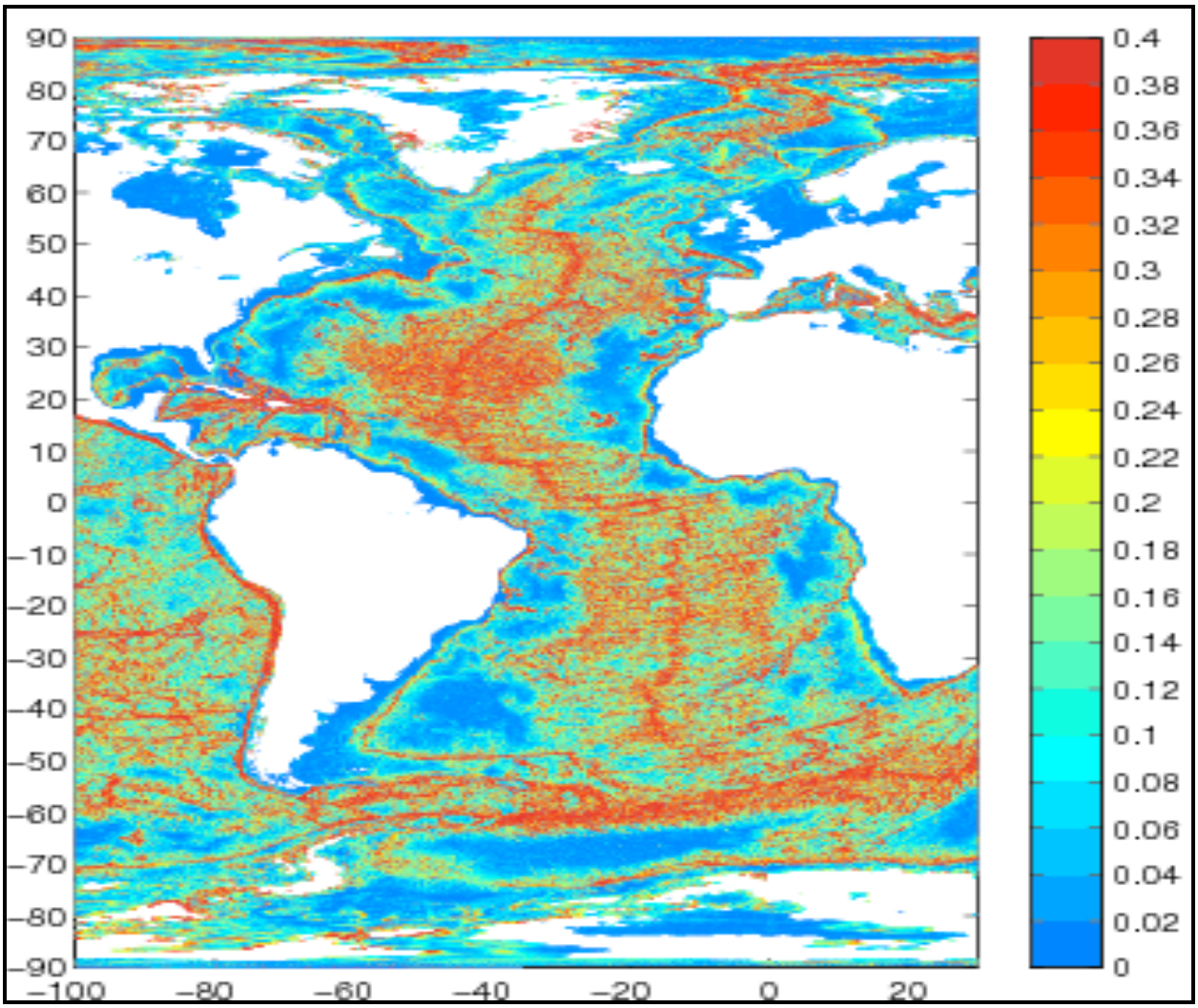

Figure 1.11. Colors are NT values (where the local water depth > 1000 m) showing potential areas of topocaustics in the Atlantic Ocean—in particular, the light-green, yellow and red regions where NT > 0.2 cycles per day. Regions near the equator are not valid. This map was constructed using the 1-minute resolution ETOPO1 data (http://www.ngdc.noaa.gov/mgg/global/global.html).

1.6. SUMMARY

Provided that TRW trapping depth scale h_{trap} is not larger than the total water depth h, TRW and IW rays are mathematically equivalent (Oey, 2008). This curious coincidence allows well-developed techniques for IW-ray tracing (e.g., Lighthill, 1978) to be applied and extended, with appropriate modifications, to study TRW's. In IW's the maximum possible local frequency is N, while in TRW's it is $N_T = N|\nabla h|$. The idea of topographic caustics (topocaustics) is introduced here. Strong current oscillations result, and they decay rapidly across a topocaustic. One unique feature of topocaustics (different from IW's) arises because of the one-sided propagation property of TRW's—it is then possible for energy to accumulate near the western end (in northern hemisphere looking generally towards shallow waters) of closed contours of N_T. Localized focusing of deep energy at a topocaustic is consistent with observed and simulated intensified currents (and rapid decay) near the Sigsbee escarpment in the Gulf of Mexico, where

strong slope gradients coupled with a bend in isobaths are conducive to the development of a topocaustic. The Gulf of Mexico model also shows that, near the northeastern portion of the Sigsbee escarpment, bursts of short-period (5~10 days) intense motions are locally forced by either the Loop Current's northward expansion, or by a warm-core ring.

1.7. OTHER IDEALIZED EXPERIMENTS

Other model experiments were conducted to support the conclusions of the main experiment described in the text. They include:

1. Changing the topography. Here we tested the case when the canyon is removed (the isobaths are strictly along the channel). There are no closed N_T-contours, and no localized regions of strong current fluctuations in topocaustics. We next tested a series of topography in which the canyon is shifted north and south of its position in the base experiment shown in Figure 1.3. The locations of strong current fluctuations are changed, but their characteristics are as predicted by the main experiment.
2. Changing the source positions and strengths. Here, provided that the forcing is still 'remote' (i.e., away from the closed N_T contours), the topocaustic locations of the main experiment are independent of the forcing. For forcing that partially covers a closed N_T-contour (corresponding to say an eddy that comes close to the Sigsbee escarpment; see Section 4), the response at the corresponding western topocaustic is much stronger, about 1.5 times stronger than the forcing.
3. Refining the horizontal resolution to 1.25 km × 1.25 km, as well as coarsening it to 5 km × 5 km. The former resolution gives very similar results as Figure 1.5, while the latter gives weaker energies, though the trapping regions can still be clearly identified.
4. Extending the (idealized) calculation to a longer period of 1080 days. Here we repeated the spectral analyses to confirm Figure 1.5a,b.

2. LOOP CURRENT CYCLE: COUPLED RESPONSE OF THE LOOP CURRENT WITH DEEP FLOWS[5]

Synopsis

By analyzing mass balances in the deep eastern Gulf of Mexico from a process experiment consisting of steady transport forcing only from the Caribbean Sea and North Atlantic Ocean, we are able to describe the Loop Current Cycle: Loop Current expansion → Yucatan's deep flows → ring separation → Loop Current retraction → eddy migration → deep flows in the Gulf → Loop Current expansion, and to provide insights into the eddy-separation process, surface-deep coupled dynamics and deep mean circulation, culminating in the prediction of a 3-layer zonal transport structure across the Gulf as shown in Figure 2.5.

Summary of the Main Results

While the upper-layer dynamics of Loop Current and eddies in the Gulf of Mexico are well-studied, our understanding of how they are coupled to the deep flows is limited. In this work, results from a numerical model are analyzed to classify the expansion, shedding, retraction and deep-coupling cycle (the Loop Current Cycle) according to the vertical mass flux across the base of the Loop. Stage A is "Loop-reforming" period with downward flux and deep divergence under the Loop Current. Stage B is "incipient-shedding" with strong upward flux and deep convergence. Stage C is "eddy-migration" with waning upward flux and deep throughflow from the western Gulf into the Yucatan Channel. Because of the strong deep coupling between the eastern and western Gulf, the Loop's expansion is poorly correlated with deep flows through the Yucatan Channel. Stage A is longest and the mean vertical flux under the Loop Current is downward. Therefore, since the net circulation around the abyssal basin is zero, the abyssal gyre in the western Gulf is cyclonic. The gyre's strength is strongest when the Loop Current is reforming, and weakest after an eddy is shed. The result suggests that the Loop Current Cycle can force a low-frequency (time scales ~ shedding periods; O(months)) abyssal oscillation in the Gulf of Mexico. The deep mean cyclonic gyre in the western Gulf necessitates an east-to-west deep transport of water which, since the mean upper-layer transport is also westward due to migrating rings, there must exist a 3-layer (zonal) circulation structure in the Gulf.

2.1. INTRODUCTION

The Loop Current is the extension of the Yucatan Current, and is the most prominent circulation feature in the Gulf of Mexico. Mainly confined in the upper 1000 m, the Loop Current has very strong speeds that can exceed 2 m s^{-1} (see Oey et al., 2005b for a review and references). Large warm-core rings (Loop Current eddies, 200~350 km wide and 500~1000 m deep) episodically separate from the Loop Current at time intervals that range from 3~18 months (Sturges and Leben, 2000; Leben, 2005). Upper-layer ($z >\approx -1000$ m) mass influx from the Yucatan Channel feeds the Loop Current, which accumulates mass and grows larger and deeper (Pichevin and Nof, 1997). Since the Gulf of Mexico is closed in the west, the expanding (and deepening) Loop forces some water out of the Straits of Florida and also through the upper

[5] This chapter is based on Chang and Oey (2011): Loop Current Cycle: coupled response of the Loop Current with deep flows. J. Phys. Oceanogr., in press.

Yucatan Channel (e.g. on the Cuban side). Since the Straits of Florida has a shallow sill depth (800~1000m), and a rather narrow width compared to the Loop, some of the displaced water also leaks into the Caribbean Sea through the deep sill of the Yucatan Channel (~2040m). As the Loop Current grows, the westward Rossby wave speed (which is $\propto -\beta R^2$, where R is the Rossby radius based on the matured deep Loop) overcomes the growth rate and the Loop sheds an eddy (Nof, 2005). As the eddy migrates westward, it also displaces water from the western Gulf, and this also generates deep flows. This cycle: expansion → Yucatan's deep flows → separation → retraction → eddy migration → deep flows in the Gulf → expansion—will be referred to as the Loop Current Cycle.

Some (surface) aspects of the Loop Current Cycle can be seen in animations of sea surface height (SSH) from satellite product (e.g. Archiving, Validation and Interpretation of Satellite Oceanographic data—AVISO, http://www.aviso.oceanobs.com) and/or numerical models. Deep outflows (in Yucatan Channel) were observed by Burkov et al. (1982) and Maul et al. (1985), and in a numerical model (the Princeton Ocean Model or POM) by Oey (1996). Oey summarized his and Maul et al.'s findings: "…correlation between shedding events and reversed bottom flow can be identified… The bottom reversed flows last from a few weeks to as long as 6 months … and in general precede sheddings ... The evidence for the two processes to be related is overwhelming. In analyzing the near-bottom current meter time series in the Yucatan Channel, Maul et al. … noted prolonged (weeks to months) southward flow, which appeared to correlate with eddy shedding inferred from satellite imagery…" Oey (1996) was more interested in relating the Yucatan deep outflow and Loop Curent eddy shedding, but noted also that the model deep outflow is correlated with upper-layer (defined as $z > -750$ m) inflow, at time scales of 1~3 months (see his Figure 6). Since the upper-layer inflow contributes to the growth of the Loop (Pichevin and Nof, 1997; Nof, 2005), the Yucatan deep outflow may also correlate with the Loop Current's expansion area. The idea was first put forth by Maul (1977), as summarized in Maul et al. (1985): "… this deep southward flow (in the Yucatan Channel) is part of the continuity adjustment process associated with eddy formation in the Gulf Loop Current: excess upper layer inflow required to form the eddies is partially compensated by time-dependent outflow in the deep layer."

Maul et al.'s (1985) idea is later examined by Bunge et al. (2002) using mooring data from September 1999-June 2000 collected during the CANEK observational program in the Yucatan Channel (Candela et al. 2002; Sheinbaum et al. 2002). The analysis was for 6 months from November 1999~April 2000 and excluded eddy shedding. The authors found some correlation between Loop Current expansion rate and Yucatan deep outflow. Subsequent analyses by Ezer et al. (2003; also a POM simulation, described in Oey et al., 2003) suggested also that deep outflow in the Yucatan Channel may be related to the Loop's expansion rate.

The Loop Current Cycle is not exact: no two realizations of Loop Current are the same and eddy sizes differ. Also, the intervals between eddy-separations, as well as the inflow and outflow transports, vary with time. It is, however, a useful concept. While the previous research suggest that the Loop's expansion may be correlated with deep outflow, we do not yet have a clear description of this and other processes involved. We do not, in particular, have a clear understanding of the upper-lower layer coupling during a Loop Current Cycle. This is due to the lack of an observational dataset that can adequately provide the three-dimensional and time-dependent evolution of the Loop Current Cycle. There are now many good numerical models of the Gulf of Mexico (see review in Oey et al., 2005b). Models now have high resolution that reduces their truncation errors, and make up for their lack of true physics with self consistency

(e.g., mass is conserved), fine spatial coverage and multi-year outputs. Here we used the POM to examine the Loop Current Cycle. An 8-year process simulation is conducted such that the model sheds eddies at a nearly constant rate of 1 eddy per 8.1 months (12 eddies total). The nearly constant rate of eddy shedding produces nearly repeatable Loop Current Cycles. The model therefore yields more easily identifiable patterns that provide insight into the coupling between the Loop Current and deep flows. The following questions will be addressed: What is the distribution of mass that enters and exits the deep Gulf during a Loop Current Cycle? What is the time-dependent coupling between the Loop Current and various inflows and outflows? How does the western deep Gulf respond to the Loop Current Cycle, and why is the circulation there cyclonic?

Our focus will almost exclusively be on deep flows and their relation to the Loop Current and eddy-shedding, as these are topics that are least understood. The approach is to compute (deep) mass transport budgets and then relate them to the Loop Current Cycle. This work therefore complements Oey (2008) who examined deep eddies and how they may generate topographic Rossby waves. It will be seen also that some of Oey's (2008) analyses support our results.

Mass-budget analyses do not directly tell us about cause-and-effect. However, mass conservation imposes powerful constraints on the dynamics of a semi-enclosed sea. In the case of the Gulf of Mexico, westward mass transport by eddies necessitates a return (i.e., eastward) transport which will be used in this work to provide an improved understanding of the dynamics of the Loop Current Cycle. A similar approach was previously used as one of the analysis tools to explain eddy-shedding behaviors of the Loop Current and heat exchanges between the Gulf and the Caribbean Sea (Chang and Oey, 2010a,b). As indicated above, Pichevin and Nof's (1997) and Nof's (2005) works suggest that the separation of an eddy from the Loop Current is primarily an upper-layer process in which the tendency for the 'bulged' Loop to bend westward due to Rossby wave dynamics overcomes the growth rate of the Loop by inflow through the Yucatan Channel. Chang and Oey's (2010a) work supports Pichevin and Nof's (1997) and Nof's (2005). By analyzing the results of a three-dimensional model with Gulf's topography and stratification, the authors demonstrate that eddy-shedding depends on Gulf-wide mass balance and zonal momentum flux in the upper layer. In this work, we will present results that also support Pichevin and Nof's (1997) and Nof's (2005) and Chang and Oey's (2010a) idea of a dominantly upper-layer forcing by the Loop Current and eddies. This idea is central to understanding the results contained herein. The following "thought experiment" is useful. Fluid in the Gulf is initially at rest. Yucatan inflow which is primarily in the upper layer (as observed, Sheinbaum et al. 2002; see also Figure 2 in Oey et al. 2005b) then initiates a growing Loop Current in the eastern Gulf[6]. The abyssal ocean then responds; an example is Maul et al.'s (1985) idea of a deep outflow through the Yucatan Channel. As the Loop bends westward, and as the eddy separates from the Loop and migrates westward, water that is displaced in the western Gulf produces return (i.e. eastward) transports both near the surface and in deep layers (Chang and Oey, 2010a). Chang and Oey (2010a) show that an eddy typically transports about 13 Sv of water westward (see their Table 2). Most of this water is returned eastward in the upper layer, but the deep return flow (under the eddy, deeper than $z \approx -800$ m) is not insignificant, roughly 1~2 Sv, and the accompanying vertical mass flux in the western Gulf is downward. As the eddy decays, and in the absence of other external forcing (i.e. surface fluxes, rivers, time-dependent large-scale transports say from the Atlantic, etc are nil), isopycnals flatten, resulting in

[6] As in Chang and Oey (2010a), it is convenient to separate the Gulf into western and eastern regions by the 90°W longitudinal line extending southward approximately off the Mississippi Delta.

upwelling in the western Gulf that is accompanied by westward deep flow from the eastern to western basins. In this idealized experiment, the causes of all these effects are clearly from the upper-layer: Yucatan inflow, Loop Current and eddies. The goal is then to describe and understand this simple case. The results presented herein will suggest that for deep motions to significantly affect the upper-layer dynamics, the forcing would be external, and the likely source is the deep flow through the Yucatan Channel.

The outline of the chapter is as follows. Section 2 describes the numerical model. Section 3 describes the Loop Current Cycle using mass balances to analyze the coupling between Loop Current, eddy-shedding and time-dependent deep flows. In section 4, we show how the Loop Current Cycle is coupled to the central and western Gulf's deep circulation. Section 5 uses a vorticity constraint for the deep Gulf to show that a cyclonic gyre must exist in the western Gulf. Section 6 is conclusion and discussion.

2.2. THE NUMERICAL MODEL

The Princeton Ocean Model (POM; Mellor, 2004) is time-dependent and three-dimensional based on the primitive equations assuming hydrostacy and Boussinesq approximation. Model domain covers the western Caribbean Sea and the Gulf of Mexico west of 78°W. It is nested within a larger-scale, coarser-grid northwestern Atlantic Ocean Model described in Oey et al. (2003). The nested model's horizontal resolution is double, approximately *5 km* in the Gulf of Mexico including the Yucatan Channel and Straits of Florida, and there are 25 vertical sigma levels. (Please visit http://www.aos.princeton.edu/WWWPUBLIC/PROFS/publications.html for publications that describe other details of the model). All surface fluxes are nil, and transport through the Yucatan Channel is very nearly constant at 23.7 Sv. The model was integrated for *12 years* initialized from the coarse grid. A quasi-equilibrium state, in which the model Loop Current sheds eddies at a nearly constant rate of 1 eddy per 8.1 months, was reached in 4~5 years. The analyses below are based on the last *8 years* of the model data.

2.3. THE LOOP CURRENT CYCLE

In the model, eddies are shed at approximately (88°W, 25.5°N). After an eddy is shed, it migrates southwestward, at about $0.07\ m\ s^{-1}$, and eventually decays in the southwestern Gulf. Meantime, the Loop Current reforms (i.e. expands) and the cycle repeats (see Oey et al., 2003 especially their Figure 5; and Oey, 2004). This regularity is idealized, but is an advantage for the present attempt to better understand processes. A description of how the deep flows (at Yucatan and between the western and eastern Gulf) are coupled to the Loop Current is non-existence even for this idealized case.

The interaction between upper and lower layers (shallower and deeper than 1000 m respectively) is examined by calculating mass balance *beneath* z = −1000 m. The reason for this will become clear shortly. Figure 2.1 shows the map of the eastern Gulf of Mexico. A control volume is defined in the deep portion of the eastern Gulf with the upper boundary at z = −1000 m. The northern, eastern and southwestern boundaries are closed because of the continental shelf break, the shallow sill of the Straits of Florida, and the bank of Campeche. There are therefore three openings bounding the control volume: at 90°W (western thick line), the deep sill of the Yucatan Channel (southern thick line) and the upper boundary at z = −1000 m. The strong constraint imposed by mass conservation in this control volume will enable us to

unambiguously describe the Loop Current Cycle. We present first time-series plots, and then explain the physics involved.

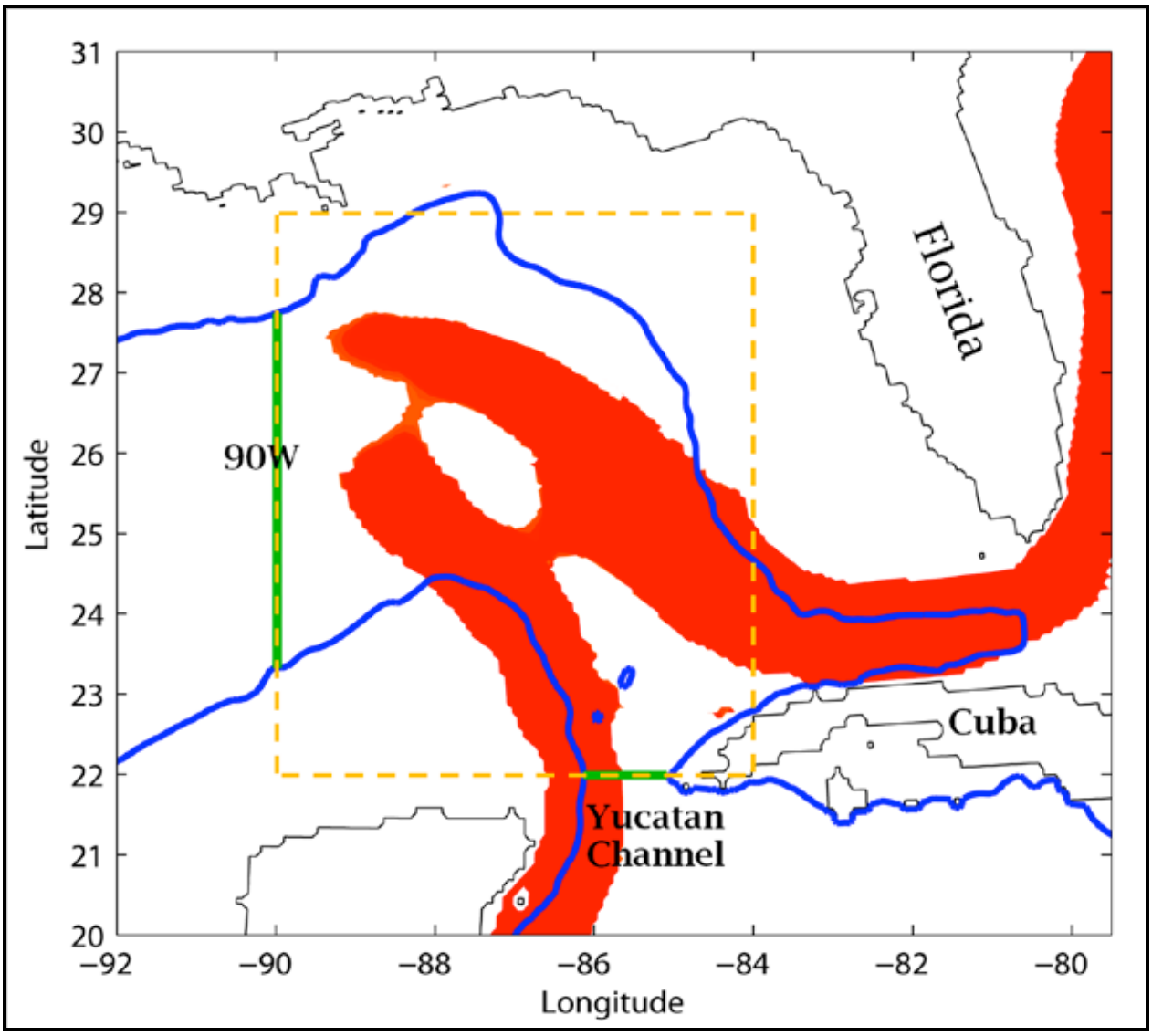

Figure 2.1. Map of the eastern Gulf of Mexico. Red shading show 8-year mean speeds > 0.15 m s-1, depth-averaged in upper 200 m, and indicates the position of the model Loop Current. Blue contour is the 1000 m isobath. Sections at 90°W and Yucatan Channel are indicated by green lines which together with the 1000 m isobath and from z = (1000 m to bottom define the deep control volume used for mass balance analysis. Dashed yellow lines define the box where the Loop's expansion/retraction area is calculated based on SSH (or speeds) in the Section 2.7, and the line (not drawn) joining the southeast to northwest corners of the box is where the Loop's expansion/retraction is rechecked using SSH (also in the Section 2.7).

Time series of transports across the three openings are plotted in Figure 2.2. Thin vertical lines represent times when eddies detach from the Loop Current. Transports at 90°W (hereinafter denoted as "Tr_{90W}"), Yucatan Channel ("Tr_{Yuc}") and across z = −1000 m ("Tr_{Z1k}") are time dependent, and they change signs (directions) at different stages of the Loop Current Cycle.

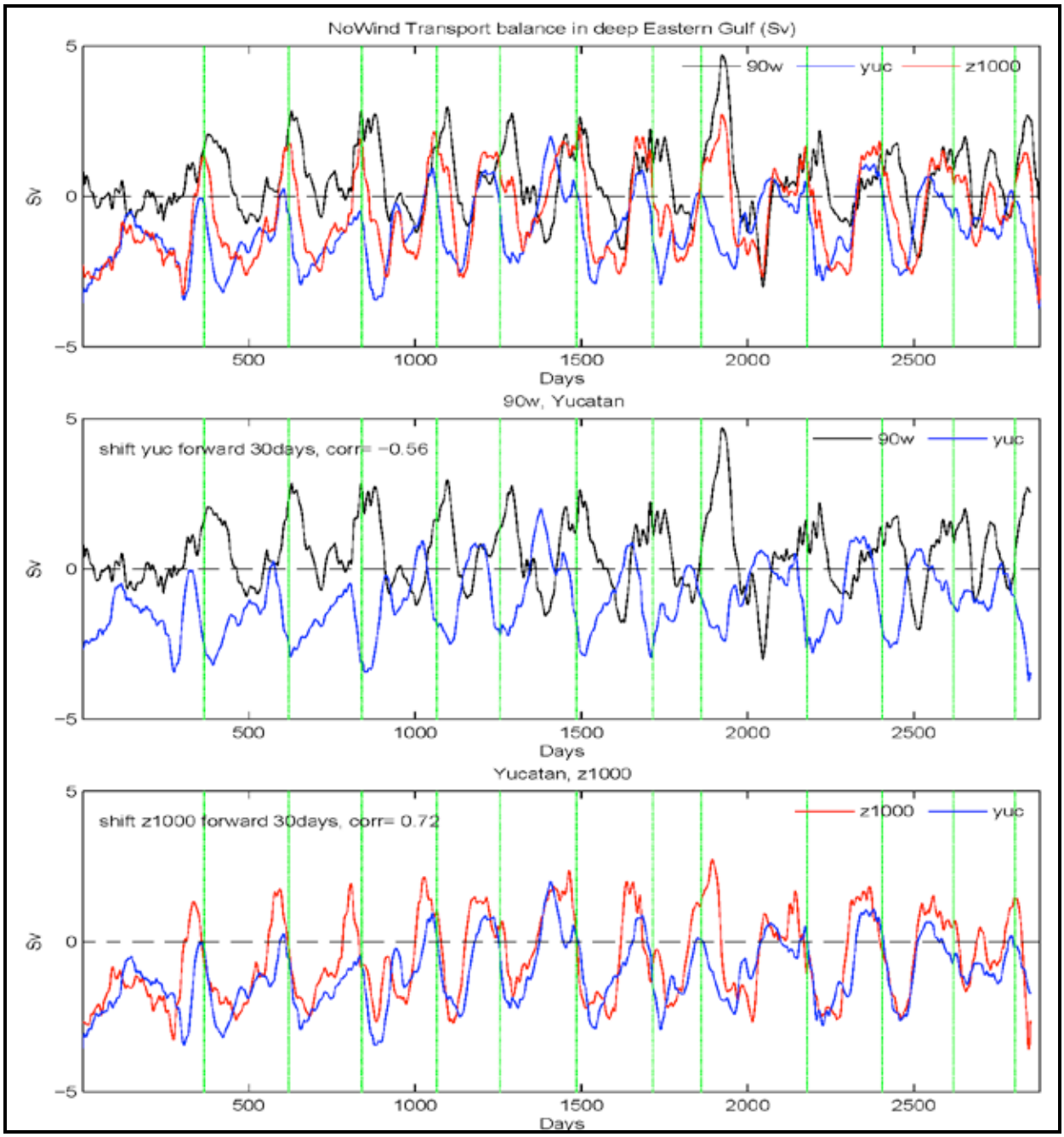

Figure 2.2. Time series of transports across the boundaries of the deep eastern Gulf control volume (see Figure 1) across 90˚W (black), Yucatan Channel (blue), and z = (1000 m (red)); (a) all three time series; (b) 90˚W and Yucatan Channel shifted forward by 30 days; (c) Yucatan Channel and z = (1000 m shifted forward by 30 days). Time is in days of the 8-year analysis period.

In the plots, the sign of transport is kept the same as the velocity: positive Tr_{90W} and Tr_{Yuc} are eastward and northward respectively, influx to the control volume, but positive Tr_{Z1k} is upward out of the control volume. The sign-retention in Tr_{Z1k} is to keep its conventional physical meaning that downward is negative, e.g., the Tr_{Z1k} tends to be < 0 representing downwelling when the Loop Current impresses upon the control volume from above as for example when the Loop expands into the Gulf of Mexico, etc. This relation between Tr_{Z1k} and the Loop Current's

expansion (and retraction, same below) is approximate (see Section 2.7), but for the time being it is quite helpful to keep a mental image of the connection. The curves and their relationships appear complicated, but on closer examination they reveal the following general pattern. Small time shifts of 1~2 months exist between Tr_{90W} and Tr_{Yuc} and also between Tr_{Yuc} and Tr_{Z1k} (Figure 2a). Transports at 90°W and Yucatan Channel (Tr_{90W} and Tr_{Yuc}, Figure 2b) are anti-correlated: maximum Tr_{90W} (i.e., maximum eastward transport at 90°W) leads minimum Tr_{Yuc} (i.e. maximum southward transport at the Yucatan Channel) by *30 days* (Figure 2b; the correlation coefficient "CC" is −0.56 at *30 day* lag).[7] On the other hand, Tr_{Yuc} and Tr_{Z1k} are positively correlated; the CC is +0.61, and = +0.72 at *30 day* lag, Tr_{Z1k} lags Tr_{Yuc} (Figure 2c). These correlations (and their respective lags) suggest closely related dynamics between Loop Current expansion, eddy shedding, eddy-passage across 90°W, which forces Tr_{90w}, vertical mass exchanges across the base of the Loop (Tr_{Z1k}), and the Yucatan deep flows (Tr_{Yuc}). To understand the relation, we choose one event from Figure 2a to examine the interaction between Tr_{Yuc}, Tr_{90W}, and Tr_{Z1k} (Figure 2.3, top panel). To confirm that our interpretations are robust (i.e., event-independent) we also calculated the corresponding ensemble time series (Figure 3, bottom panel). Since each event is distinct (each with a different time period), each ensemble is for simplicity taken as the average from 115 days before to 125 days after each eddy shedding. The two plots in Figure 3 are similar, and the following descriptions apply to both of them. Three stages are defined based on the variation of Tr_{Z1k} as will be explained shortly. Figure 2.4a-c shows the states of the Loop Current at these stages as plots of the corresponding ensemble averages of sea surface height and surface currents. Figure 2.5 gives schematic sketches that the reader may find useful in following the descriptions below.

2.3.1. Stage A

This corresponds to a state when the Loop Current is reforming and expanding after an eddy has shed and propagated away from the eastern Gulf of Mexico (Figure 2.4a). The Loop Current at this stage is near the Yucatan Channel. Continuity requires that the Loop Current's expansion is accompanied by downwelling beneath it so that $Tr_{Z1k} < 0$, though some mass may also leak into the Straits of Florida (c.f. Maul et al. 1985; Nof, 2005; Chang and Oey, 2010a). This period of downwelling ($Tr_{Z1k} < 0$) is taken to define Stage A. Figure 2.3 shows that it coincides in general with stronger deep outflow in the Yucatan Channel ($Tr_{Yuc} < 0$). However, the responses in Stage A are different prior to (Stage A1) and after (Stage A2) the shedding of an eddy. Although the Loop Current is reforming in both these sub-stages, it is clear that in Stage A1, the deep, predominantly divergent flow in the eastern Gulf of Mexico, is associated with the downwelling mass flux; i.e. Stage A1 is consistent with Maul et al.'s (1985) hypothesis. This is drawn in Figure 2.5a. The Stage A2 is different, however. Both deep eastward flow across 90°W ($Tr_{90W} > 0$)

[7] All quoted correlation coefficients in the chapter are significant at the 95% significance level.

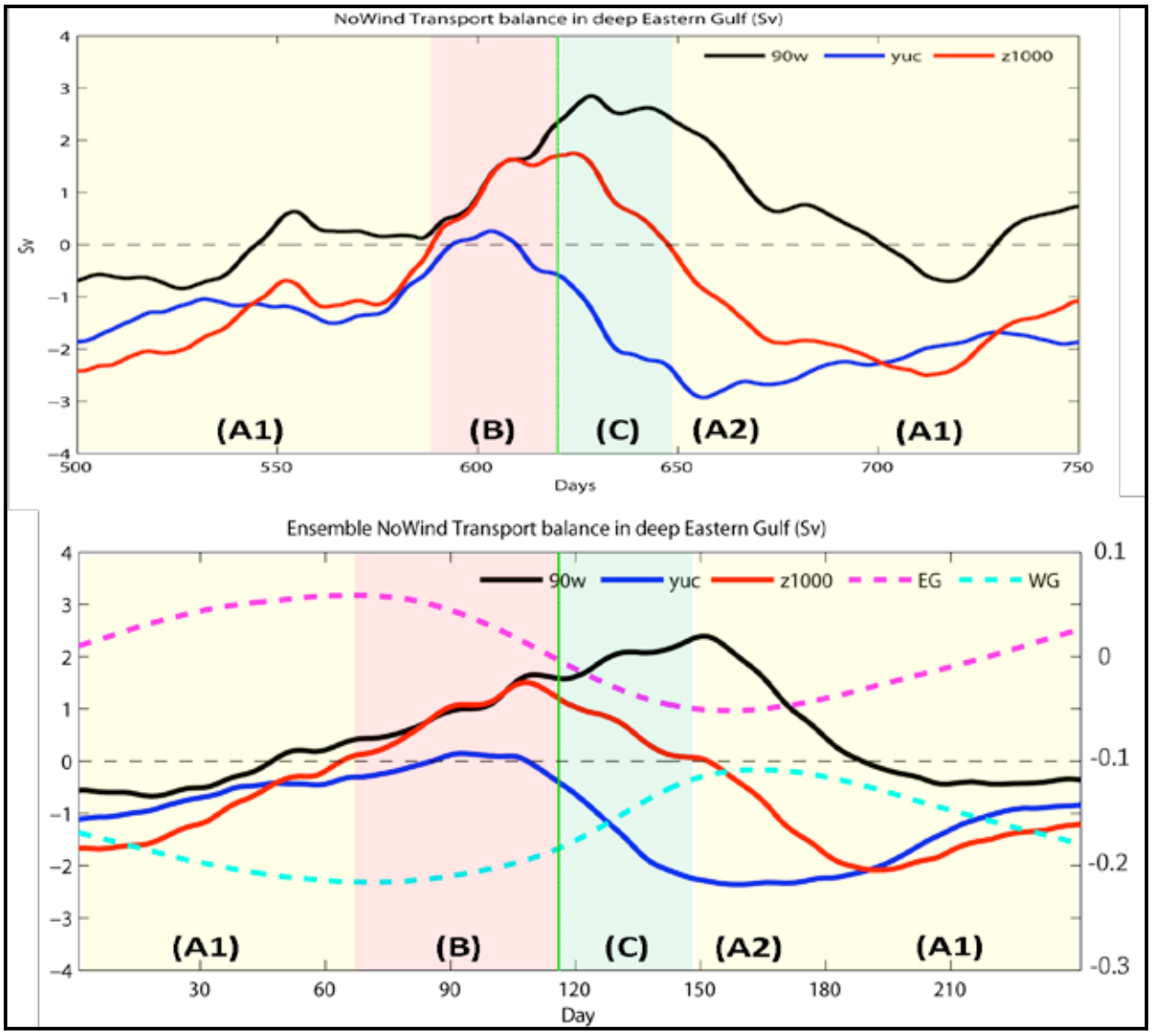

Figure 2.3. Top panel: same as Figure 2.2a, but only for one event showing how the various stages (color shadings) are defined in the text. Bottom panel: the same transport time-series but ensemble averaged before and after the time of each eddy-shedding event (see text for details). Dashed curves are ensemble eastern (EG) and western (WG) Gulf's area-averaged SSH's in meters (right ordinate).

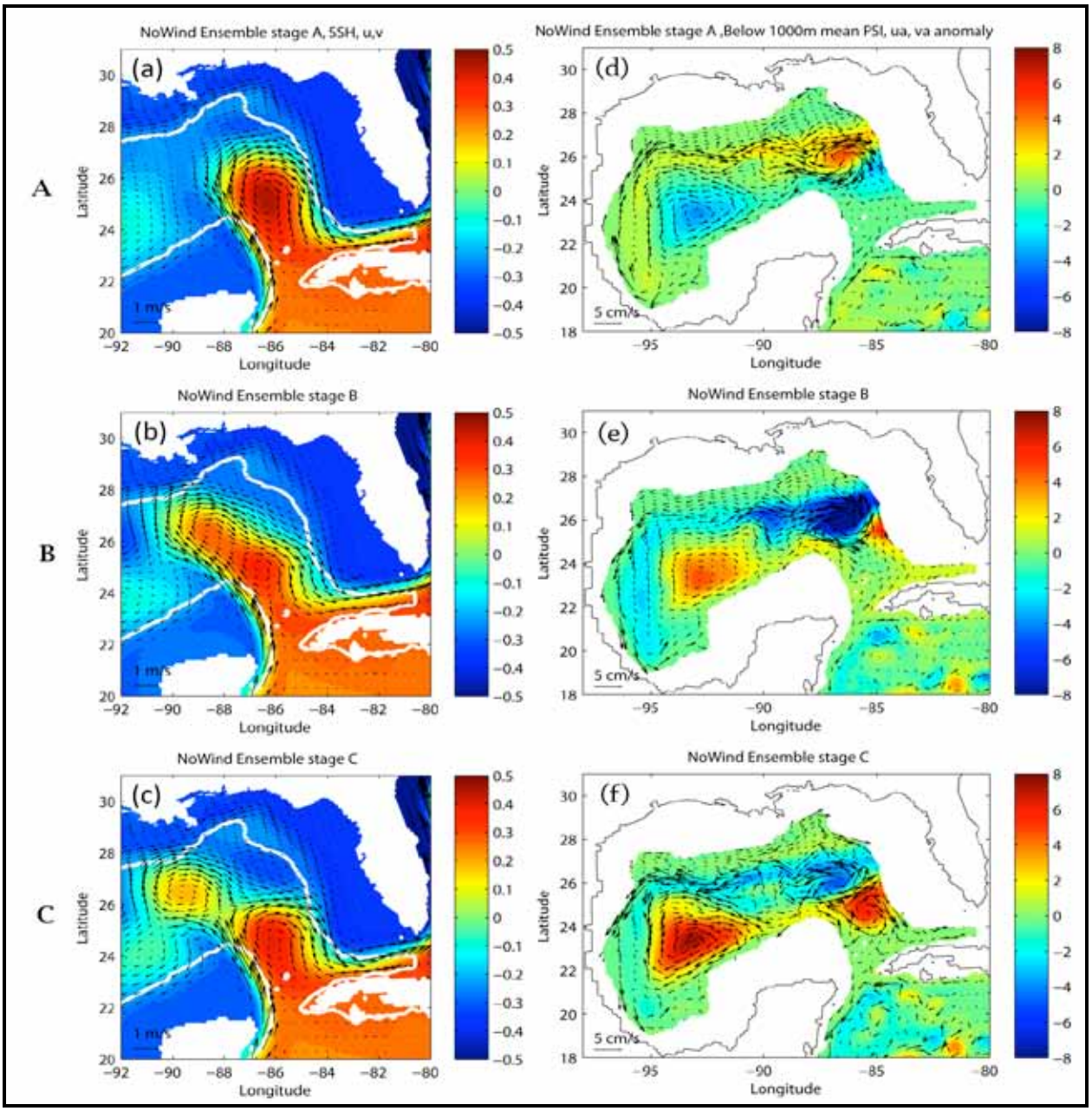

Figure 2.4. Sea-surface height and surface currents (at the 1st sigma level), ensemble-averaged during Stages A, B and C (as indicated) of the Loop Current Cycle. Panels d, e and f are deep currents anomalies depth-averaged from bottom to z = (1000 m (vectors)), and their corresponding (approximate) stream function (color), also ensemble-averaged during Stages A, B and C.

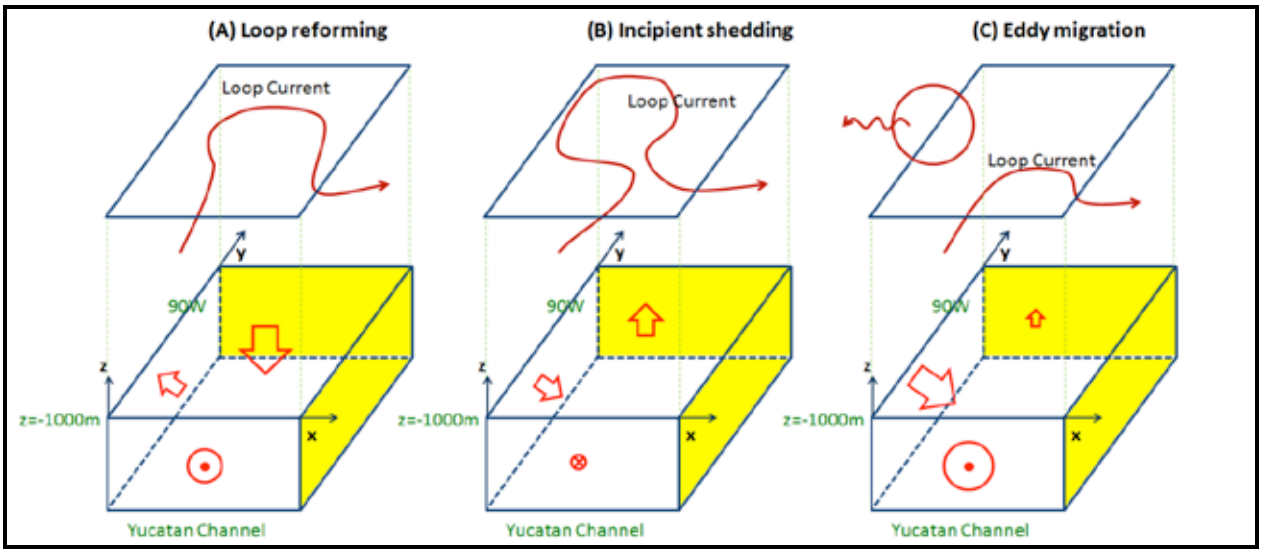

Figure 2.5. A schematic illustration of the 3 stages of the Loop Current Cycle (i.e., a cycle of Loop Current expansion, eddy shedding, retraction and deep-coupling, see text). Lower box shows the mass balance in the deep control volume (see Figure 2.1) bounded by 90°W (west), Yucatan Channel (south) and the depth of z = (1000m (upper)). Arrows and symbol circles indicate the directions and (approximate) magnitudes of the transports. Yellow shading indicates a closed boundary. Projected upper layer shows the condition of the Loop Current during stage (A) Loop reforming, (B) incipient eddy-shedding, and (C) westward eddy migration across 90°W.

and downward mass flux beneath the Loop Current ($Tr_{Z1k} < 0$) contribute to the strong outflow in the Yucatan Channel ($Tr_{Yuc} < 0$). In fact, Tr_{Yuc} reaches a minimum in this Stage A2 (i.e., maximum outflow; Figure 2.3), balancing the summed contributions from Tr_{90W} (> 0) and Tr_{Z1k} (< 0). However, the contribution from Tr_{90W} is dominant. From Figure 2.3, it is clear that the large Tr_{90W} in Stage A2 is caused by the continued forcing of the westward-propagating eddy (from Stage C, see below) that forces an eastward returned deep flow (since the western Gulf is closed and mass is conserved; Chang and Oey, 2010a). As Stage A2 transits to Stage A1, Tr_{90W} weakens and Tr_{Z1k} reaches its minimum (strong downwelling). The strong downwelling feeds the deep outflow at Yucatan, Tr_{Yuc}, and the latter continues to weaken because of the weakened contribution from Tr_{90W}. Alltogether Tr_{Yuc} appears to lead Tr_{Z1k} in Figure 2.2c, i.e., the minimum of Tr_{Yuc} precedes the minimum of Tr_{Z1k}. The strong downwelling also squashes vortex lines, and induces negative vorticity in the deep layers, consistent with Oey's (2008) EOF analysis of the relative vorticity stretching term when the Loop is reforming (see his Figure 4).

The existence of Stage A2 (and Stage C, below) suggests that within approximately two months after an eddy is shed, the deep outflow at Yucatan can be quite unrelated to the Loop Current's expansion (which is related to $Tr_{Z1k} < 0$; see Section 2.7). This may explain why in Bunge et al's (2002) Figure 2.3, the rate of Loop's expansion (and retraction) does not correlate well with the observed deep flow in the Yucatan Channel, especially at the beginning of the time series which was 1~2 months after a huge eddy (Eddy Juggernaut) separated from the Loop Current.

2.3.2. Stage B

This corresponds to the period of incipient eddy-shedding when Tr_{Z1k} changes sign to become positive or upwelling, and continues to increase to its maximum value, around which time an eddy separates from the Loop (Figure 2.3). The upwelling lags the sign change of deep eastward flow across 90°W ($Tr_{90W} > 0$) and is almost entirely fed by it because the deep flow in the Yucatan Channel is very weak. This result shows that eddy shedding is related more to the westward movement of the Loop's water mass (because westward Rossby wave speed exceeds the rate of mass influx from the Yucatan), proposed by Nof (2005), rather than to local instability (see also Hurlburt and Thompson, 1980). The deep eastward flow $Tr_{90W} > 0$ is therefore caused by pressure produced by westward-propagating eddy following Rossby-wave dynamics. From the SSH plots in Figure 2.4 (bottom panel),[8] the steepest fall in eastern SSH occurs when the eddy separates from the Loop Current (from stages B to C, below). This agrees with long Rossby-wave dynamics which, assuming geostrophy and reduced-gravity for the upper layer, is:

$$\partial h/\partial t - \beta R^2 \partial h/\partial x = 0$$

where h is the upper-layer depth. Thus $\partial h/\partial t$ in the eastern Gulf is largest (and negative) for a matured Loop/eddy when the Rossby radius R is largest, and $\partial h/\partial x < 0$ for an eddy exiting westward from the eastern Gulf. Westward detachment of the Loop's water mass forces a deep returned (i.e. eastward) flow across 90°W, $Tr_{90W} > 0$, leaves a "vacuum" in the area once occupied by the Loop, and "sucks" deep water upward, $Tr_{Z1k} > 0$. Upwelling stretches fluid column and results in deep cyclone that is often seen when an eddy separates from the Loop Current (Schmitz, 2005; Oey, 2008). The ensemble Loop Current takes on the shape of an elongated peanut (with shell; Figure 2.4b). The narrowest region (or neck) of the peanut is where the most intense upwelling and cyclone reside. The fact that Tr_{90W} precedes Tr_{Z1k} and that the two transports nearly balance each other prior to eddy-shedding (i.e., when the matured Loop spreads westward) suggests that the cyclone is a by-product of the shedding process, rather than its cause.

The timing of eddy separation can depend on mass and momentum balances between the western and eastern Gulf of Mexico (i.e. fluxes across 90°W; Chang and Oey, 2010a), hence also on the deep transport Tr_{90W}. The above result that the deep flow in the Yucatan Channel is weak during Stage B then suggests that externally-imposed small perturbations in the deep portion of the channel may sufficiently alter the balances across 90°W to delay or hasten eddy-shedding. This is an interesting topic of potential importance, perhaps to be pursued in a future study.[9]

2.3.3. Stage C

This corresponds to the period immediately after an eddy has separated from the Loop Current, and lasts approximately 1 month (Figure 2.3). The ensemble Loop Current (Figure

[8] Because of area averaging, Figure 2.3 includes the background effect of SSH in the east to be always higher than that in the west. The important point here is that the curves show rising and falling SSH's in the east during Loop reforming and eddy-shedding stages respectively, and the opposite trends in the west.

[9] Hurlburt and Thompson (1980) found in their 2-layer model experiment that eddy-shedding ceases if Yucatan deep inflow is increased, and explained their finding in terms of topographic torque. Their results are also consistent with PNN's and Chang and Oey's (2010a) reasoning based on mass and momentum balances. The two are not contradictory, and their relative importance in more realistic simulations and/or observations should be investigated in the future.

2.4c) shows a separated eddy that is crossing 90°W. As the eddy moves westward, the compensating deep eastward flow $Tr_{90W} > 0$ continues to increase, while upwelling ($Tr_{Z1k} > 0$) weakens and Yucatan outflow increases ($Tr_{Yuc} < 0$). The Yucatan outflow continues to increase and becomes a maximum (large negative Tr_{Yuc}) in Stage A2. The observational evidence of such a large outflow a few months after an eddy is shed may be seen in Bunge et al. (2002; their Figure 2.3a near the beginning of the transport time series). Since in this Stage C the forcing for the outflow is due to Tr_{90W}, Maul et al.'s (1985) hypothesis is not valid.

2.3.4. A Summary of Stages A, B and C

Figure 2.5 shows a summary of the three stages discussed above. For simplicity, Stage A1 only is given (Figure 2.5a), while Stage A2 is understood to be a continuation of Stage C (Figure 2.5c) with weak downwelling instead of upwelling. Figure 2.5a (Stage A1) is when the Loop Current is reforming. There is downward transport under the Loop, and flow divergence in the deep portion of the eastern Gulf, with outflow in the Yucatan Channel and westward flow to the deep basin of the western Gulf. Figure 2.5b (Stage B) is when the Loop Current begins to shed an eddy. There is strong upward transport at the base of the Loop Current, induced by the rapid westward movement of the nascent ring separating from the Loop Current. The flow is therefore convergent in the deep basin of the eastern Gulf. The upwelling is primarily fed by the eastward deep flow across 90°W, while deep flow in the Yucatan Channel is weak. Figure 2.5c (Stages C and A2) is when the eddy has separated and now propagates westward. The compensating eastward flow across 90°W is strong, and it is primarily balanced by the outflow at the Yucatan Channel.

It is clear that the Maul et al.'s (1985) hypothesis applies (approximately) only during Stage A1. So far, we have only used Tr_{Z1k} to infer Loop's expansion. In the Section 2.7, we further examine the relations of the three transport time series (Figure 2.3) with the Loop's area. We find that, as can be expected from the above discussions, the correlation between the rate of Loop's expansion with Yucatan outflow is not high, since the interaction with the western Gulf cannot be neglected.

The net transport is southward in the deep portion of the Yucatan Channel ($Tr_{Yuc} < 0$). This is a consequence of the constraint imposed by the semi-enclosed Gulf. Mass transport into the Gulf by the Loop Current ($Tr_{Z1k} < 0$) and westward-propagating eddies ($Tr_{90W} > 0$) must be returned out of the Gulf, and a portion of it exits the Gulf as deep outflow through the Yucatan Channel.

2.4. THE GULF OF MEXICO OSCILLATOR

What is the Gulf-wide deep circulation? While numerous observational and modeling studies have been devoted to describing the upper-layer dynamics, the deep circulation is still poorly understood. Oey (2008) studied transient (deep) eddy motions (including topographic Rossby waves) but did not consider the Gulf-wide circulation. Oey and Lee (2002) showed that (see in particular their Figure B1) the deep mean circulation is cyclonic. Lee and Mellor (2003) also obtained a deep cyclonic gyre in their Gulf of Mexico simulation. Based on historical data, DeHaan and Sturges (2005) gave observational evidence of the cyclonic deep gyre. Weatherly et al. (2005) presented SOFAR floats that indicated a cyclonic gyre at $z \approx -900$ m. Several driving mechanisms have been proposed, some of which are local and quite detailed (see summary in Oey et al. 2005b). Here we offer a simple one related to the Loop Current Cycle.

We apply the same three-stage ensemble averaging but for the depth-averaged deep circulation below z = –1000 m (Figures 2.4d-f; it is not necessary to distinguish between Stages A1 and A2 which are therefore lumped into Stage A). Stage A occurs 63% of the time (1803 days), Stage B 20% (567 days) and Stage C 17% (510 days). The anomaly is shown, but since Stage A is dominant, the 8-year mean (not shown) is similar to Figure 2.4d, the corresponding cyclone being stronger and anticyclone weaker. Stage A has a cyclonic gyre in the western Gulf. In the eastern Gulf, a tripolar-circulation structure exists, with an anticyclone near (87°W, 26°N) sandwiched between two smaller cyclones north and south. The anticyclone also has a zonal "tail" that produces zonal eastward flow along 26°N; this eastward flow is sandwiched between two westward zonal currents south and north. In Stage B, there is a cyclone in the eastern Gulf, and an anticyclone in the western Gulf. Stage C is a transition stage when the western anticyclone strengthens, and in the eastern Gulf the cyclone weakens and an anticyclone appears. It is straightforward to see that these variations of the strengths of eastern and western circulations depend on stretching and compression imposed at the deep layer's upper boundary at z = –1000 m, i.e., on Tr_{Z1kW} and Tr_{Z1kE} (= Tr_{Z1k}), where the subscripts "*W*" and "*E*" denote region of the Gulf west and east of 90°W, respectively. Since $Tr_{Z1kW} = -Tr_{90W}$, i.e., westward deep transport across 90°W is balanced by upwelling (across z=–1000 m) in the western Gulf, and vice versa, we see from Figure 2.3 (lower panel) that except during the short-period Stage A2, Tr_{Z1kW} and Tr_{Z1kE} are anti-correlated; i.e., upwelling or stretching of deep layer in one (sub)basin corresponds to downwelling or compression in the other. By conservation of potential vorticity, then, as the Loop Current is reforming in Stage A ($Tr_{Z1kE} < 0$ and $Tr_{Z1kW} > 0$) the lower-layer vorticity in the eastern Gulf becomes more anticyclonic while the cyclone in the western Gulf strengthens (Figure 2.4d). During incipient shedding Stage B, the deep layer of the eastern Gulf gains cyclonic vorticity due to the strong upwelling there, and the western Gulf's cyclone weakens as downwelling there compresses vortex lines (i.e., anticyclonic anomaly, Figure 2.4e). Stage C is a transition period when upwelling in the eastern Gulf wanes but downwelling in the western Gulf intensifies (Figure 2.4f, as Tr_{90W} continues to rise, Figure 2.3). The process then repeats with a new Loop Current Cycle. This coupled upper-lower layer response may be referred to as the Gulf of Mexico oscillator (see further discussions below). The amplitude of the deep vorticity (ζ) oscillation may be estimated using $\partial(\zeta/f)/\partial t \approx \partial w/\partial z$, which gives $|\zeta|/f \approx 0.005$ (using the values of $w \approx \pm 0.4$ *m day*$^{-1}$ and a time scale ≈ 30 days; Figure 2.3), corresponding to a horizontal shear of about 0.05 m s^{-1} over 200 km (Figure 2.4d,e,f).

2.5. WHY IS THE DEEP MEAN CIRCULATION CYCLONIC?

It was mentioned previously that the 8-year mean deep circulation in the western Gulf is cyclonic similar to that shown in Figure 2.4d. More detailed analyses indicate that the mean downwelling under the Loop penetrates below z ≈ –2000 m, and the western cyclonic gyre is also strongest below that level (not shown). Deeper than this depth, the abyssal basin of the Gulf of Mexico is closed and fluid motion shows little vertical variations (Oey, 2008). We therefore model the abyssal Gulf as a homogeneous fluid layer with vertical mass flux across its top. A reduced-gravity model is used and the solution applies only to Stage A. Yang and Price (2000) show that for a basin with inflows or outflows across its lateral boundary, and in steady state:

$$\oint \boldsymbol{U}_h \bullet \boldsymbol{n} \; \frac{f+\zeta}{H+\eta} \; ds = \; -r \oint (\boldsymbol{u}_h \bullet \boldsymbol{l}) \; ds \qquad (1)$$

where ($\boldsymbol{n}$, $\boldsymbol{l}$) is the unit vector at the boundary of the basin with outward normal $\boldsymbol{n}$, and tangential unit vector $\boldsymbol{l}$, s is the coordinate along the boundary (positive anticlockwise), r is the bottom linear friction coefficient, H = depth of lower layer at rest (i.e. bottom topography), η = depth anomaly, $\boldsymbol{u}_h$ is the horizontal depth-averaged velocity, $\zeta = \nabla\times \boldsymbol{u}_h$ is the corresponding relative vorticity, $\boldsymbol{U}_h = \boldsymbol{u}_h(H+\eta)$ is the depth-integrated transport. For a closed basin, the LHS vanishes, so that the circulation $\forall\ (\boldsymbol{u}_h.\boldsymbol{l})ds = 0$. Therefore, since the mean vertical flux in the eastern Gulf of Mexico is downward (the red curve in Figure 2.3), the resulting anticyclonic circulation must be compensated by cyclonic circulation somewhere else in the basin. We use a numerical model to show that the cyclonic circulation is in the deep portion of the western Gulf of Mexico.

The reduced-gravity model is also based on POM. The domain is the Gulf of Mexico deeper than 1000 m, and is closed at the Straits of Florida and the Yucatan Channel. (The choice of $z < -1000$ m to define the deep layer is for computational convenience only; it has no impact on the result since the Yucatan Channel is closed in the model). Table 2.1 gives various model parameters and their meanings. Weak dissipation is included as A_H for numerical stability. A mass influx of 0.25 Sv is specified (i.e., downward into the deep layer) over an area 250 km × 250 km under the Loop Current, and the model is integrated until steady state. The depth anomaly η and depth-averaged velocity $\boldsymbol{u}_h$ are plotted in Figure 2.6, which clearly shows cyclonic gyre in the deep western Gulf. Apart from the weaker strength, the resulting circulation is in good agreement with Figure 2.4d, including the weak eastward zonal flow just north of the 3000 m isobaths in the northern Gulf.

Table 2.1

Reduced-Gravity Model Parameters

Parameters	Meanings	Values
g'	$g\Delta\rho/\rho_o$	$0.013\ m\ s^{-2}$
H	topography below z = –2000 m	*variable*
$\Delta x, \Delta y$	constant x and y grid spacings	*10 km*
A_H	horizontal viscosity	$100\ m^2\ s^{-1}$
r	linear friction coefficient	$1.36\times10^{-4}\ s^{-1}$

The mean cyclonic circulation in the deep western Gulf (say west of 90°W) requires an inflow (i.e. westward) across 90°W ($\boldsymbol{U}_h.\boldsymbol{n} < 0$ in equation 1) below the sill depth of the Yucatan Channel, consistent with downwelling across $z \approx -2000$ m mentioned above and a corresponding upwelling in the western Gulf. The *net* transport integrated from z = -1000 m to bottom, $\langle Tr_{Z1kW}\rangle$ (<.> = mean), must still be *eastward* however (Figure 2.3), since it must balance the mean westward mass transport by LC eddies. The vertical flux across z=-1000 m in the western Gulf is therefore downward. There is then vertical convergence for -1000 m > z > -2000 m in the western Gulf, and the mean transport at 90°W has a 3-layer structure as shown in Figure 2.7. We caution, however, that while useful for understanding the overall circulation, the 3-layer structure belies a complex latitudinal flow structure (not shown).

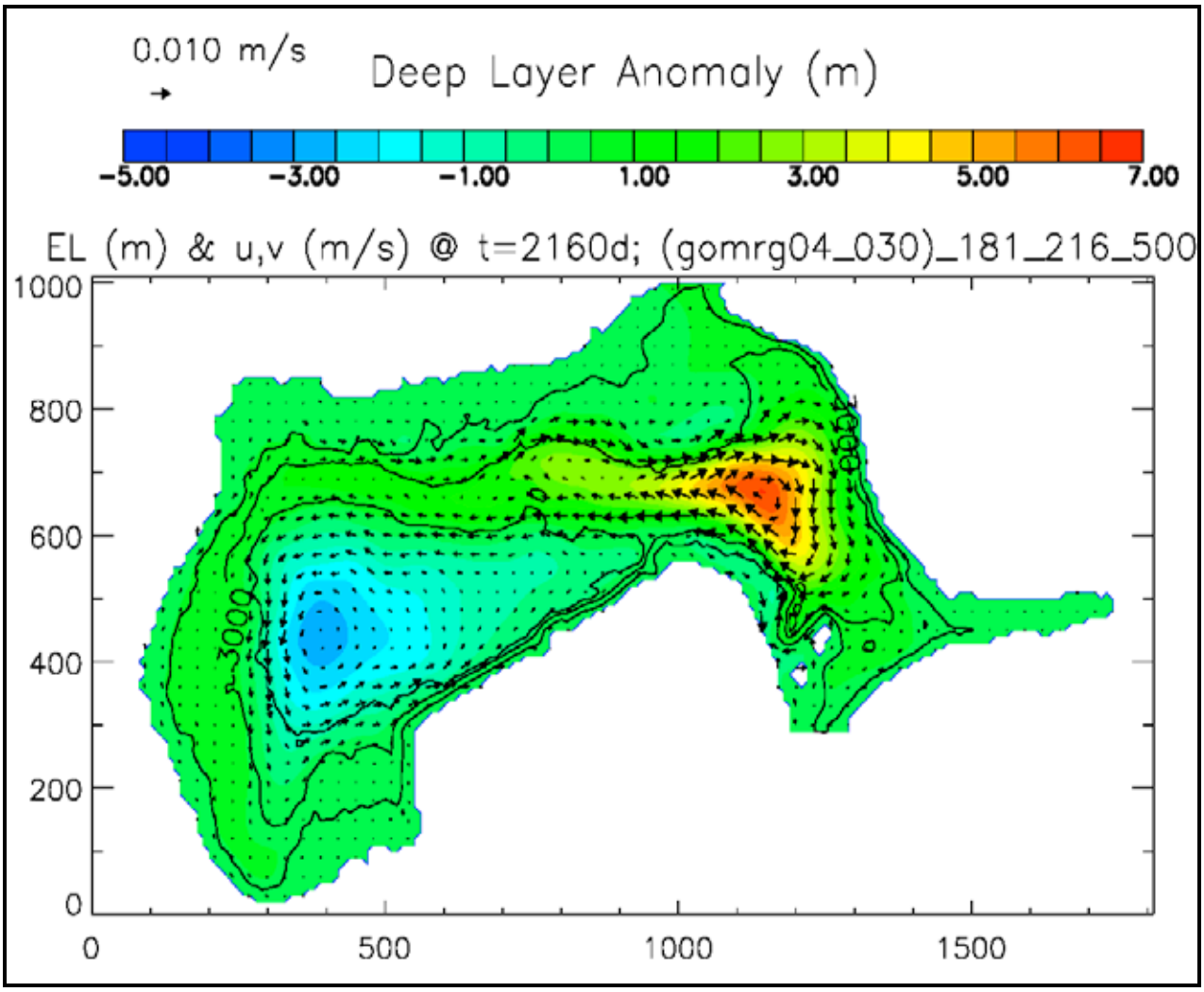

Figure 2.6. The reduced-gravity model result at steady state. Color is layer anomaly in meters and vectors are the depth-averaged currents.

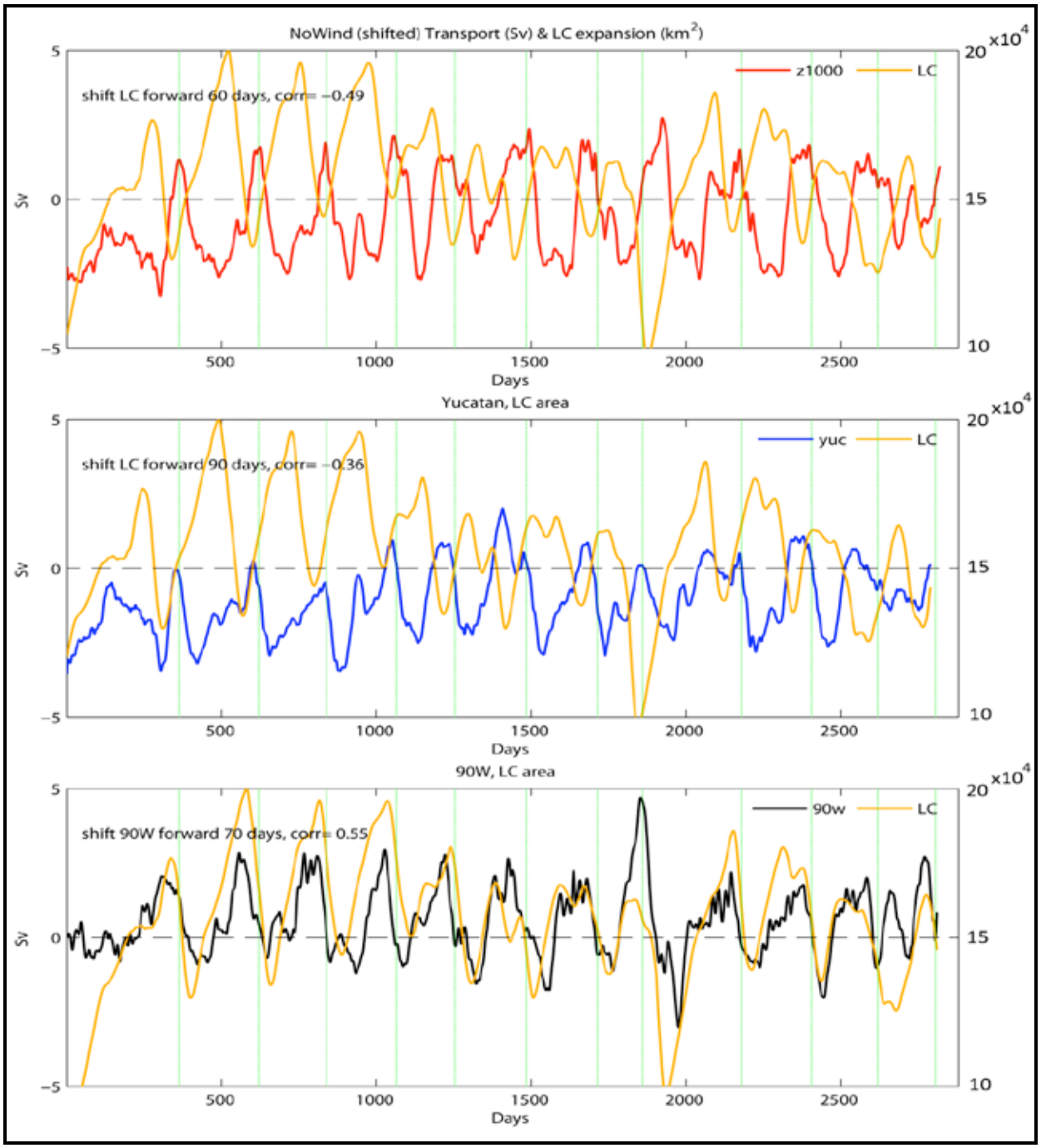

Figure 2.7. Time series of Loop Current's area (brown; defined as where SSH > 0.15 m) plotted together with transports across z = (1000 m (top panel)), through the Yucatan Channel (blue; middle panel), and across 90˚W (black; lower panel). The time series have been shifted as indicated. Time is in days of the 8-year analysis period.

2.6. CONCLUSION AND DISCUSSION

Conclusions are summarized and discussed below:

1. The expansion, eddy-shedding and retraction of Loop Current, and its coupling with the deep flows, is classified into various stages depending on the vertical mass flux across the base of the Loop ($z \approx -1000$ m) in the eastern Gulf:
   a. Stage A1 is the "Loop-reforming" stage prior to eddy-shedding; it has downward flux and deep divergence;
   b. Stage B is the "incipient-shedding" stage; it has deep convergence from the west (i.e., the central Gulf) that leads upward flux under the Loop, while the Yucatan Channel's deep flow is weak;
   c. Stage C is the "eddy-migration" stage; it too has an upward flux, though a decreasing one, and deep flow from the west supplies the deep Yucatan outflow; and
   d. Stage A2 is the beginning of the Loop-reforming stage after eddy-shedding. It has a downward flux but the deep influx (of Stage C) from the central Gulf remains substantial. Together they contribute to strong deep outflow in the Yucatan Channel.
2. Stage B results support Pichevin and Nof (1997) and Nof (2005) that eddy shedding is primarily by westward detachment of the matured Loop by Rossby wave dynamics. The dynamical response of a weak Yucatan deep flow during this stage suggests that eddy-shedding may be sensitive to external deep perturbations (e.g., from the Caribbean)—an interesting future research topic.
3. There exist significant deep coupling between the western and eastern basins of the Gulf, and this leads to a poor correlation between the Loop Current expansion (area) and deep outflow in the Yucatan Channel. The vertical flux Tr_{Z1k} is correlated with Yucatan deep flow Tr_{Yuc} (CC = +0.72 at *30 day* lag, Tr_{Z1k} lags Tr_{Yuc}; Figure 2.2c), and is negatively correlated (CC = –0.5) with the Loop's area expansion rate $d(A_{Loop})/dt$ (Section 2.7). The less-than-perfect correlations in both cases are caused by deep exchanges Tr_{90W} between the western and eastern Gulf. We find therefore that $d(A_{Loop})/dt$ and Tr_{Yuc} are only weakly correlated with CC = –0.36 which is also the level of correlation found by Ezer et al. (2003) from a realistic numerical simulation, and also by Bunge et al. (2002) from observations. In commenting on the latter's work, Rivas et al. (2005) noted that "… there is little relation between the variation of the surface area extension of the Loop Current and the evolution of the near-bottom eddy flow in the Yucatan Channel…," except perhaps during a Loop growth period in October-November 1999 after an eddy (Eddy Juggernaut) was shed. During this period, a strong outflow lasting 40~50 days and with

peak transport of −2 Sv in the Yucatan Channel occurred. This period corresponds to, and agrees well with, Stages C and A2 (Figure 2.3).

4. The net downward flux under the Loop is because the Loop Current spends a relatively longer time "reforming" (stage A: 63% time). Together with the compensating deep flow from the western Gulf, the net deep transport at Yucatan is southward. This is a consequence of the constraint imposed by the semi-enclosed Gulf. Mass transport into the Gulf by the Loop Current ($Tr_{Z1k} < 0$) and westward-propagating eddies ($Tr_{90W} > 0$) are returned out of the Gulf, and a portion of it exits the Gulf as deep outflow through the Yucatan Channel.

5. The Yucatan's deep outflow of about −1 Sv compares reasonably well with Sheinbaum et al.'s (2002) observation of −0.7 to −0.8 Sv below the 5.7°C isotherm ($z \approx -900$m; see also Rivas et al. 2005) over a ten-month period from Sep/1999 to Jun/2000. As noted above, the stronger deep outflow shortly after an eddy is shed has also been observed (Sheinbaum et al. 2002; Bunge et al. 2002).

6. The cyclonic gyre that appears west of approximately 90°W is because the mean vertical mass flux at the base of the Loop Current due to the Loop Current Cycle is downward, which locally inputs a negative vorticity. Since the deep Gulf is closed for $z < -2000$ m, the net circulation around the abyssal basin is zero, and a deep cyclonic gyre must exist in the western Gulf. The gyre's strength varies with the Loop Current Cycle, being strongest when the Loop Current is reforming, and weakest after an eddy is shed. The deep vertical mass fluxes in the western and eastern Gulf are nearly out of phase. These results suggest that during a period when the Loop Current is growing, the deep cyclonic gyre in the western Gulf ought to be strengthened.

7. The coupled surface and deep motions in the Gulf of Mexico resulting from the separation of warm rings from the Loop Current may be idealized as a west-east oscillator (about a mean). The SSH curves in Figure 2.4 (lower panel) show the connection between flow and pressure. As the Loop Current expands, pressure builds up and the isopycnal tilts eastward (deeper east than west; eastern SSH rises). As ring separates and propagates westward, strong transport from east to west ensues in the upper layer, and the isopycnal tilts westward (deeper west than east; eastern SSH falls). Downwelling in the west pushes lower-layer fluid into the eastern Gulf's deep basin, where it upwells as well as leaks into the Caribbean Sea through the Yucatan Channel. Then, in the western Gulf, the ring decays and produces upwelling, while in the eastern Gulf, the Loop reforms and produces downwelling. The isopycnal tilts eastward, and the cycle repeats. Thus rising SSH in the east corresponds to downwelling there, and also to falling SSH in the west and upwelling there, and vice versa for falling SSH in the east (Figure 2.3).

8. The west-east oscillation is the dominant mode of variability in our idealized model. The standard deviation (of the oscillation) of the gyre-scale currents is O(0.05 m s^{-1}) (Figure 2.4d-f). The Loop Current Cycle can therefore produce

deep currents that vary slowly at the eddy-shedding time scales. Also, because the oscillation depends on the west-east pressure difference, the behaviors of the Loop Current, including how often it sheds eddies, may depend on the existing conditions of the Gulf itself, e.g., how many rings it already has. For the same reason, model parameterizations of dissipation and diffusion which in part determine how eddies decay, can affect the shedding rate. These are interesting and important topics for future research.

9. The above idealization is useful for understanding the overall response of the Loop Current Cycle, but there are also important details. A three-layer mean transport structure at 90°W exists because of the strong potential vorticity constraints placed on the abyssal circulation (because the deep Gulf is closed), and also westward mass transport by eddies must be returned to the eastern Gulf.

2.7. LOOP AREA AND DEEP TRANSPORTS

The Loop Current's expansion and retraction are more readily observed (e.g., from satellite) than the vertical mass flux beneath the Loop Current, Tr_{Z1k}, so here we wish to see how closely they are related. We use the Loop's area (A_{Loop}) defined by SSH > 0.1 m as a proxy of its expansion and retraction (Figure 2.1). Virtually the same results are obtained using time series of the Loop's edge measured along the line that connects the southeastern to northwestern corners of the dashed box in Figure 2.1.

Figure 2.7 shows A_{Loop} plotted together with Tr_{Z1k}, Tr_{Yuc}, and Tr_{90W}. The A_{Loop} is anticorrelated with, and lags Tr_{Z1k} by 60 days (= $\pi/2$ for a shedding period of 240 days); the maximum lagged CC is –0.5. Thus d(A_{Loop})/dt and Tr_{Z1k} are anticorrelated. As the Loop expands (retracts), it forces a downward (upward) flux across its base. On the other hand, Figure 2.2 already shows that Tr_{Z1k} lags the Yucatan deep flow Tr_{Yuc} by 30 days (CC = 0.72), so that Tr_{Yuc} must lead A_{Loop} by 90 days and is anticorrelated with it, with CC = $-0.5 \times 0.72 = -0.36$, as shown in the middle panel of Figure 2.7. The less-than-perfect correlations in all of the above cases, but in particular in the CC between Tr_{Yuc} and A_{Loop}, are caused by deep exchanges Tr_{90W} between the western and eastern Gulf. Indeed, there is a much more robust correlation between A_{Loop} and Tr_{90W}, with the latter lagging the former by 70 days and the corresponding CC = 0.55 (Figure 2.7 bottom panel). Physically, while the expansion of the Loop Current causes the Yucatan outflow to strengthen, it is not the only cause. The maximum outflow is actually controlled more by eddy shedding and propagation (across 90°W) when Tr_{90W} increases.

3. LOOP CURRENT CYCLE AND TRIGGER MECHANISM FOR LOOP CURRENT RING SEPARATIONS[10]

Synopsis

While theory does not preclude the possibility that flow variations in the Straits of Florida can trigger Loop Current ring separations, they are neither necessary nor sufficient.

Summary of the Main Results

Chang and Oey (2010a) demonstrate that a change in x-momentum flux in a control volume in the eastern Gulf of Mexico (Pichevin and Nof, 1997) can lead to a change in the eddy-shedding period of the Loop Current. They suggest then that eddy-shedding can depend on an externally imposed momentum flux through the Straits of Florida. The paper by Sturges et al. (2010) appears to show observational evidence of this phenomenon. The authors present cable data in the Straits of Florida (as well as other data) and conclude that the data indicate Loop Current ring separation that is "triggered" downstream by fluctuations in the Straits' transport. This is potentially a significant finding. However, we think that Sturges et al's paper is misleading. Here we show that in addition to being insufficient as implied by Sturges et al.'s data, the "downstream trigger" mechanism is also not necessary, at least not necessary in theory, for Loop Current ring separations. This does not, however, preclude the possibility that the downstream-trigger mechanism is real, as suggested above; it just means that the observational evidence is, at the present time, incomplete. The mechanism should be investigated in the future by a rigorous observational demonstration, as well as dynamically and also rigorously through process and/or analytical modeling.

3.1. INTRODUCTION

Sturges et al. (2010) noted pulses of increased and decreased transports inferred from cable data at the northern end of the Straits of Florida (Jupiter to Settlement Point). The authors suggested that the pulses originated as SSH fluctuations in the open Atlantic Ocean and that they triggered Loop Current ring separations in the Gulf of Mexico. Although transport pulses appeared throughout the time series, the authors suggested that only those pulses that were seen just before eddy shedding were responsible for the ring separations. They concluded that "if the Loop Current is in a position where a ring-shedding event is poised to happen—but the separation has not yet occurred . . . these pulses provide the mechanism that causes the instability to go forward and the rings to separate." One infers from above conclusion that the "downstream trigger mechanism" is insufficient for Loop Current ring separations; however, the authors seem to suggest that it is necessary.

Sturges et al.'s idea is interesting, and "downstream trigger mechanism" maybe a possibility. However, the conclusions can be misleading as explained below. At the same time, this chapter will also compare downstream trigger mechanism for Loop Current ring separations with recent theoretical advances of the Loop Current dynamics (Chang and Oey, 2010a,b) and in particular with the idea of Loop Current Cycle (Chang and Oey, 2011).

[10] This chapter is based on Oey and Chang, 2011: Loop Current Cycle and trigger mechanism for Loop Current ring separations. *Proc. BOEM Info. Trans Meet,* New Orleans, LA. [Available online at http://www.aos.princeton.edu/WWWPUBLIC/PROFS/PUBLICATION/LCCycleTriggerMechanismv8.pdf.]

3.2. WHY DO WE THINK THAT THE DOWNSTREAM-TRIGGER MECHANISM AS PRESENTED BY STURGES ET AL. CAN BE MISLEADING?

Firstly, occurrences of transport pulses are not proof of cause and effect to ring separations. The pulses may be part of the natural Loop Current's variability, or that they may reflect transport variations through side channels (e.g. the Old Bahamas Channel) rather than through the western end of the Straits of Florida between Key West and Cuba (Hamilton et al. 2005). Hamilton et al. (2005) observed little correlation between transports through the two ends (western and northern) of the Straits of Florida. Secondly, and perhaps more importantly, while it is almost impossible from observations to show that the downstream trigger mechanism is not necessary,[11] several model calculations from existing literature prove just that. In other words, models cited below produce eddy-shedding without the necessity of invoking a downstream trigger in the Straits of Florida.

If downstream trigger is indeed the mechanism that causes Loop Current rings to separate, then existing models without an active Atlantic Ocean would not produce eddy separation. These include, for examples, the models of Hurlburt and Thompson (1980), Oey (1996), Pichevin and Nof (1997) and others (see Oey et al. 2005 for a review) which specified (various) open-boundary, outflow conditions downstream of the Straits of Florida. There are also models that include an inert or passive Atlantic Ocean, e.g., Oey et al. (2003, their experiments A and B) and Oey (2004), as well as the more recent works by Chang and Oey (2010a,b). That these models could produce eddy-shedding at a reasonable rate (one eddy per 6~11 months) suggests that the downstream trigger mechanism is not necessary.[12] Sturges et al. (2010) also cited Pichevin and Nof's (1997) Figure 8 (which shows a rise and fall in those authors' modeled outflow, i.e., Florida transport) as a supporting theoretical evidence of the downstream trigger mechanism. However, since Pichevin and Nof's (1997) model does not have an active Atlantic Ocean, their results are actually inconsistent with the downstream trigger mechanism.

The occurrences of pulses of Atlantic Ocean's origin are therefore neither necessary nor sufficient to trigger Loop Current ring separations. Whatever transport variations that might exist in the above idealized models must originate upstream. It is of interest to show clearly why these transport variations arise (when they arise) in the idealized model; this we do in the followings with a simple mass balance analysis.

3.3. METHOD

We use Chang and Oey's (2010a) Gulf of Mexico model based on the Princeton Ocean Model (POM); see that paper for details. The model domain covers the western Caribbean Sea and the Gulf of Mexico west of 78°W. Steady transport and T/S values (plus radiation conditions, etc.) are specified at 78°W. All surface fluxes are nil, and transport through the Yucatan Channel is nearly constant at approximately 24 Sv. The model's horizontal resolution is variable approximately 3~5 km and it has 25 terrain-following vertical levels. The model was integrated for 12 years initialized from a previous model that was run for about 25 years (c.f. Oey et al.'s (2003) Experiment A). A quasi-equilibrium state, in which the model Loop Current sheds eddies at a nearly constant rate of 1 eddy per 8.1 months, was reached in 4~5 years. The analyses below are based on the last 8 years of the model data with 12 Loop Current ring

[11] For that one has to find a sufficiently long period (months ~ years) when the Atlantic Ocean is void of storms, eddies and other disturbances that may cause SSH fluctuations.

[12] There is of course the possibility that these models were all wrong; we assume however that this is not so.

separation events. The near-regularity of the separation events allows us to define a "Loop Current Cycle" with a period of ~240 days (Chang and Oey, 2011) over which ensemble averaging is then computed for transports across the faces of a control volume. The control volume encloses the eastern Gulf of Mexico: western face is across the central Gulf at longitude = 90°W from the Yucatan Peninsula in the south to the Mississippi Delta in the north; eastern face is the Straits of Florida at longitude = 80.6°W from the northern coast of Cuba to the southern tip of Florida; southern face is the Yucatan Channel and the northern face is the U.S. coastline.

The analysis is simplified by focusing on the deep control volume below z = -1000 m (see discussions in Chang and Oey (2011). Since the sill depth of the Straits of Florida at 80.6°W is shallower than 1000 m, that boundary is closed. Vertical mass transport across the z = -1000 m horizontal plane (henceforth z1000m-plane) then is balanced by the (difference) transports through the deep portions of the lateral boundaries at 90°W and the Yucatan Channel. Figure 3.1 shows deep transports across 90°W (this transport is denoted by "90w"), the Yucatan Channel

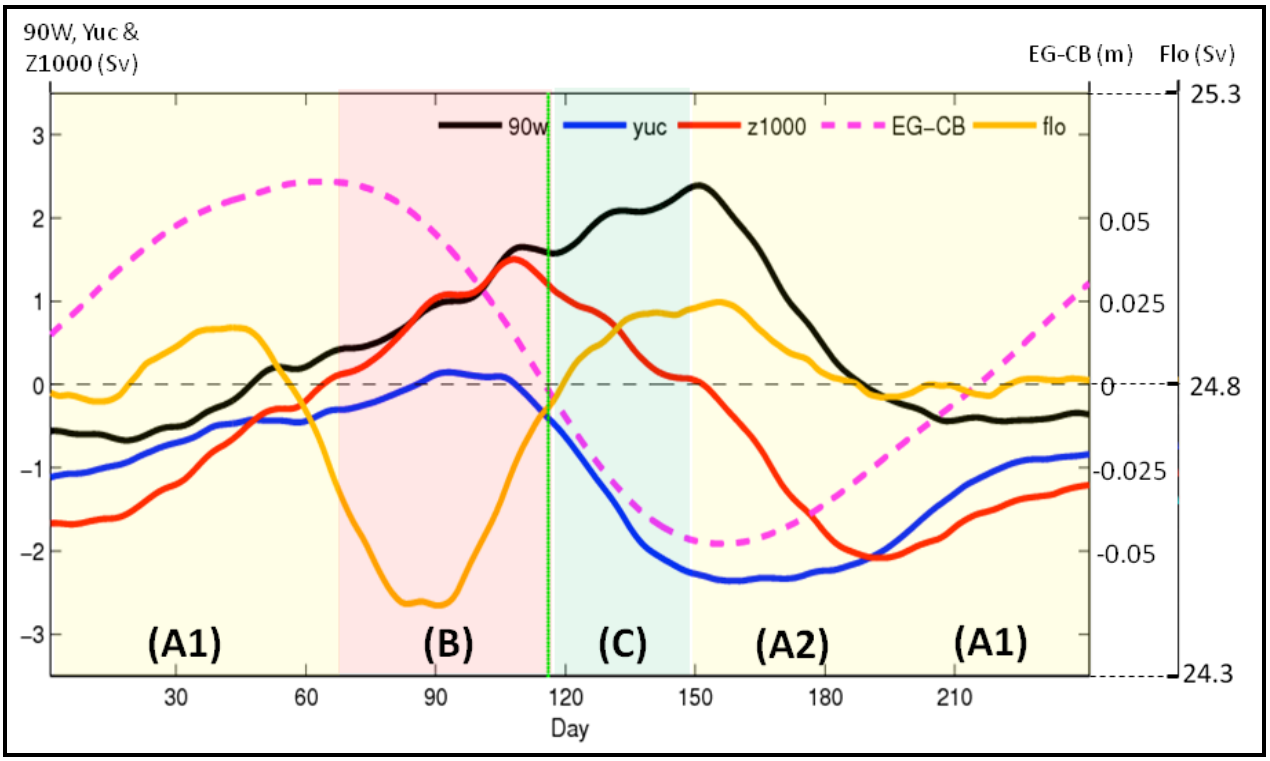

Figure 3.1. Ensemble averaged time-series of transports across the boundaries of the deep eastern Gulf control volume (see text) across 90°W (black), Yucatan Channel (blue), and z = (1000 m horizontal plane (red)). Also plotted are the Florida transport (gold curve) and the difference between the area-mean SSH in the eastern Gulf and the Caribbean Sea (dashed). The time-axis is over the Loop Current Cycle of 240 days with Stages A, B and C as discussed in text (see also Chang and Oey, 2011). To show more clearly the relationship between the different variables during a Loop Current Cycle, a 30-day running-average has been applied to all the time series.

(denoted by "yuc") and the z1000m-plane (denoted by "z1000"), ensemble-averaged over all 12 eddy-shedding events. Figure 3.1 also shows the total (i.e. from surface to bottom) transport at the western end of the Straits of Florida at 80.6°W (denoted by "Flo," = total transport through the Yucatan Channel), as well as the difference between area-mean SSH in the eastern Gulf and the Caribbean Sea (denoted by "EG-CB")[13]. Usual sign convention is used for the transport, e.g., negative is westward or southward etc.

3.4. RESULTS

In the eastern Gulf of Mexico, the Loop Current and rings are generally dominant; their movements and strenghts force vertical fluxes across the z1000m-plane (as well as horizontal fluxes). Since the idealized model has no other forcing except a steady transport (and T/S etc) specified in the Caribbean Sea, deep flows across lateral boundaries respond passively to the Loop Current and rings. As the Loop expands (or reforms after each shedding), it forces downward flux, z1000 < 0, across the z1000m-plane. This period of downward flux is Stage A1 in Figure 3.1 which shows that, in response, the deep flow is divergent (both "90w" and "yuc" are negative). It is also a period when "EG-CB" increases (days 0~70 and 180~240).

As the Loop Current expands northwestward in accordance to Rossby wave dynamics (Hurlburt and Thompson, 1980), it forces a deep return flow across 90°W ("90w" turns positive)—this is Stage B. A large portion of the Loop Current has now moved westward away from the entrance to the Yucatan Channel, the deep flow in the channel becomes weak ("yuc" ≈ 0), and the deep return flow across 90°W is nearly wholly balanced by upwelling across the z1000m-plane, i.e., 90w ≈ z1000 > 0 (e.g. days 80~115). The resulting deep-layer stretching produces cyclonic anomaly in the eastern Gulf as well as a drop in "EG" (hence also in "EG-CB") prior to eddy-shedding. Before this drop, however, the peak pressure (near day 70) due to "EG" decelerates the Yucatan Channel's northward inflow which (because the deep channel's flow is weak at this Stage B) is mainly confined in the upper layer, and which supplies the transport to the Straits of Florida. That is why the minimum "Flo" lags the peak in "EG-CB" and Figure 3.1 shows that the lag is 20~30 days (i.e. near day 90 in Figure 3.1). The phase lag *very roughly* follows a one-dimensional (Yucatan) channel-flow balance: $\partial v/\partial t = -g\partial\eta/\partial y$, so that minimum "v" lags the peak in SSH gradient $\partial\eta/\partial y$.[14]

The "EG" drops steeply during eddy-shedding (days 90~125), and our model follows closely Pichevin and Nof (1997) and Nof (2005) that eddy is shed when the westward Rossby wave speed based on the matured eddy overcomes the growth rate due to inflow through the Yucatan Channel (see Chang and Oey 2010a,c). After eddy-shedding, in Stage C, the deep eastward flow across 90°W continues to rise as eddy transports mass westward—since the western Gulf is closed, eddy forces a return deep flow (Chang and Oey 2010a,b).[15] The upward flux across the z1000m-plane weakens (days 115~150). The resulting strong convergence in the deep eastern Gulf then forces a correspondingly strong outflow through the Yucatan's deep channel, i.e., yuc < 0 (which has been observed, Chang and Oey (2011)), hence also a strong upsurge in the inflow transport in the upper layer of the channel. The strong upsurge is apparently sufficient to

[13] This is dominated by EG (i.e., EG ≈ EG-CB), the SSH in the eastern Gulf.

[14] This formula is very rough because the flow is not one-dimensional, and SSH gradient also drives flow through the Straits of Florida. That explains why "Flo" in Figure 1 rises prior to $\partial\eta/\partial y$ changes sign.

[15] Note that the deep transport "90w" cannot be neglected when assessing the relation between Loop Current's expansion and deep transport in the Yucatan Channel. The neglect explains why in previous studies the Loop's expansion and deep Yucatan flow were not always correlated (Chang and Oey, 2011).

cause the transport "Flo" through the Straits of Florida to "overshoot" after eddy-shedding (days 120~150).

3.5. CONCLUSION AND DISCUSSION

In conclusion, the rise and fall of "Flo" is a natural variation of the Loop Current ring separation, and it agrees well with Pichevin and Nof's (1997) Figure 8, though the two models are very different; it is not due to a "downstream trigger mechanism." The minimum in "Flo" before an eddy is shed is closely tied with the peak SSH (around day 70) that builds up in the eastern Gulf some 40 days before an eddy is shed. If the Loop Current Cycle is considered as an "oscillator" of the Gulf of Mexico (Chang and Oey 2011), the subsequent rise in "Flo" would be an "overshoot" after the pressure is released—after the eddy is shed. In both our and Pichevin and Nof's (1997) time series, the time scales are longer than Sturges et al's (2010). Hamilton et al. (2005) observed that transport through the western end of the Straits of Florida is dominantly of longer periods, and is uncorrelated with the transport at the northern end, where the variation is of shorter periods (~10 days). Hamilton et al.'s (2005) observations are consistent with (though are not proof of) our view that, to the "leading" order, Loop Current ring separation is perhaps not triggered by downstream transport pulses. If daily time-series (instead of 30-day running averaged as in Figure 3.1) is used for the ensemble, we obtain short-period, small-amplitude oscillations (not shown) of "Flo" superimposed on the dominant slow variation shown in Figure 3.1. Though these oscillations have similar time scales as Sturges et al.'s (2010), about 10~20 days, we do not consider them to be significant. The idealized model has the dominant 240-day Loop Current Cycle that is also reflected in the ensemble in Figure 3.1. In the real ocean, the Loop Current Cycle has variable periods, from 3~18 months, which tend to cancel when they are ensembled about the shedding times; this may explain why no slower variation can be seen in Sturges et al's (2010) ensemble (their Figure 4). If the time-axis is scaled by the shedding period T or some power of it, T^{α}, for some α which may be fractional, it will be interesting to see if observational points may be made to collapse about a common curve of the Loop Current Cycle.

On the other hand, as we suggested previously (Chang and Oey, 2010a), a change in x-momentum flux in a control volume in the eastern Gulf of Mexico can lead to a change in the eddy-shedding period of the Loop Current., so that eddy-shedding can also depend on an externally imposed momentum flux through the Straits of Florida. The study of this potentially interesting phenomenon should be carried out through careful observations and analyses, and should be proven dynamically and rigorously through process and/or analytical modeling.

4. COMPARISON OF MODELED AND OBSERVED VARIABILITY IN AN EDDY-DOMINATED REGION OF THE GULF OF MEXICO: DEEP DYNAMICS[16]

Synopsis

Modeled currents in the deep layer of the central Gulf of Mexico are compared with observations from the Exploratory Study.

Summary of the Main Results

This study compares the deep current response of a data-assimilated model of the Gulf of Mexico with observations from the Central Gulf's Exploratory Study from 2003-2004. The model is assimilated in the upper layer only and the deep layer (below z ≈-1000 m) is "free" or fully prognostic. Previous studies have indicated that deep currents in the Gulf of Mexico can be energetic dominated by topographic Rossby waves. We focus therefore on comparing current statistics and EOF's rather than one-to-one time-series comparisons. There have been significant improvements in the modeled response when compared against observations since this exercise was last performed by using an earlier, less highly resolved version of the model and more limited observations. The EKE levels and current profile characteristics at the mooring sites compare well with the observations. Depth profiles of velocities below 1000 m are highly coherent and quasi-barotropic as observed. The velocity PDF's have similar distributions with extreme events exceeding the normal distribution, and the frequency content and Lagrangian spatial scales of the flows are approximately similar. However, comparison of the frequency and wavenumber contents of the model and observations revealed some discrepancies. The identification of these discrepancies will lead to future model improvements.

4.1. INTRODUCTION

The circulation below ~ 1000 m in the Gulf of Mexico is characterized by almost depth-independent motions with dominant periodicities of between 10 and 100 days. Observations show highly coherent flows that are often bottom intensified and have little direct relation to the fluctuations of the upper-layer eddies. The upper-layer eddies result from shedding by the Loop Current (LC) of large anticyclones or LC eddies that interact with the continental slope topography and with other eddies to produce a complex field of both cyclones and anticyclones. The LC and LC eddies also generate peripheral cyclonic frontal eddies.

The lower layer, which is defined as below the direct influence of the eddies that extend down through ~ 800 to 1200 m depths and the top of the bottom boundary layer, has fluctuations that can be largely accounted for by appeal to the theory of Topographic Rossby waves (TRW), first given by Rhines (1970). These are linear, transverse and dispersive potential vorticity waves controlled by the bottom slope and water column stratification. They were first shown to be a good description of observations of deep currents in many parts of the deep basin of the northern Gulf by Hamilton (1990). Subsequently, Oey (1996), Oey and Lee (2002), and Oey (2008) described modeled deep currents in terms of propagating TRWs generated by the LC, and LC eddies translating westward across the deep basins of the Gulf. In Oey (2008), results from a

[16] This chapter is based on Hamilton and Oey (2011): Comparison of modeled and observed variability in an eddy-dominated region of the Gulf of Mexico: deep dynamics. Manuscript to be submitted.

high resolution (3 to 5 km grid spacing) model were used to investigate the transfer of energy to the lower layer under the LC by baroclinic instabilities that produced deep lower-layer eddies. The movement of these deep eddies to the west in the model produced radiating TRWs that propagated towards the base of the northern slope where there is a steep escarpment (the Sigsbee Escarpment). Hamilton and Lugo-Fernandez (2001) and Hamilton (2007) had observed very energetic (amplitudes > 50 cm/s) short period (~ 10 days) bottom intensified currents at the base of the Sigsbee around 90 °W, and Oey's (2008; also Oey et al. 2009) mechanism is a plausible explanation of their generation, and accounts for some of their characteristics.

In an extensive review of deep currents that included the results of recent major observational studies in the western, central and eastern parts of the Gulf, Hamilton (2009) showed that observed kinetic energies and periodicities along the central part of the Sigsbee Escarpment were compatible with TRW ray paths emanating from the LC. Moreover, Hamilton (2009) also showed, from upper and lower layer relative vorticities, evidence of baroclinic instabilities in the northern part of the LC that favored the 20 to 30 day period TRWs that dominate the lower layer at this site. Oey's (2008) model also predicted that this region, adjacent to the steep west Florida slope, is also a region of strong baroclinic instability. There are some differences between Hamilton's (2009) interpretation of the observed velocities from current meters and deep RAFOS float tracks as being dominated by TRWs, and Oey's (2008) interpretation of model simulated deep currents in the vicinity and immediately west of the LC as being a mixture of deep eddies and radiating TRWs. This paper will attempt to shed more light on these issues.

The main purpose of this study is to investigate the modeled deep current variability in terms of processes described by the observations. Model-data comparisons have previously been conducted on basic statistics such as mean flow and EKE, and EOF's (e.g., Oey et al. 2004; Wang et al., 2003; Lin et al. 2007). In this paper, frequency content, coherence and higher order quantities such as vorticity and TRW parameters as well as basic statistics will be quantified. The observational database is similar to that used by Hamilton (2009), excluding the far western Gulf, but with some additional moorings in the central and eastern Gulf. Indeed the starting points for the comparisons and analyses are similar to the analyses given in Hamilton (2009), and thus there will be extensive references to that work. The model is similar to that used in Oey (2008), but now assimilates satellite SST and SSH data as described in various previous works (e.g. Lin et al. 2007). It is noted that the assimilation scheme only operates down to 600-800 m and thus, the lower layer results are essentially from a free running model forced by an upper layer that assimilates the observed eddy field.

4.2. OBSERVATIONAL DATA

The deep current database is derived from the same sources as in Hamilton (2009) (see his Table 1) excluding the western Gulf moorings (Figure 4.1). The moorings in Figure 4.1a are full depth, measuring currents from ~ 40 m below the surface to ~ 100 m above bottom (mab) with various spacing between instruments. This study is mainly concerned with the central gulf and deep flows along the Sigsbee escarpment, which was the focus of the Exploratory Program array (Donohue et al., 2006), deployed for 1-year in April 2003. The Exploratory array (Figure 4.1b) consisted of full-depth moorings, short near bottom moorings with current meters 100 and 500 mab, and pressure equipped inverted echo sounders (PIES; Meinen and Watts, 2000). Additions to the Hamilton (2009) database are from a 2-year deployment of *L7* beginning in May, 2000 (Inoue et al., 2008), and an 11 month deployment of *L5* beginning in July, 2001 (McKone et al., 2007). A 2-character ID such as *L7* will refer to the mooring locations, for both the observations

and model, and for the most part coordinate axes for (u, v) velocities will be east and north. In some analyses isobath coordinates will be used where the v-component axis is aligned with the general trend of the local isobaths. The quality assurance and concatenation procedures for the observed records were the same as given in Hamilton (2009), and any tidal or inertial signals were removed by applying a 40-hour low pass (HLP) Lanzcos filter and decimating to 6-hour intervals.

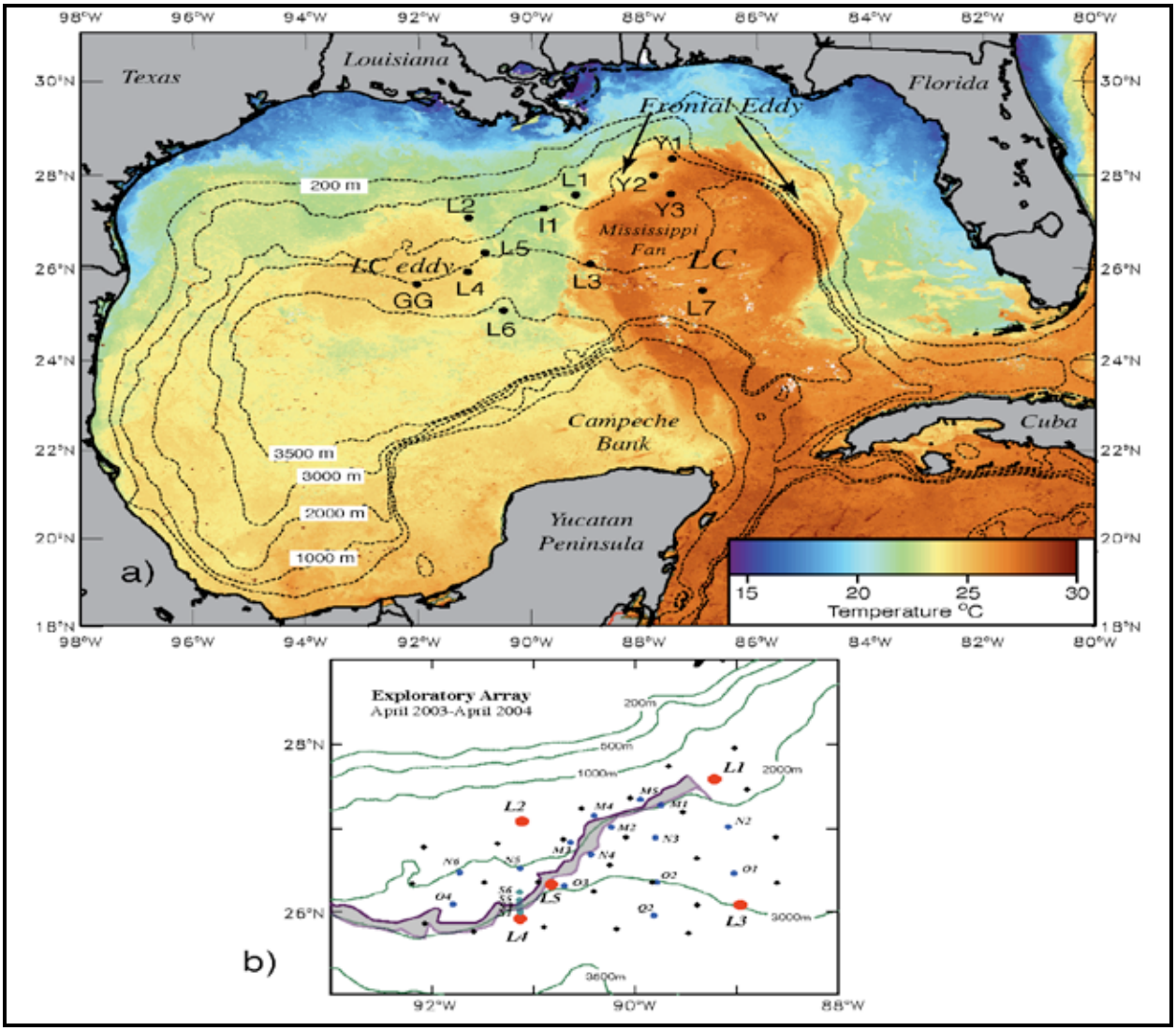

Figure 4.1. a) Locations of the principal full-depth moorings used in the analyses. The SST image is a 3-day composite centered on February 5, 1998, and shows an extended Loop Current (LC) and a detached LC eddy (named eddy El Dorado). Image courtesy of John Hopkins University Applied Physics Laboratory. b) Exploratory program array: red dots—full depth moorings, blue dots—short near bottom moorings, cyan dots—near bottom cross escarpment array, diamonds—pressure equipped inverted echo sounders (PIES). The Sigsbee escarpment (500 m depth change) is shaded gray.

The database also includes the same RAFOS float paths as given in Hamilton (2009), where the emphasis is on the last 6 months of the tracks for floats that were deployed at 1500 m and

below. Sound source failures in the first 6 months of the one-year float deployments resulted in short records with substantial gaps. After restoration of the sound sources in October 2003, good continuous records were obtained for the second six-months (Donohue et al. 2006). Float tracks were smoothed and filtered and re-sampled at 6-hour intervals as described in Hamilton (2009).

4.3. MODEL

The model used for the comparisons has been given in previous papers: Oey (2008), and Chang and Oey (2010a,b,c). In this study, the model assimilates satellite SSH and SST data (Oey et al. 2005; Lin et al. 2007) in the upper layer. Simulation data were extracted at the mooring locations (Figure 4.1) at a standard set of depths (20-m intervals between 0 and 100 m; 50-m intervals between 100 and 300 m; and 100-m intervals between 300 m and bottom). Model data, available from December 2003 to January 2006, was daily averaged and included (u, v) velocity components, temperature and salinity (T, S), and relative vorticity ($\zeta = \partial_x v - \partial_y u$) by calculating the circulation around each grid cell and dividing by the cell's area.

4.4. RESULTS

4.4.1. Loop Current Upper Layer

Both model simulations (Oey, 2008) and observations (Hamilton, 2009) have shown the importance of the region under the LC around *L7* that is north of the Campeche Bank. The model predicts that it is a region of active baroclinic instability, and the measurements indicate that it is a region of high lower-layer kinetic energy that may be radiating long-period TRWs towards both the Yucatan and the Sigsbee escarpment. Because the analysis is comparing Eulerian flows at a number of fixed mooring sites, and LC variability is a major forcing for the lower-layer, it is necessary to evaluate whether the data assimilation captures the major features of the LC upper layer at a given mooring site. Figure 4.2 compares the upper layer temperature and current profiles for the 2003-2004 deployment at *L7*. The model captures the major features of the warm and cold events caused by movements of the LC front quite well. There are some timing issues that may be caused by the temporal resolution of the AVISO SSH data that are used in the assimilation, and clearly the currents are not as strong as observed, even allowing for the daily averaging. However, the major flow events are well captured, and this gives some confidence that the model can reproduce realistic LC forcing to the lower layer. Comparison of upper-layer eddy fields and basic statistics to assess the accuracy of the assimilation method will be given separately (Oey et al. manuscript in preparation).

4.4.2. Lower Layer Variability

A feature of the lower layer observed current fluctuations at any one site is their high coherence for all levels below 1000 m. Usually one complex empirical orthogonal function (CEOF) mode accounts for greater than 80% and often greater than 90% of the total variance of the records below 1000 m for a given mooring (Hamilton, 2009). Moreover, the (complex) mode eigenvector is essentially unidirectional; thus, above the boundary layer there is little turning with depth. Before exploring the regional distribution of the vertically coherent variability, it is useful to compare the lower-layer CEOF velocity modes from the model and measurements. For the *L3* mooring (Figure 4.1) the CEOF's were calculated using the same depth levels in the model as for the observations, and also for the model using all available depth levels (100 m spacing from 1000 to 2900 m). The model velocity time series were 2-years long

versus 1-year for the measurements (analysis was done for the model using the same interval as the measurements at *L3* with virtually the same results).

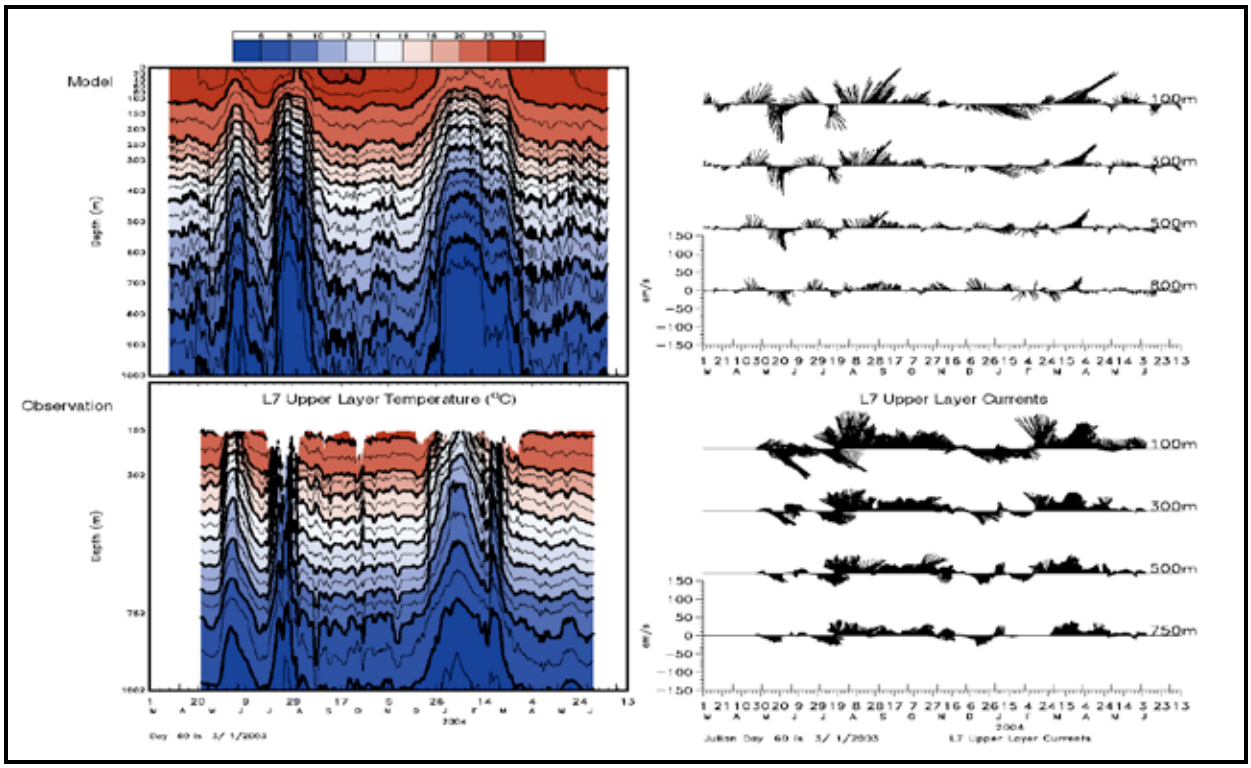

Figure 4.2. Isotherm contours (LH-panels) and upper layer current vectors (RH-panels) for the L7 site from the model (upper panels)and observations (lower panels) for the Exploratory period. The observed isotherm depths are corrected for mooring draw down using observed pressure records. The model currents are daily averages and the measurements use 40-HLP records.

The observational and model CEOF mode 1's are given in Figure 4.3, and they account for ≥90% of the total variance of the records at 1000 m and below. The observational mode 1 accounts for nearly all the variance (98%) whereas the equivalent model mode is about 8% less. The observations show an increase in amplitude between 1000 and 2000 m and then a slight decrease between 2000 m and 100 mab. The bottom boundary layer, for an unstratified water column, is estimated to be ~ 30-40 m thick. This is consistent with Reid and Wang (2004) analysis of TRW velocity profiles in an exponentially stratified ocean, which is more characteristic of the Gulf than the uniform stratification assumed by the standard theory (Rhines, 1970). The model mode 1, using the same levels as the observations, shows a depth-independent response between ~ 1500 and 2500 m with slight decreases above and below (more decrease above than below), where the coherence with the mode also decreases. The mode that uses all model depth levels has the same shape and therefore, the model lower-layer currents are more barotropic than observed, and slightly less coherent through the lower water column (the difference in sign between the two model mode 1's is an artifact of the CEOF analysis—the respective amplitude time series also have the opposite sign, so the reconstructed currents are nearly identical). On the other hand, the magnitudes of the observed fluctuations at *L3* are very well reproduced by the model results. Similar, nearly barotropic shapes of the lower-layer model

mode 1's, are also found at the other full-depth mooring sites, whereas the observational mode 1's (see Figure 4.3a in Hamilton (2009)) show a little more variety ranging from bottom intensified to essentially depth independent. For the observed and model currents, the CEOF mode 1's, where the analysis is performed separately for each mooring site, explain the majority (~ 90%) of the lower-layer variance for both model and observations (Table 4.1).

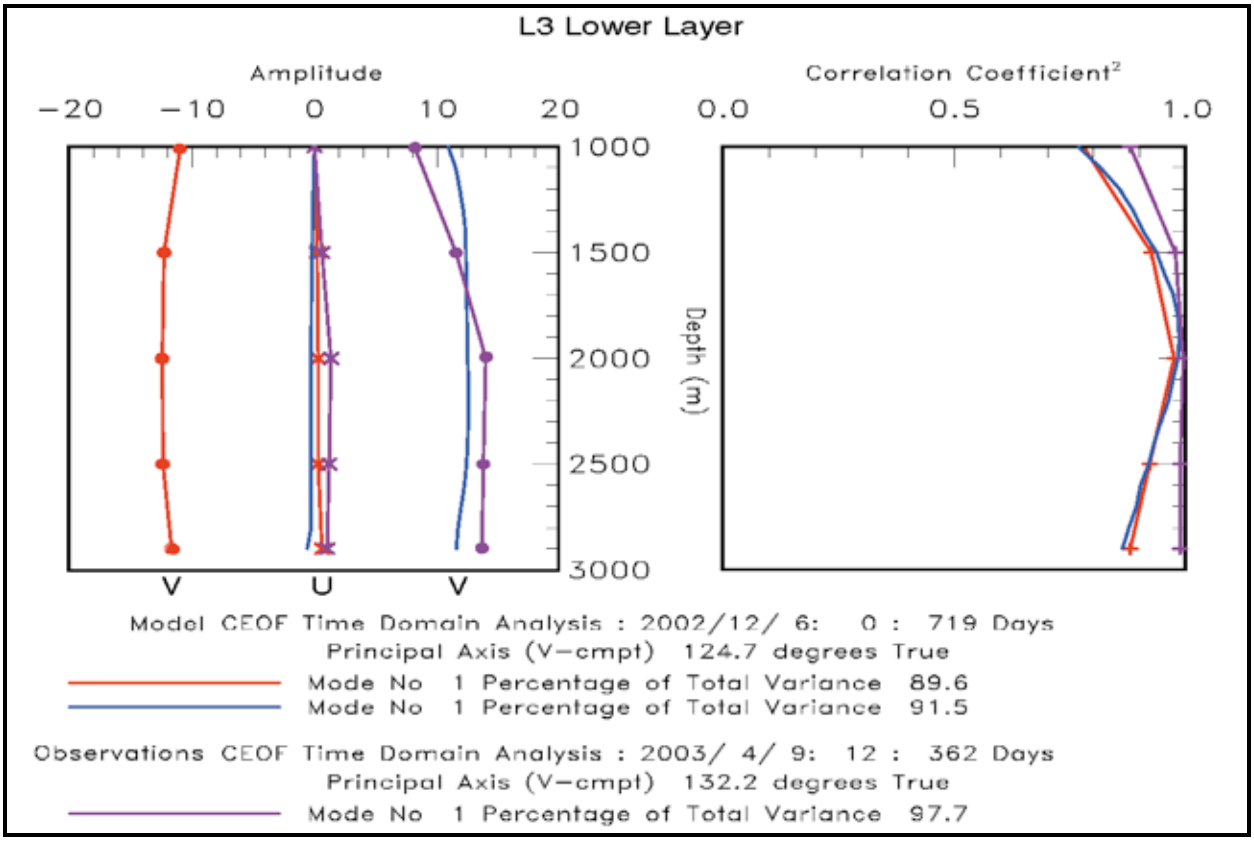

Figure 4.3. CEOF lower layer mode 1's for mooring L3 from model simulations using the same depths as observed (red), using all model depths with 100 m spacing (blue), and from the observations (purple). The LH plot shows the mode amplitudes (cm/s), and the RH plot gives the respective coherence squared of the input series with the mode.

The mode 1 standard deviation ellipses and the depth-integrated eddy kinetic energy, EKE_H, for observed and modeled lower-layer currents are given in Figure 4.4, where

$$EKE_H = \tfrac{1}{2} < \int U^* U dz > = \tfrac{1}{2} \sum_n < A_n^*(t) A_n(t) > \int_{-H+50m}^{-1000m} e_n^*(z) e_n(z) dz \quad (1)$$

and the CEOF modes are given by

$$U^*(z,t) = \sum_n A_n^*(t) e_n^*(z),$$

where z = 0 at the surface, z =-H is ocean's bottom, $e_n(z)$ is the eigen vector for mode n, the amplitudes are normalized, $< A_n^* A_n > = 3$, < > denotes time average, and the complex velocity

vectors, *U*, have record means removed. All quantities are complex variables and only one mode ($n = 1$) is used in the following. EKE_H is a better measure of the vertically coherent kinetic energy contained in the lower water column than the (u, v) variances, though using the latter to estimate lower layer EKE_H would not significantly change the results. The observational CEOF analyses use the available time series, which are usually about 1-year, with the exception of I1 (2 years). Model analyses use 2-years of daily averaged currents that overlap the Exploratory program *L* moorings (Table 4.1). The model is able to match the variances and integrated energy levels very well. The principal axes of the fluctuations are slightly more along isobath at abyssal depths, away from the escarpments (e.g., *L3, L6* and *Y2*), and there is a little less variance in the northern part of the LC (*Y2* and *Y3*) than in the observations. A similar comparison of variances for all bottom current meters of the Exploratory program (Figure 4.1b) using the same time interval as the observations produced similar agreements.

4.4.3. Spectral Analysis

The normalized mode amplitudes, *A(t),* for both the model and observations are shown in Figure 4.5 for the Exploratory interval where they overlap. The periodicities of the fluctuations are similar, particularly at longer periods, but not unexpectedly given the uncertainty in the generation mechanisms and the dispersive nature of the wave-like lower-layer flows (Hamilton, 2009), there is little correspondence between observed and simulated events. However, if the model is simulating the correct transfer of energy from the data assimilating upper layer eddies to the lower layer, the simulations should have some correspondence in the spectral content and characteristics of the lower-layer flows. For the observations, the spectral distribution of EKE_H roughly follows water depth in that low (> 50 day) to high (< 20 day periods) frequency energy tends to dominate in deeper to shallower depths, respectively. Hamilton (2009) argued that given generally bowl-shaped basins in which bottom slope is inversely proportional to water depth, this inhomogeneity with location of spectral content supported the idea of dispersive TRWs of differing frequencies propagating along differing paths, with lower frequencies confined to deeper water.

Table 4.1

Lower-Layer EOF Analysis of Currents by Mooring for Observations and Model Simulation

		Observations:		Modes 1/2 Percent of Total Variance				Model Modes: Percent of Total Variance				No. of Levels ≥ 1000 m
Mooring	Levels (m)	Start Date (yy-mm-dd)	Length (days)	CEOF	Frequency Bands (cpd)			CEOF	Frequency Bands (cpd)			
					0.01-0.03	0.024-0.05	0.05-0.2		0.008-0.02	0.02-0.05	0.05-0.1	
GG	725, 1650	87-11-15	346	71.8	71.6	80.8	-	90.5	89.8	81.5	-	20
I1	1000, 1200, 1600, 1800	99-09-02	525	88.9	83.7	87.9	84.8	91.0	88.2	94.6	85.0	9
L3	1000, 1500, 2000, 2500, 2900	03-04-09	363	97.7	94.0	83.2	73.5	91.5	85.7	78.4	73.0	20
L4	1000, 2000, 2500, 2900, 3250	03-04-05	365	97.0	97.8	77.0	-	88.1	87.6	74.0	-	23
L5	1165, 1415, 1677, 1925, 2175, 2625, 2925	03-04-22	411	95.0	96.1	96.7	84.4	92.3	88.9	84.9	-	18
L5	1128, 1378, 1628, 1878, 2128, 2578, 2878	01-08-05	297	95.5	83.4	88.6	86.3					
L6	1005, 1479, 1985, 2490, 2995, 3308	03-05-16	465	97.2	80.6	87.9	-	94.8	77.7/20.1	61.7/33.9	58.6	25
L7	500, 2000, 3000, 3187, 3256	03-04-24	410	85.5	70.4/23.6	69.9/21.6	-	93.6	67.7/26.6	62.7/32.8	56.0/33.7	23
L7	700, 2500, 3000, 3187, 3256	00-06-05	720	85.2	66.7/27.6	73.1/20.0	-					
Y1	729, 1224, 1472, 2479	05-01-26	276	84.5	-	-	-	71.4	-	-	-	16
Y2	1037, 1284, 1532, 2035	05-01-25	359	81.0	66.6/20.0	76.9/14.0	53.3/28.4	81.4	63.5/25.6	72.1	51.8	15
Y3	987, 1234, 1482, 1985, 2489, 2689	05-01-24	361	92.7	89.2	78.8	-	88.9	73.8	59.9/32.6	67.9	18

Model analysis start date: 2002-12-06, time series length: 720 days.
Model analysis depth levels are at 100 m intervals for 1000 m and below. Depth levels below 100 mab are excluded.

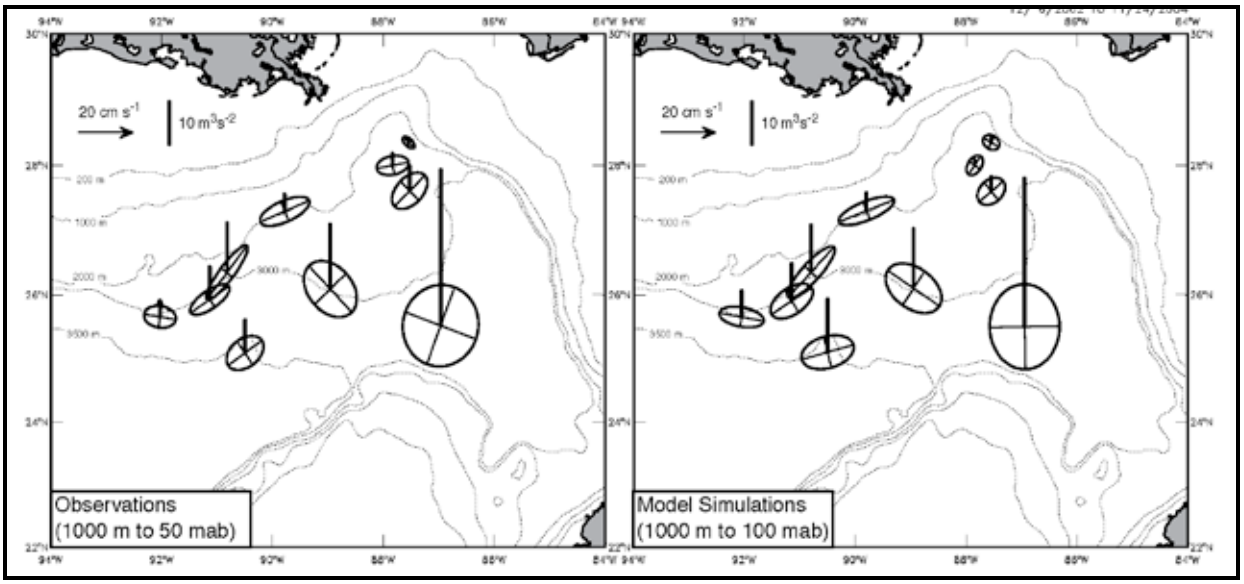

Figure 4.4. Depth average standard deviation ellipses and depth-integrated eddy kinetic energy (thick vertical lines) from CEOF mode 1 lower layer velocities from observations (LH panel) and model simulations (RH panel).

Figure 4.6 gives the spectra of the normalized amplitudes from the model and observational CEOF mode 1 analyses. In the observations, the deepest moorings (*L4*, *L6* and *L7*) have a consistent low frequency peak at ~ 50 to 60 days. For the same sites in the model, there is less consistency and *L7* favors both longer (not shown in the figure) and shorter (~ 30 to 40 day) peaks. Similarly, for shallower abyssal locations (*GG*, *L5* and *Y3*) the observations show a consistent peak ~ 25 to 40 days, whereas the model is less consistent and favors a peak at shorter periods. The short period (10 to 20 day) large amplitude fluctuations observed at I1 (Hamilton, 2007) are shifted to ~ 25 days in the model though there is a weaker peak around 12 days. The energy at *L3* is observed to be of a broadband nature for periods longer than 10 days, with peaks at 15 days, 20~29 days and 40~50 days. In the model, peaks are more distinct at 13, 17 and 28 days. At *Y2* both observational and model spectra have a similar peak ~ 20 to 30 days.

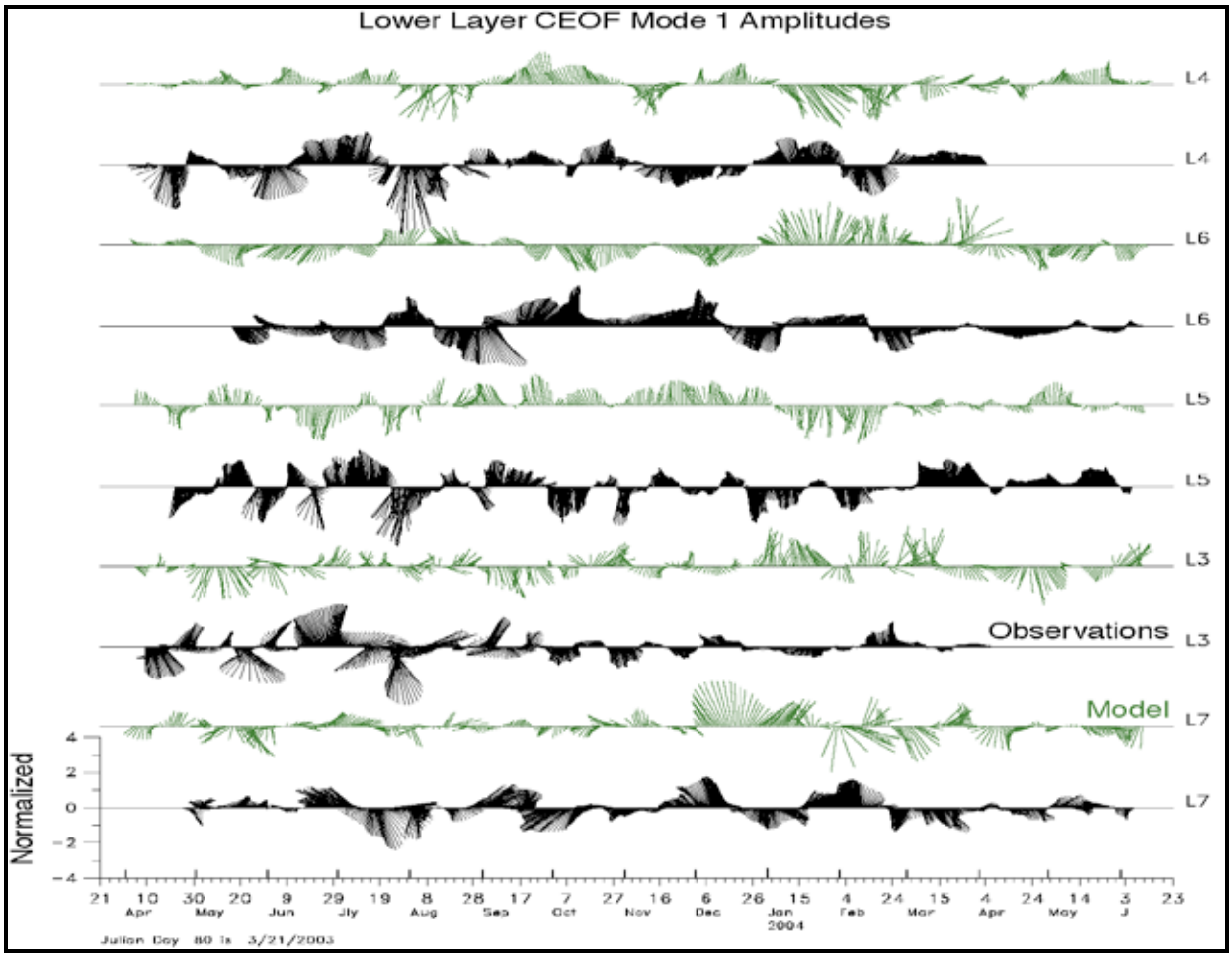

Figure 4.5. Normalized CEOF mode 1 amplitudes from the observational (black) and model (green) analyses for the lower layer currents at each L mooring location for the overlap with the Exploratory program. Up is the direction of the major principal axis at each site.

In Hamilton (2009), frequency domain EOF's were calculated for a low (35-100 days), medium (20-40 days) and high (5-20 days) bands based on the major peaks of the observed spectra. This was done also for the model locations, using slightly different bands that better encompass the model spectral peaks. The total variance explained for each band is given in Table 4.1 for both model and observations. Similar to the CEOF's, the observational modes account for higher percentages than the model. In a few cases two modes are significant. The depth-integrated EKE from the EOF modes for the three frequency bands are given in Figures 4.7a and b for the observed and modeled deep currents, respectively. The distributions of EKE_H confirm the differences in spectral energy shown in Figure 4.6 in that shorter period fluctuations tend to be more prominent, with a greater spread across the bands for the model relative to the observations. For example, at *L7* under the LC, the longest period fluctuations (> 50 days) dominate the observations with no significant energy at periods less than 20 days (Figure 4.7a). For the model, the 20-40 days fluctuations dominate at *L7*, and significant energy is present at the shortest 10-20 day periods (Figure 4.7b).

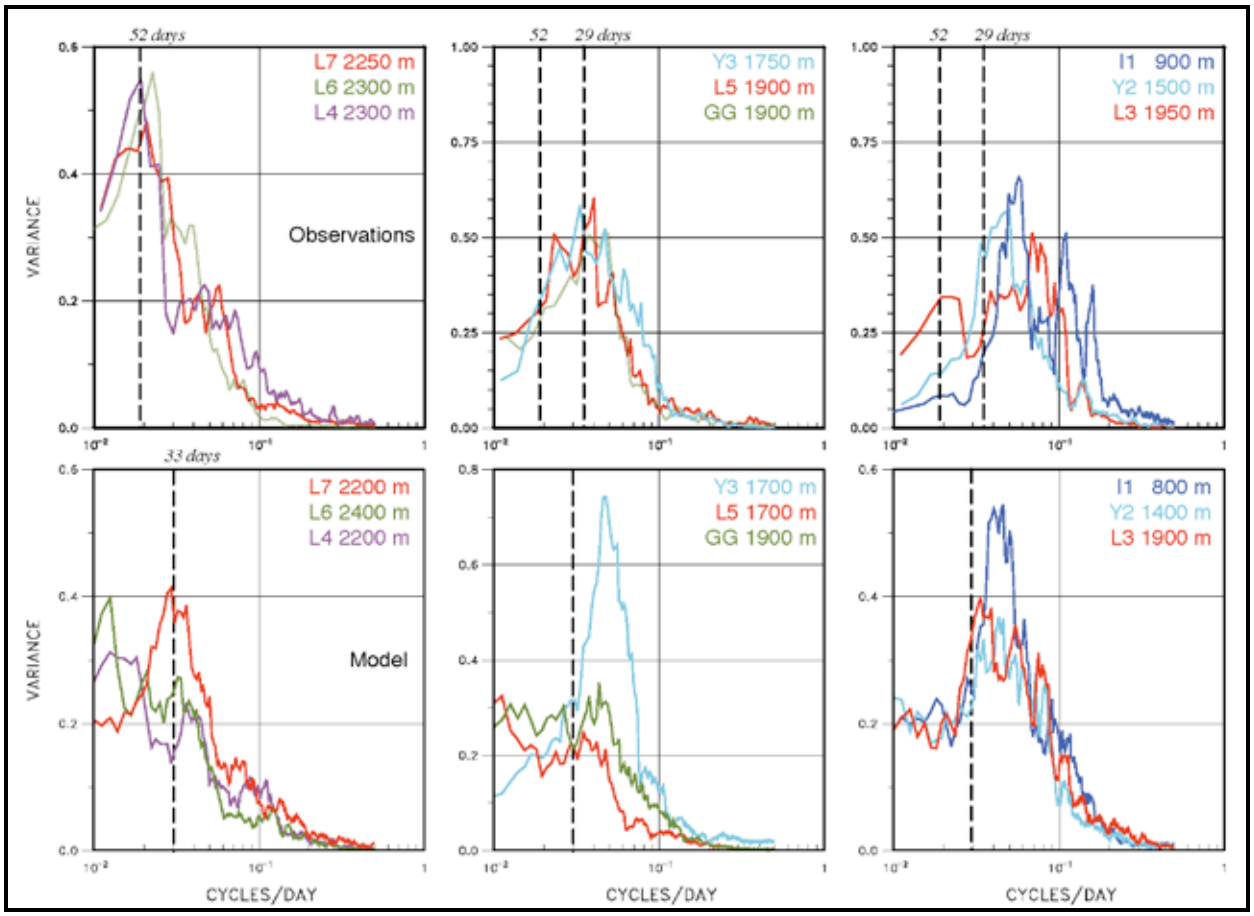

Figure 4.6. Spectra, in variance preserving form, for the normalized CEOF mode 1 amplitudes of the lower-layer currents. Upper row are from the available observations (1-year analyses), and the lower row from the model (2-year analyses). The color codes give the mooring location and lower-layer thickness, and red is used for the largest depth-integrated EKE in each group.

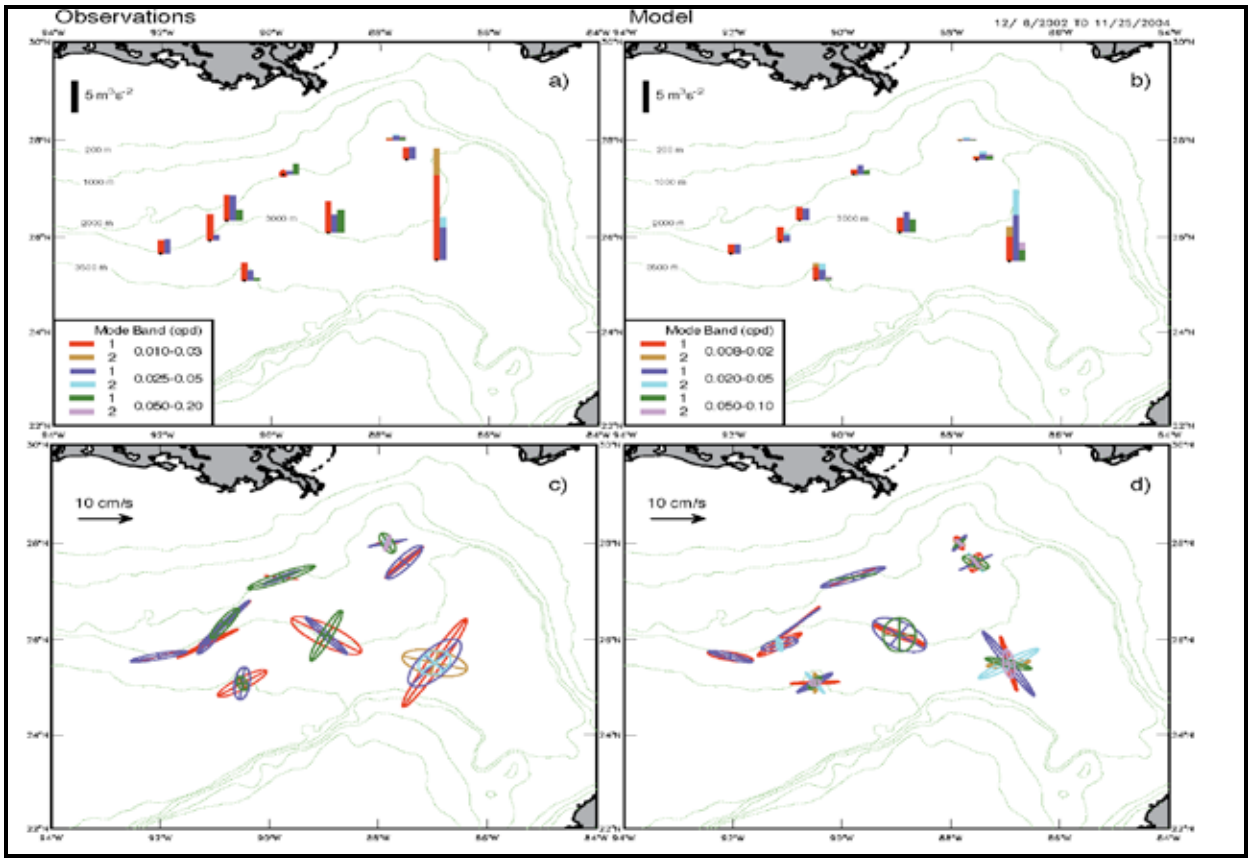

Figure 4.7. Top panels depth-integrated EKE for the indicated frequency bands and EOF modes for observed (a) and modeled (b) currents, where the height of the bar represents the total EKEH and the colors the split between modes. Bottom panels are the equivalent (c—observed; d—modeled) depth-averaged mode eigenvectors represented as hodographs.

The equivalent depth-averaged lower-layer mode currents for observations and model are given in Figures 4.7c and d, respectively. A significant characteristic of the observed modes for moorings in abyssal depths that are not influenced by adjacent steep escarpments is the rotation of the major principal axis from across the isobath to more along the isobath trend with decreasing frequency. This, along with nearly rectilinear motions, are characteristics of TRWs predicted by the dispersion equation (Rhines, 1970; Thompson, 1977). One potential problem in comparing the directions of principal axes is that the model bathymetry may influence the results through the general trend of the isobaths at a given location. For the observations, the isobath direction was derived from the published charts and checked against a least square plane fit to the Smith and Sandwell, (1997) bathymetry using a 50 x 50 km region centered on the mooring location. The directions usually compared with less than 10° difference. The same least square plane fit was used with the gridded bathymetry for the model locations, and in all the cases discussed herein where flows are analyzed in the along and across isobath directions, the model-derived isobath is within 10° of the along-isobath axis used for both the observational and model results. Therefore, the influence of model bathymetry on the comparisons is considered minimal.

At *L3* the rotation is anticlockwise and at *L6* it is clockwise (Figure 4.7c), consistent with TRWs of differing frequencies propagating towards shallower and deeper water, respectively (The group velocity of TRWs is directed along the direction of the major principal axis of the fluctuations with shallower water on the right—see discussion in Oey and Lee, 2002). The

model hodographs (Figure 4.7d) at *L3* also shows an anticlockwise rotation and at *L6* a clockwise rotation, though the motion is more circular at the higher frequencies at *L3* and mode 2 is also required at *L6* in order to account for the variances in the frequency bands when compared to the observational results.

In Hamilton (2009), the broad band fluctuations at *L3* were examined in isobath coordinates with power wavelet spectra using the Morlet wavelet and the methods given in Torrence and Combo (1998). The results show differences in the responses of the cross-isobath (u), and along-isobath (v) components, which were significant at short (10-20 day periods) and long (50-100 day periods), respectively. These different u and v responses, again, were interpreted as being caused by short and long period TRWs propagating through the site, and further there seemed to be an increase in power prior to and during the separation eddy Sargassum from a well extended LC, but not during the separation of eddy Titanic 5 months later, which occurred close to the

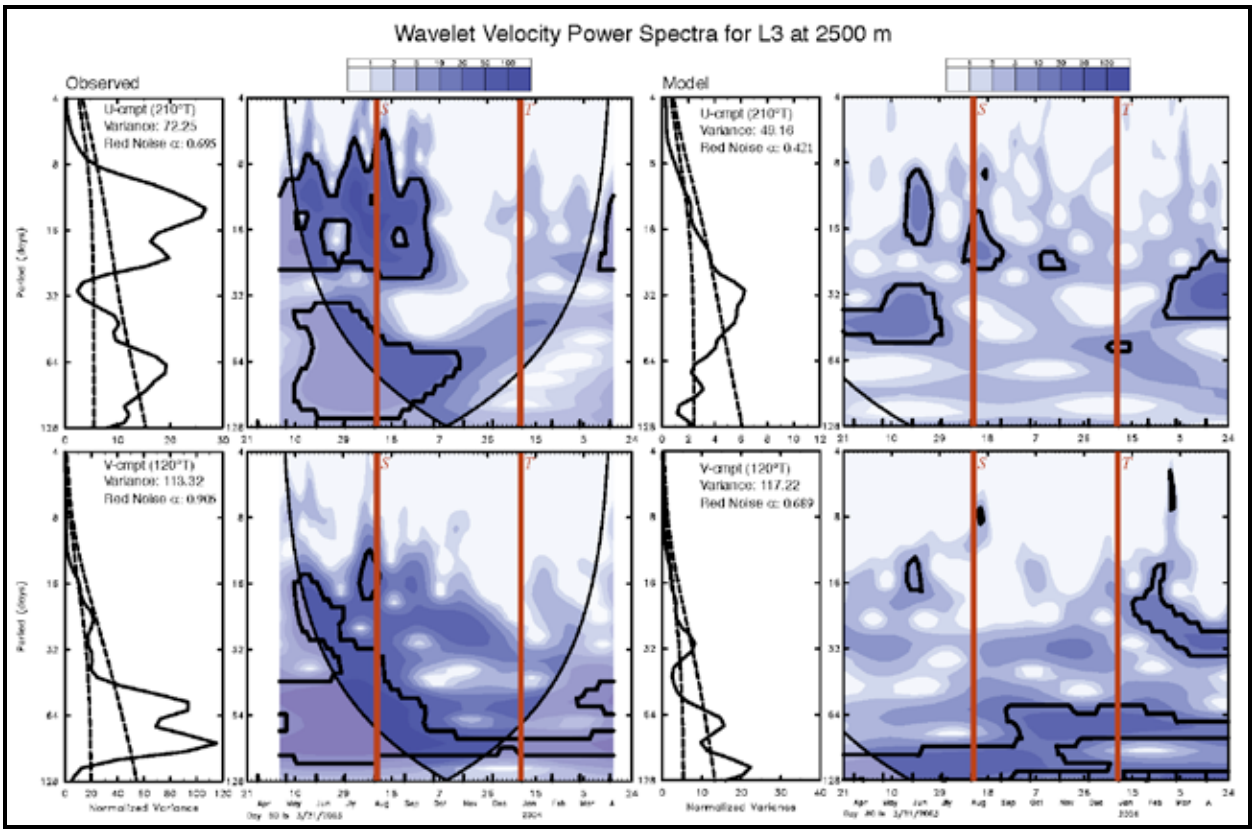

Figure 4.8. The contour plots show the local wavelet power spectrum of the velocity components from observations (LHS) and model (RHS) L3 at 2500 m for the Exploratory time interval using the Morlet wavelet normalized by the variances of the respective series. The thick solid contours enclose regions of greater than 95% confidence for a red-noise process with the indicated lag-1 (α) coefficients. The lighter shades indicate the "cone of influence" where edge effects become important. The red event lines show the detachment dates of LCE's Sargassum and Titanic (from Leben, 2005). The line plots show the respective global (time-averaged) wavelet spectrum (solid lines). The dashed lines show the mean red noise spectrum (lower), and the 95% confidence levels (upper) for the global wavelet spectra, given their respective α's.

Campeche Bank (Figure 4.8). The same wavelet methods were applied to the *L3*, 2500-m current fluctuations from the model and the comparison is given in Figure 4.8. There is a similar difference between u- and v-components, except that the short period u-component fluctuations occur at 20-40 day periods. There is also v-component power at 100-200 days that is not shown, but was not resolved by the shorter observed time series. Therefore, these signals could also be caused by TRWs with somewhat different frequency content than observed. The time variability of the fluctuations in different frequency bands is less marked, particularly for the significant long-period v-components, than in the observations, and there is less apparent response to the separation of the two eddies.

4.4.4. Lagrangian Comparisons

The Exploratory program deployed 36 RAFOS floats at 500-m intervals below 1000 m, with the majority at 1500 m nominal depth. There were problems with the sound sources, but good locations were produced for the first 3 months and the last 6 months of the 1-year deployments. The float paths had two general characteristics: oscillations with both clockwise and anticlockwise loops with weak dispersion over restricted regions of the abyssal basin, and rapid westward translation in a narrow region adjacent to the Sigsbee escarpment. The latter seems to be the major pathway by which deep water parcels are transported from eastern to western basins. No floats at 1500 m and below crossed the Sigsbee escarpment from the abyssal basin to the lower northern continental slope (Hamilton, 2009). The oscillatory looping paths were interpreted as being compatible with the abyssal regime being dominated by TRWs rather than by translating closed-core deep eddies (Hamilton, 2009). Lower-layer cyclones, translating westward from the LC with lifetimes of ~ 1 month, are a feature of the model results (Oey, 2008), where they act as a generating mechanism for northwestward, up-slope propagating TRWs. Translating deep eddies have been produced in other models also, although they are associated more with translating rings (e.g., Welsh and Inoue, 2000). An alternative explanation of the observed oscillatory float tracks is that they may be the result of geostrophic turbulence that produces a field of transient quasi-stationary eddies. This would produce isotropic velocity fluctuations that the observations (e.g., Figure 4.8) do not support.

To examine this issue using similar data, the model was seeded with 26 floats that had the same initial locations, times and durations as the last six months (October 2003 – April 2004) of the equivalent observed float tracks. All the model floats were at 1500 m, whereas the observations had a few floats at deeper depths. However, this is not significant because of the nearly depth-independent nature of the lower-layer fluctuations. A subset of the equivalent observed and modeled float tracks, restricted to the eastern Gulf, are given in Figure 4.9. As with the Eulerian comparisons, it is not expected that there will be a direct correspondence between observed and simulated pathways; however, if the model is close to reality, the statistics should be similar. Under the west side of the LC (particularly floats *0467*) the oscillatory looping paths are remarkably similar. To the west in the Exploratory region, the model tracks have a less looping behavior than the equivalent observations. Of particular note are the model float tracks for *0466* and *0458* that both translate westward and do two cyclonic loops, similar to paths produced by rapidly westward translating closed-core cyclones. Similar behavior was not found in any of the observed float tracks in the central and eastern Gulf. Another difference is that the same two model floats make more than one circuit of a large deep cyclone adjacent to the west Florida escarpment between ~26° and 27°N, a feature not sampled by the observations.

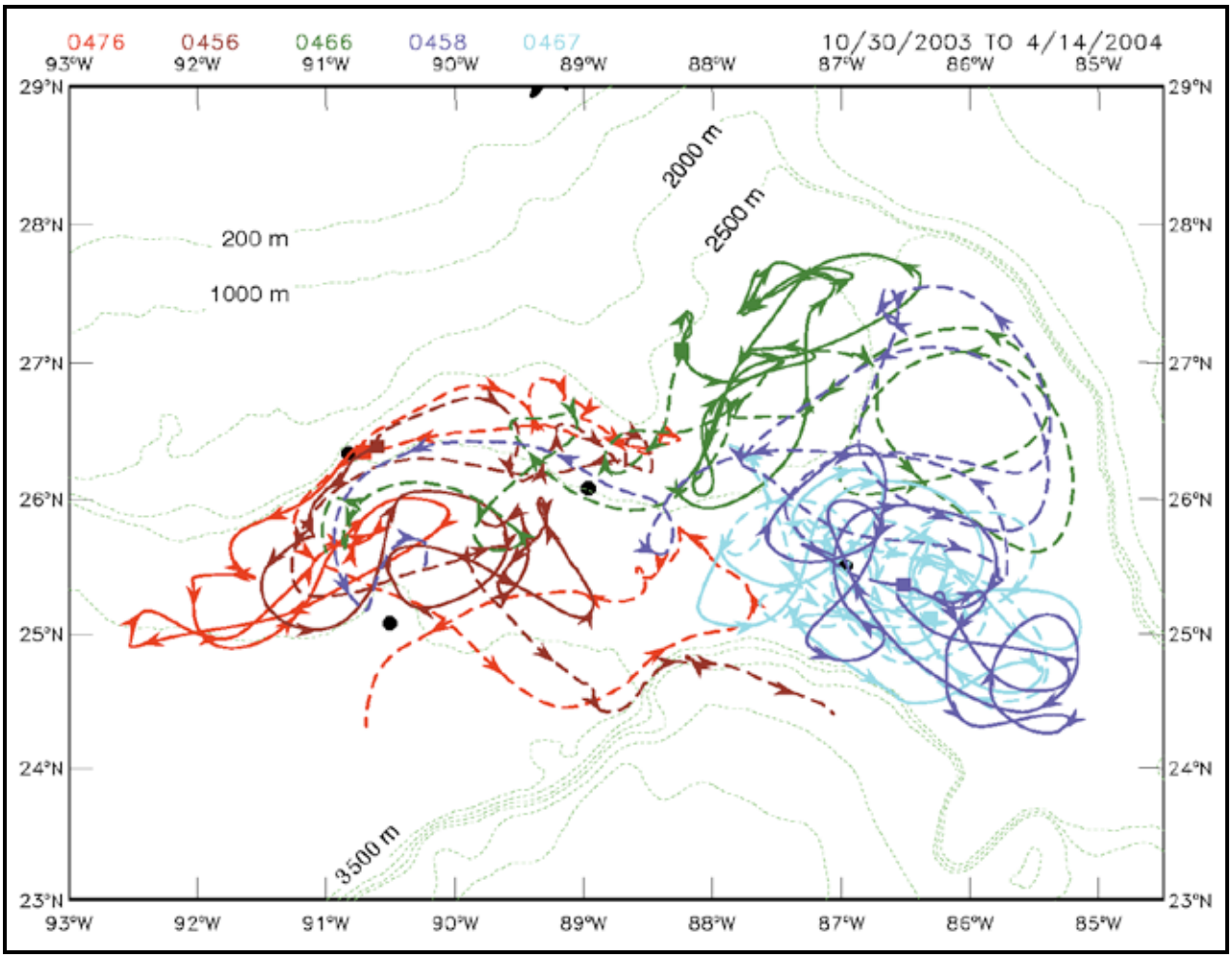

Figure 4.9. Float tracks from the model (dashed) and RAFOS deployed in the Exploratory program (solid) for the same initial locations (given by the solid squares) and time intervals. Arrow heads are at 10-day intervals, and paths are color coded by the RAFOS float number above the plot. All model and RAFOS floats were at 1500 m, except for RAFOS 0476 at 2500 m. Mooring locations, noted in the text, are shown by the black dots.

For the five observed and model floats in Figure 4.9, the east (u) and north (v) component velocity autocorrelations were calculated from the demeaned 6-month records, and then ensemble averaged (Figure 4.10). The integral timescales were also calculated from the ensemble autocorrelations, where the integral was terminated at the first zero crossing. For Lagrangian autocorrelations, the removed mean should be a space dependant function (e.g., Chiswell et al., 2007), and this is available for the model simulations, but not easily obtained for the observations. Therefore, simple record length means were removed to make comparable statistics. Both model and observed Lagrangian autocorrelations show periodic behavior after the initial decay, with the observations having larger amplitudes and slightly longer characteristic periodicities. The longer periodicity is characteristic of strongly looping tracks (Veneziani et al., 2004). The Lagrangian integral timescales are comparable with the model's being slightly shorter.

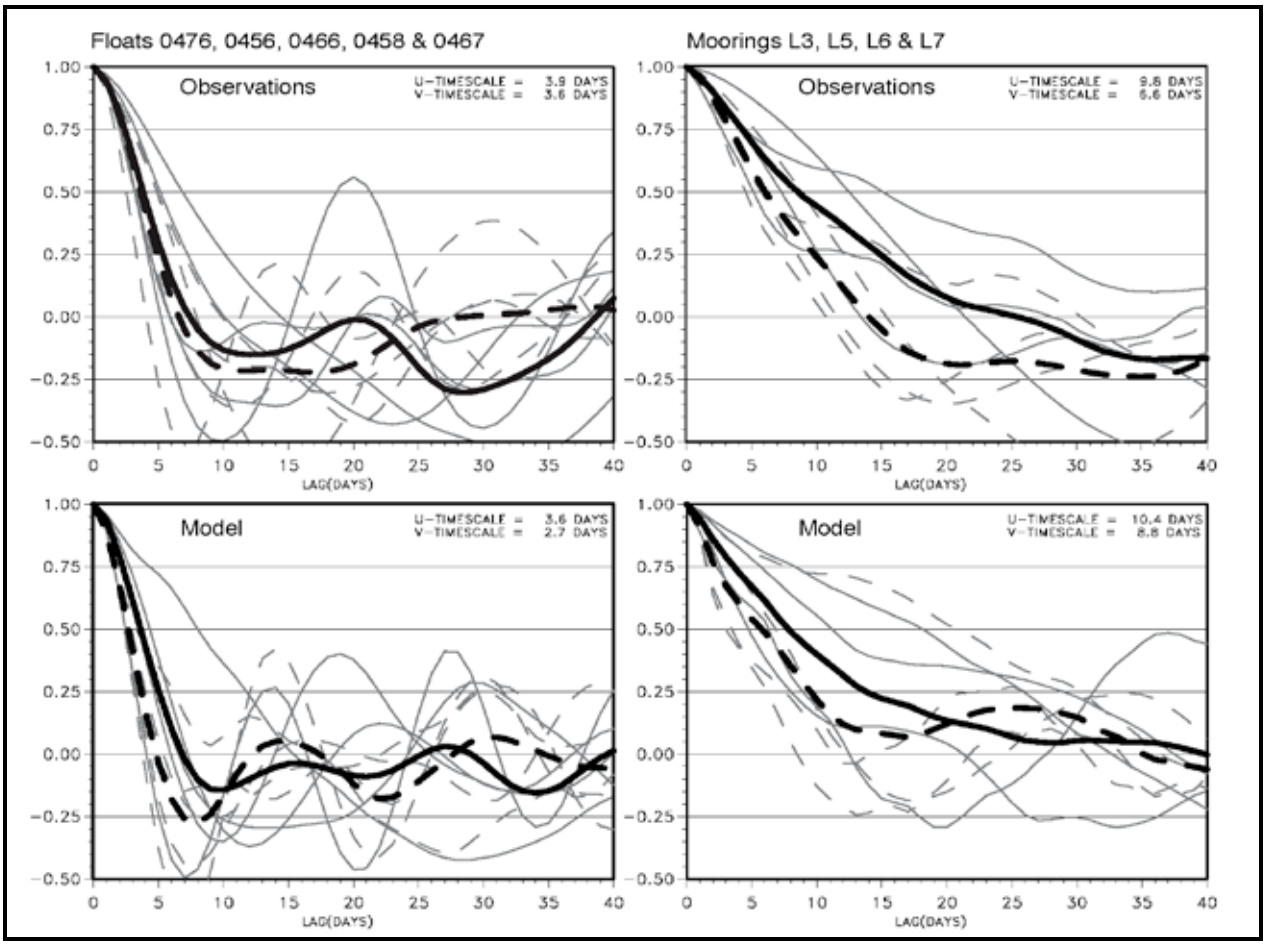

Figure 4.10. 1500-m depth autocorrelations from floats (LH panels) and current meters (RH panels) for observations (upper row) and model simulations (lower row). Solid and dashed lines are east (u) and north (v) components, respectively. The heavy lines are the ensemble autocorrelations for the indicated floats and moorings.

The model Eulerian timescales, calculated using the velocity records at 1500 m for mooring locations *L3*, *L5*, *L6* and *L7*, are longer than obtained from the equivalent observations. It is usually the case that Lagrangian timescales are shorter than Eulerian timescales for geophysical flows, because the characteristic length scales of the eddies are shorter than the distance traveled by drifters in one Eulerian timescale. Therefore, a drifter's velocity becomes decorrelated in time faster than the Eulerian timescale because a drifter advects into regions that are spatially decorrelated (Middleton, 1985). There is some indication from the estimated timescales in Figure 4.10 that the model eddy (i.e. Lagrangian) length scales are shorter than observed and the characteristic Eulerian timescales of the fluctuating flows are longer than observed. Both model and observed north (v) component timescales are shorter than their respective east (u) components, indicating shorter characteristic periodicities across the general east-west trend of the bathymetry than along bathymetry, which is consistent with the wavelet powers given in Figure 4.8.

Comparison of float and current meter basic statistics are given in Table 4.2, where 1°x1° squares were defined centered on each of the four mooring locations shown in Figure 4.9, and velocities extracted from all the float trajectories that entered each box. Velocities were

calculated at 6-hour intervals for both the floats and current meters at 1500 or 2000 m, but at 1-day intervals for the model Eulerian currents, using all available records so as to produce similar number of velocity estimates at each mooring location. The velocities were decomposed into across- (u) and along- (v) isobath coordinates where the isobath direction was defined at the center of each box. The standard deviations are very similar between the Lagrangian and Eulerian estimates, and between the observations and model statistics. Perhaps the largest discrepancies are at L6, south of the escarpment, where the model indicates somewhat higher energy levels than observed, which is also consistent with the Eulerian EKE_H comparison in Figure 4.4. Following Bracco et al. (2000), the velocity estimates were used to construct probability density functions (PDF) where the records were demeaned and normalized by the standard deviations in Table 4.2 for each box before being binned. The resulting PDFs are given in Figure 4.11 where, similar to other high-energy regions (LaCasce, 2008), there are significant deviations from the Gaussian distribution in that the tails are extended, implying an excess of velocities greater than the standard deviation. However, based on Figure 4.11, the model PDFs are closer to a Gaussian distribution than the observations.

Table 4.2

Lagrangian and Eulerian Statistics at 1500 m

	Observations					Model				
	Floats			Current Meters		Floats			Eulerian[a]	
Location (Isobath Direction from N)	No. of Tracks in 1°x1° Box	No. of Velocity Estimates	$\langle u'^4\rangle^{3/4}/\langle v'$	No. of Velocity Estimates	$\langle u'^4\rangle^{3/4}/\langle v'^4\rangle$	No. of Tracks in 1°x1° Box	No. of Velocity Estimates	$\langle u'^4\rangle^{3/4}/\langle v'^4$	No. of Velocity Estimates	$\langle u'^4\rangle^{3/4}/\langle v'^4\rangle^{3/4}$
L3(115°)	25	1356	5.93/7.30	1451	7.05/9.32	30	2223	5.30/8.57	1440	7.19/10.55
L5(048°)	38	2870	3.14/5.73	1644	2.95/10.45	29	1182	5.05/9.89	1440	3.21/10.49
L6(093°)	38	2821	4.94/6.36	1861	5.25/5.82	48	2326	6.99/10.24	1440	6.01/9.46
L7(138°)	29	1465	11.02/9.21	1642[b]	13.59/12.53[b]	27	1159	12.47/12.45	1440	11.80/12.67

a 1-day interval data
b 2000-m Instrument

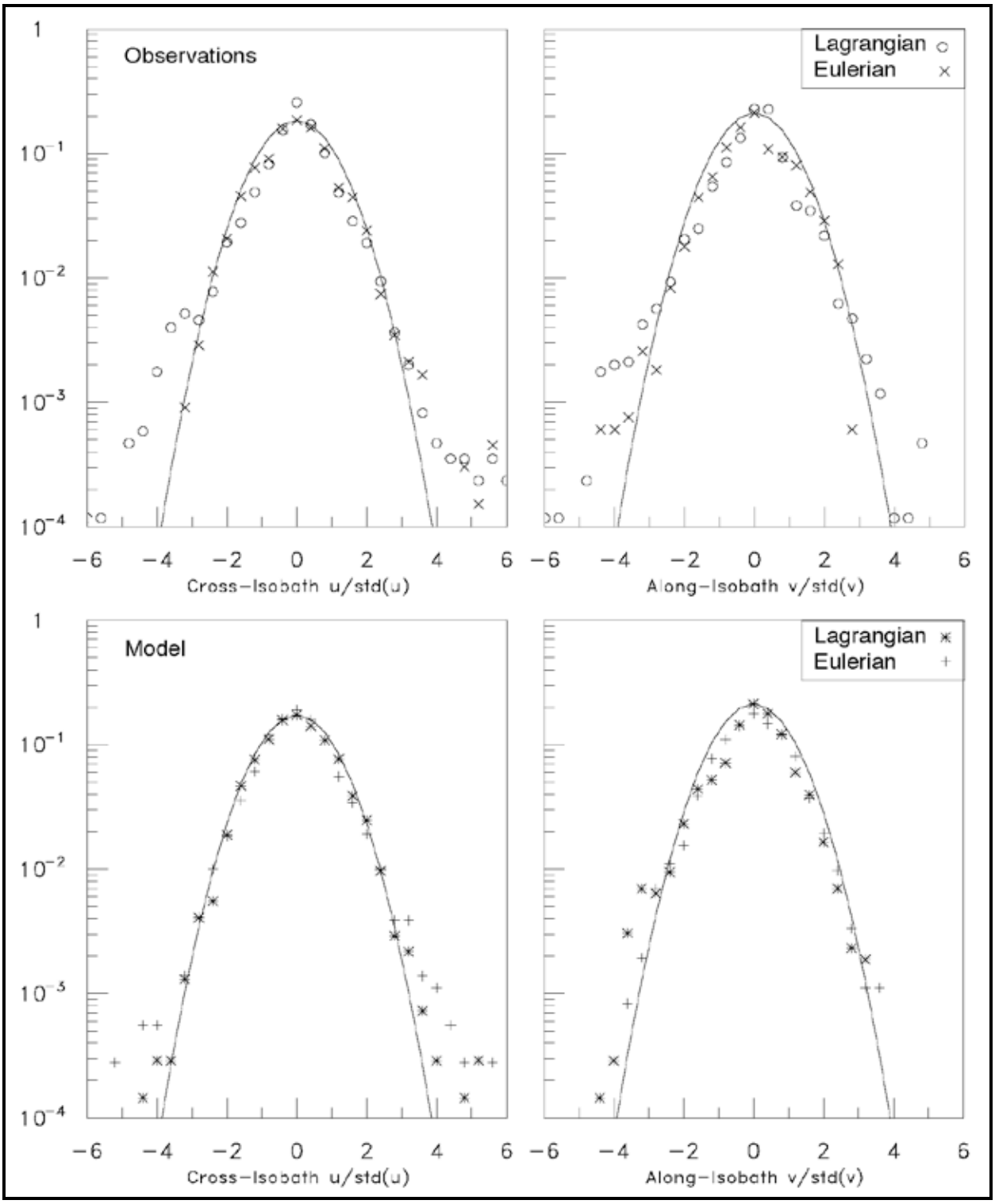

Figure 4.11. PDF's for cross (u) and along (v) isobath currents from deep floats and current meters (nominal depth 1500 m), normalized for locations L3, L5, L6 and L7. Top panels from observations in the Exploratory program; bottom panels from model simulations. The lines are gaussian distributions.

4.5. DISCUSSION AND CONCLUSIONS

This study has investigated the response of the lower layer of a data assimilating Gulf of Mexico model, where the assimilation is confined to the upper layer and comparisons of the upper layer eddy circulations to the observed are generally reasonable. The free response of the model lower layer has been compared to contemporary observations that have previously been analyzed and interpreted as being dominated by TRWs (Hamilton, 2009). There have been large gains in model fidelity to the lower layer observations since this exercise was last performed by Oey et al., using an earlier, less highly resolved, version of the model and more limited observations. Key areas of improvement for the lower layer are the impressive agreements with EKE levels and current profile characteristics at the mooring sites. Depth profiles of velocities below 1000 m are highly coherent and quasi-barotropic as observed. The velocity PDF's have similar distributions with extreme events exceeding the normal distribution, and the frequency content and Lagrangian spatial scales of the flows are approximately similar.

Examination of the frequency and wavenumber contents of the model and observations revealed some discrepancies, which can be summarized as follows. At sub-inertial frequencies, model lower-layer current fluctuations are less bottom-intensified than observed. Model currents tend to have energetic responses at longer and shorter periodicities than observed, and this is also reflected in a larger difference between Lagrangian and Eulerian integral time scales for the model results. The model floats also show some evidence of the deep westward propagating eddies, discussed by Oey (2008), and a long-lasting deep cold eddy adjacent to the northwest Florida slope that were not apparent in the equivalent RAFOS float tracks.

General conclusions on lower-layer model performance are that even though basic statistics of the fluctuations are good, the lower layer currents are not predicted. This undoubtedly related to the details of the genesis of the lower layer current fluctuations by the LC and LC eddies. Being of smaller scales and highly dispersive, the lower layer currents are much less predictable. There is evidence, however that instabilities and the generation of TRWs differ in the model from what can be surmised from the limited observational array in the northern part of the LC. Thus, model lower layer flows in the eastern Gulf seem to be more of a mixture of eddies and TRW's than the more TRW dominated regime inferred from the observed currents. It is possible that the stochastic nature of the upper to lower layer exchanges precludes a predictable lower layer current field without direct assimilation of lower layer measurements. Future work is necessary to clarify these issues.

5. CONCLUSIONS

The Loop Current and warm-core rings that episodically separate from the Loop are powerful features which dominate the upper (surface to depths of *500~1000 m*) circulation in the Gulf of Mexico [e.g., Oey et al., 2005]. The Loop and rings are well-studied because they are prominently important. They are also very obvious manifestations of the circulation system of the Gulf, being more readily observable especially in recent decades with satellite data. The Loop and rings affect, either directly or indirectly through their smaller-scale subsidiaries, just about every aspect of oceanography in the Gulf. One such aspect concerns deep motions which are much less accessible, much less known, much less understood and probably also much less predictable. Here, by "deep" we mean depths from (approximately) *1000 m* below the surface to the seafloor. At these depths, the Gulf's is virtually closed except for the deep narrow opening at Yucatan Channel. Loop and rings are therefore the major sources of energy for deep motions, which are generated and dissipated within the Gulf. Deep motions provide mixing below the thermocline and may play a crucial role in the overall energy balance which in turn may affect the Loop and its behaviors including the separation of rings.

In recent years, deep circulations of the Gulf have received increased attention spurred in part by concerns with potential environmental impacts of oil and gas activities in deeper waters of the Gulf (the industry is also concerned with strong deep currents that can cause havoc to pipelines and oil rigs), and in part by our curiosity to explore the unknowns, and a desire to understand them. It is the goal of the proposed research, therefore, using numerical modeling techniques guided by observations, to:

1. advance to a high level our understanding of deep motions: if, why and how they are forced by, and coupled to, the processes in the upper layers—the Loop and rings, in particular; and
2. provide a realistic simulation of the Gulf's circulation processes.

The improved model-observation syntheses of the deep-Gulf circulation should lead to more accurate assessments of their impacts on contaminant-transports and dispersions—topics that are of interest to the BOEM.

These goals have been accomplished in this project.

We have identified stages of Loop Current expansion, eddy shedding propagation, and retraction, and explain their coupling to the deep Gulf in terms of mass flux across the z = -1000 m surface in the eastern Gulf of Mexico. Main conclusions are:

1. there is a net downwelling across the z =-1000 m surface in the eastern Gulf of Mexico because on average the Loop Current spends more time accumulating mass (reforming) and expanding than shedding eddies;
2. the net deep flow in the Yucatan Channel is an outflow, from the Gulf to the Caribbean Sea;
3. the deep outflow variation in the Yucatan Channel is poorly correlated with the expansion and retraction of the Loop Current because the latter also produces deep (zonal) flow exchanges between the eastern and western Gulf.

The idea of a good correlation has been falsely presumed in many previous studies including that of this author (in Ezer et al. 2003);

4. the Yucatan deep outflow becomes very weak (nearly zero) during the time of an incipient eddy-shedding. This suggests that, because of the deep coupling between the eastern and western Gulf of Mexico (see below), the eddy-separation process can be sensitive to deep transport perturbations and exchanges between the Gulf and the Caribbean Sea; that is because these perturbations and exchanges can sufficiently offset the mass balance of the Loop;
5. the close coupling between deep flows in the western and eastern Gulf of Mexico has a profound implication to Loop Current eddy shedding and eddy propagation, as well as to deep circulation, in the idea of a Gulf of Mexico Oscillator: when the eastern Gulf thermocline rises, that of the western Gulf falls, and vice versa. The implication is that the oscillation can be modified in a nonlinear manner by the relative pressure difference between the western and eastern Gulf, so that the period of eddy shedding can also change with time; an example is provided in Chang and Oey (2010a). This "local" idea is in stark contrast (and complements) that of the remote forcing idea explained in Oey et al. (2003);
6. the net downwelling in the eastern Gulf of Mexico is shown to lead to a net cyclonic circulation in the deep western Gulf below the sill depth of the Yucatan Channel at $z \approx -2000$ m. The reason is because at these deep levels, the Gulf is closed, and the net circulation around the (closed) Gulf is zero. The net transport at these deep levels is from east to west across approximately the 90^{o}W;
7. the net cyclonic circulation in the deep western Gulf necessitates upwelling across the $z \approx -2000$ m surface, and since net transport in the upper layer is westward (due to eddies), there must be convergence in the intermediate layer in the western Gulf (-1000 m $> z >-2000$ m). A 3-layer zonal transport structure must therefore exist in the Gulf of Mexico; and, finally,
8. the modeled deep currents in the Gulf of Mexico have been extensively compared against observations. Improvements of the strengths of modeled deep currents (compared to a previous comparison) are noted. However, there are areas where the model may be improved. In particular, some of the model physics—eddies versus waves for example, may need further re-examination both in the model as well as in observations.

5.1. RECOMMENDATIONS FOR FUTURE STUDIES

It is clear that from the above conclusions that east-west coupling is important. Future observational studies by BOEM should strive to collect enough information to compute mass transport at the key south-north vertical section in the central Gulf (90^{o}W is good). Coupled with measurements at the Yucatan Channel, the 90^{o}W section holds the key to our understanding of the Loop Current fluctuations, eddy-shedding and propagation, and deep flows.

REFERENCES

Berntsen, J. and L.-Y. Oey. 2010. Estimation of the internal pressure gradient in σ-coordinate ocean models: comparison of second-, fourth-, and sixth-order schemes. Ocean Dyn. 60:317-330.

Bracco, A., J.H. LaCasce, and A. Provenzale. 2000. Velocity pdfs for oceanic floats. J. Phys. Oceanogr. 30:461-474.

Bunge, L., J. Ochoa, A. Badan, J. Candela, and J. Sheinbaum. 2002. Deep flows in the Yucatan Channel and their relation to changes in the Loop Current extension, J. Geophys. Res. 107(C12), 3233, doi:10.1029/2001JC001256.

Burkov, V. A., L. I. Galerkin, and A. B. Zubin. 1982. New data on water exchange through the Yucatan Strait (in Russian). Dokl. Akade. Nauk SSSR 265(1):190-195. [Available as a translation from Oceanology, 1984:198-200.]

Candela J., J. Sheinbaum, J. Ochoa, A. Badan, and R. Leben. 2002. The potential vorticity flux through the Yucatan Channel and the Loop Current in the Gulf of México. Geophys. Res. Lett. 29:2059,doi:10.1029/2002GL015587.

Chang,Y.-L. and L.-Y. Oey. 2010a. Why can wind delay the shedding of Loop Current eddies? J. Phys. Oceanogr. 40:2481-2495.

Chang,Y.-L. and L.-Y. Oey. 2010b. Eddy and wind-forced heat transports in the Gulf of Mexico. J. Phys. Oceanogr. 40:2728-2742.

Chang,Y.-L. and L.-Y. Oey. In press. Loop Current Cycle: coupled response of Loop Current and deep flows. J. Phys. Oceanogr. 2011: http://journals.ametsoc.org/doi/pdf/10.1175/2010JPO4479.1.

Chiswell, S.M., G.J. Rickard, and M.M. Bowen. 2007. Eulerian and Lagrangian eddy statistics of the Tasman Sea and southwest Pacific Ocean. J. Geophys. Res. 112:C10004, doi:10.1029/2007JC004110.

Cochrane, J.D. 1972. Separation of an anticyclone and subsequent developments in the Loop Current (1969). In: Capurro, L.R.A. and J.L Reid, eds. Contributions on the physical oceanography of the Gulf of Mexico. Vol. 2, Texas A&M University. Houston, TX: Gulf Pub. Co. Pp. 91-106.

Cooper, C., G.Z. Forristall, and T.M. Joyce. 1990. Velocity and hydrographic structure of two Gulf of Mexico warm-core rings. J. Geophys. Res. 95:1663-1679.

DeHaan, C. and W. Sturges. 2005. Deep Cyclonic Circulation in the Gulf of Mexico. J. Phys. Oceanogr. 35(10):1801-1812.

Donohue, K., P. Hamilton, K. Leaman, R. Leben, M. Prater, D.R.Watts, and E. Waddell. 2006. Exploratory study of deepwater currents in the Gulf of Mexico. Volume II: Technical report.

U.S. Dept. of the Interior, Minerals Management Service, Gulf of Mexico OCS Region, New Orleans, LA. OCS Study MMS 2006-074. 430 pp.

Elliott, B.A. 1982. Anticyclonic rings in the Gulf of Mexico. J. Phys. Oceanogr. 12(11):1292-1309.

Ezer, T. and G.L. Mellor. 1994. Continuous assimilation of Geosat altimeter data into a three-dimensional primitive equation Gulf Stream model. J. Phys. Oceanogr. 24(4):832-847.

Ezer, T., L-Y. Oey, H-C. Lee, and W. Sturges. 2003. The variability of currents in the Yucatan Channel: Analysis of results from a numerical ocean model. J. Geophy. Res. 108(C1):3012, 10.1029/2002JC001509.

Forristall, G.Z., K.J. Schaudt, and .C. Cooper. 1992. Evolution and kinematics of a Loop Current Eddy in the Gulf of Mexico warm-core rings. J. Geophys. Res. 97:2173-2184.

Gill, A.E. 1982. Atmosphere-Ocean Dynamics. New York: Academic Press. 662 pp.

Hamilton, P. 1990. Deep currents in the Gulf of Mexico. J. Phys. Oceanogr. 20:1087-1104.

Hamilton, P. 2007. Deep current variability near the Sigsbee escarpment in the Gulf of Mexico. J. Phys. Oceanogr. 37:708–726.

Hamilton, P. 2009. Topographic Rossby waves in the Gulf of Mexico. Progress in Oceanography doi:10.1016/j.pocean.2009.04.019: 31 pp.

Hamilton, P. and A. Lugo-Fernandez. 2001. Observations of high speed deep currents in the northern Gulf of Mexico. Geophys. Res. Lett. 28:2867-2870.

Hamilton, P. and L.-Y. Oey. 2011. Comparison of modeled and observed variability in an eddy-dominated region of the Gulf of Mexico: deep dynamics. Manuscript to be submitted.

Hamilton, P., J.C. Larsen, K.D. Leaman, T.N. Lee, and E. Waddell. 2005. Transports through the Straits of Florida. J. Phys. Oceanogr. 35:308-322.

Huang, N.E., Z. Shen, S.R. Long, M.C. Wu, H.H. Shih, Q.Zheng, N.-C Yen, C.C. Tung, and H.H. Liu. 1998. The empirical mode decomposition and the Hilbert spectrum for nonlinear and non-stationary time series analysis. Proc. R. Soc. London A 454:903-995.

Hurlburt, H.E., and J.D. Thompson. 1980. A numerical study of Loop Current intrusions and eddy shedding. J. Phys. Oceanogr. 10:1611-1651.

Inoue, M., S.E. Welsh, L.J. Rouse, Jr., and E. Weeks. 2008. Deepwater currents in the Eastern Gulf of Mexico: Observations at 25.5°N and 87°W. U.S. Dept. of the Interior, Minerals Management Service, Gulf of Mexico OCS Region, New Orleans, LA. OCS Study MMS 2008-001. 95 pp.

Johns, W.E., T.L. Townsend, D.M. Fratantoni, and W.D. Wilson. 2002: On the Atlantic inflow to the Caribbean Sea. Deep Sea Res. Part I. 49:211–243.

LaCasce, J.H. 2008. Statistics from Lagrangian observations. Progress in Oceanography 77,doi:10.1016/j.pocean.2008.02.002:1-29.

Lai, R.J. and N.E. Huang. 2005. Investigation of vertical and horizontal momentum transfer in the Gulf of Mexico using Empirical Mode Decomposition method. J. Phys. Oceanogr. 35:1383-1402.

Leben, R.R. 2005. Altimeter-derived Loop Current metrics. In: Sturges, W. A. and A. Lugo-Fernandez, eds. Circulation in the Gulf of Mexico: Observations and Models, Vol.161. American Geophysical Union, Geophysical Monograph Series, Washington, DC. Pp. 181-201.

Lee, H.-C., and G.L. Mellor. 2003. Numerical simulation of the Gulf Stream System: The Loop Current and the deep circulation. J. Geophys. Res. 108(C2):3043, doi:10.1029/2001JC001074.

Lighthill, J. 1978. Waves in Fluids. New York: Cambridge Univ. Press. 504 pp.

Lin, X.-H., L.-Y. Oey, and D.-P. Wang. 2007: Altimetry and drifter data assimilations of Loop Current and eddies. J. Geophys. Res. 112:C05046, doi:10.1029/2006JC 003779.

Maul, G. A. 1977. The annual cycle of the Gulf Loop Current, part I, Observations during a one-year time series, J. Mar. Res. 35:29–47.

Maul, G.A., D.A. Mayer, and S.R. Baig. 1985. Comparison between a continuous three-year current meter observation at the sill of the Yucatan Strait, satellite measurements of Gulf Loop Current area, and regional sea level. J. Geophys. Res. 90:9089-9096.

McKone, K., N.D. Walker, and E. Weeks. 2007. Full-water column currents near the Sigsbee Escarpment (91-92ºW. Longitude) and relationships with the Loop Current and associated warm and cold-core eddies, U.S. Dept. of the Interior, Minerals Management Service, Gulf of Mexico OCS Region, New Orleans, LA. OCS Study MMS 2007-056. 107 pp.

Meinen, C.S. and D.R. Watts. 2000. Calibrating inverted echo sounders equipped with pressure sensors. J. Atmos. Oceanic Technol. 15:1339-1345.

Mellor, G.L. and T. Ezer. 1991. A Gulf Stream model and an altimetry assimilation scheme. J. Geophys. Res. 96:8779-8795.

Mellor, G.L. 2004. User's guide for a three-dimensional, primitive equation, numerical ocean model. Program in Atmospheric and Oceanic Sciences, Princeton University. 42 pp.

Mellor, G.L., L.-Y. Oey, and T. Ezer. 1998. Sigma coordinate pressure gradient errors and the seamount problem, J. Atmos. Oceanic. Technol. 15(5):1122-1131.

Middleton, J.F. 1985. Drifter spectra and diffusivities. J. Mar. Res. 43:37-55.

Nof, D. 2005. The momentum imbalance paradox revisited. J. Phys. Oceanogr. 35:1928-1939.

Nowlin, W.D. Jr. 1972. Winter circulation patterns and property distributions. In: Capurro, L.R.A. and J.L Reid, eds. Contributions on the physical oceanography of the Gulf of Mexico. Vol. 2, Texas A&M University. Houston, TX: Gulf Pub. Co. Pp. 3-51.

Oey, L-Y. 1996. Simulation of mesoscale variability in the Gulf of Mexico, J. Phys. Oceanogr. 26:145–175.

Oey, L.-Y. 2004. Vorticity flux in the Yucatan Channel and Loop Current Eddy shedding in the Gulf of Mexico. J. Geophys. Res. 109:C10004,doi:10.1029/2004JC002400.

Oey, L.-Y. 2008. Loop Current and Deep Eddies. J. Phys. Oceanogr. 38:1426-1449.

Oey, L.-Y. and Y.-L. Chang. 2011. Loop Current Cycle and trigger mechanism for Loop Current ring separations. *Proc. BOEM Info. Trans Meet,* New Orleans, LA. [Available online at http://www.aos.princeton.edu/WWWPUBLIC/PROFS/PUBLICATION/LCCycleTriggerMechanismv8.pdf.]

Oey, L.-Y. and H.-C. Lee. 2002. Deep Eddy Energy and Topographic Rossby Waves in the Gulf of Mexico. J. Phys. Oceanogr. 32(12):3499-3527.

Oey, L.-Y. and H.-C. Zhang. 2004. A mechanism for the generation of subsurface cyclones and jets. Cont. Shelf Res. 24:2109-2131.

Oey, L.-Y., P. Hamilton, and H.-C. Lee. 2003a. Modeling and data analyses of circulation processes in the Gulf of MexicoMMS 2003-074, 129 pp.

Oey, L.-Y., H.-C. Lee, and W.J. Schmitz Jr. 2003b. Effects of Winds and Caribbean Eddies on the Frequency of Loop Current Eddy Shedding: A Numerical Model Study, J. Geophys. Res. 108(C10):3324,doi:10.1029/2002JC001698.

Oey, L.-Y., C.Winant, E. Dever, W.R. Johnson, and D.-P. Wang. 2004. A Model of the Near-Surface Circulation of the Santa Barbara Channel: Comparison with Observation and Dynamical Interpretations. J. Phys. Oceanogr. 34(1):23-43.

Oey L.-Y., T. Ezer, G. Forristall, C. Cooper, S. DiMarco, and S. Fan. 2005a. An exercise in forecasting Loop Current and eddy frontal positions in the Gulf of Mexico. Geophys. Res. Lett. 32:L12611,doi:10.1029/2005GL023253.

Oey L.-Y., T. Ezer, and H.J. Lee. 2005b. Loop Current, Rings and Related Circulation in the Gulf of Mexico: A Review of Numerical Models and Future Challenges. In: Sturges, W. A. and A. Lugo-Fernandez, eds. Circulation in the Gulf of Mexico: Observations and Models, Vol.161. American Geophysical Union, Geophysical Monograph Series, Washington, DC. Pp. 31-56.

Oey, L.-Y., M. Inoue, R. Lai, X.-H. Lin, S. Welsh, and L. Rouse Jr. 2008. Stalling of near-inertial waves in a cyclone. Geophys. Res. Lett. 35:L12604,doi:10.1029/2008GL034273.

Oey, L.-Y., Y.-L. Chang, Z.-B. Sun, and X.-H. Lin. 2009. Topocaustics. Ocean Modeling 29:277-286.

Pichevin, T. and D. Nof. 1997. The momentum imbalance paradox. Tellus 49:298–319.

Reid, R.O. and O. Wang. 2004. Bottom-trapped Rossby waves in an exponentially stratified ocean. J. Phys. Oceanogr. 34:961–967.

Rhines, P.B. 1970. Edge-, bottom-, and Rossby waves in a rotating stratified fluid. Geophys. Fluid Dyn. 1:273-302.

Rivas, D., A. Badan, and J. Ochoa. 2005. The ventilation of the deep Gulf of Mexico. J. Phys. Oceanogr. 35:1763-1781.

Schmitz, W.J. Jr. 2005. Cyclones and westward propagation in the shedding of anticyclonic rings from the Loop Current. In: Sturges, W. A. and A. Lugo-Fernandez, eds. Circulation in the Gulf of Mexico: Observations and Models, Vol.161. American Geophysical Union, Geophysical Monograph Series, Washington, DC. Pp. 241-261.

Sheinbaum, J., J. Candela, A. Badan, and J. Ochoa, 2002: Flow structure and transport in the Yucatan Channel, Geophys. Res. Lett., 29(3), 1040,doi:10.1029/2001GL013990.

Smith, W.H.F. and D.T. Sandwell. 1997. Global sea floor topography from satellite altimetry and ship depth soundings. Science 277:1956-1962.

Sturges, W. and R. Leben. 2000. Frequency of ring separations from the Loop Current in the Gulf of Mexico: A revised estimate. J. Phys. Oceanogr. 30:1814–1818.

Sturges, W., N. Hoffmann, and R. Leben. 2010. A trigger mechanism for Loop Current ring separations. J. Phys. Oceanogr. 40:900–913.

Swaters, G.E. 1991. On the baroclinic instability of cold-core coupled density fronts on a sloping continental shelf. J. Fluid Mech. 224:361-382.

Thompson, R.O.R.Y. 1977. Observations of Rossby waves near site d. Progress Oceanogr. 7:135-162.

Torrence, C. and G.P. Combo. 1998. A practical guide to wavelet analysis. Bulletin American Meteorological Society 79:61-78.

Veneziani, M., A. Griffa, A.M. Reynolds, and A.J. Mariano. 2004. Oceanic turbulence and stochastic models from subsurface Lagrangian data for the north-west Atlantic Ocean. J. Phys. Oceanogr. 34:1884-1906.

Vukovich, F.M. 1995. An updated evaluation of the Loop Current's eddy-shedding frequency. J. Geophys. Res. 100(5):8655-8659.

Vukovich, F.M. and B.W. Crissman. 1986. Aspects of warm rings in the Gulf of Mexico. J. Geophys. Res. 91(C2):2645-2660.

Wang, D.-P., L.-Y. Oey, T. Ezer, and P. Hamilton. 2003. Nearsurface Currents in DeSoto Canyon (1997-1999): Comparison of Current Meters, Satellite Observation, and Model Simulation. J. Phys. Oceanogr., 33(1):313-326.

Weatherly, G., N. Wienders and A. Romanou. 2005. Intermediate-depth circulation in the Gulf of Mexico estimated from direct measurements. In: Sturges, W. A. and A. Lugo-Fernandez, eds. Circulation in the Gulf of Mexico: Observations and Models, Vol.161. American Geophysical Union, Geophysical Monograph Series, Washington, DC. Pp. 315-324.

Welsh, S.E. and M. Inoue. 2000. Loop current rings and deep circulation in the Gulf of Mexico. J. Geophys. Res. 105:16951-16959.

Yang J. and J.F. Price. 2000. Water-mass formation and potential vorticity balance in an abyssal ocean circulation. J. Mar. Res. 58:789–808.

Yin, X.-Q. and L.-Y. Oey. 2007. Bred-ensemble ocean forecast of Loop Current and rings. Ocean Modeling doi:10.1016/j.ocemod.2007.02.005.

The Department of the Interior Mission

As the Nation's principal conservation agency, the Department of the Interior has responsibility for most of our nationally owned public lands and natural resources. This includes fostering the sound use of our land and water resources, protecting our fish, wildlife and biological diversity; preserving the environmental and cultural values of our national parks and historical places; and providing for the enjoyment of life through outdoor recreation. The Department assesses our energy and mineral resources and works to ensure that their development is in the best interests of all our people by encouraging stewardship and citizen participation in their care. The Department also has a major responsibility for American Indian reservation communities and for people who live in island communities.

The Bureau of Ocean Energy Management

The Bureau of Ocean Energy Management (BOEM) works to manage the exploration and development of the nation's offshore resources in a way that appropriately balances economic development, energy independence, and environmental protection through oil and gas leases, renewable energy development and environmental reviews and studies.